Multi-cavity lasers

by

Ashok Pappachen Kanjamala

A Dissertation Presented to the

FACULTY OF THE GRADUATE SCHOOL

UNIVERSITY OF SOUTHERN CALIFORNIA

In Partial Fulfillment of the

Requirements for the Degree

DOCTOR OF PHILOSOPHY

(Electrical Engineering)

May 1998

Acknowledgments

During the course of my Ph.D I have relied on my family, friends and colleagues for personal as well as professional support. I would like to express my deep appreciation for their kindness and assistance which made my stay at USC a pleasant one.

I am deeply indebted to my parents, brother and sister for their patience and constant support while I travelled far away from them to fulfill a personal goal. The knowledge of their support and hopes for me was crucial to help me through the most trying moments over the last five years.

I am grateful to my advisor Prof. A. F. J. Levi for taking a me as a research student and guiding me through my Ph.D. Working with him in the laboratory was an invaluable learning experience which most graduate students rarely get. His insights and overview of the field was crucial in helping me to ask the right questions which guided the course of my Ph.D. He provided the environment and resources to let me pursue my Ph.D without too many distractions. I am also grateful for the advice and help he provided during my search for a suitable job.

I am grateful to Dr. Newton Frateschi, Dr. Robert Marsland and Dr. Peymann Hadizad who trained me on essential skills I needed to become a better researcher. I also enjoyed the wide ranging discussions that we had.

I am indebted to Kim Reid for the numerous times she went out of her way to help me. Besides being very efficient she was extremely pleasant to work with. She was an invaluable buffer between me and the University administration.

I owe my colleagues David Cohen and Sumesh M. Thiyagarajan for their help in maintaining the laboratory and for their understanding in allowing me to a disproportionate amount of space on the optical table. Besides providing me with free access to

their computer expertise they were also invaluable to bounce ideas off.

Bharath Raghavan and Bindu Madhavan helped me with many of my questions on UNIX. Bindu provided me with insights into the world of CMOS and IC technology. Bharath besides proof reading also provided support at crucial moments over the last three years.

My colleagues Tsu-Yau Chuang, David Cohen, William Cui, Yerko Dekovic, Newton Frateschi, Young-Gook Kim, Binhu Madhavan, Mark Mendez, Bharath Raghavan, Jeff Sondeen, Sumesh M. Thiyagarajan, Panduka Wijetunga and Sherali Zeadalli provided an extremely pleasant environment in which to work. I enjoyed the discussions as well as daily interactions I have had with them.

Besides the people mentioned above I am extremely lucky to have good friends too numerous to list here who have made my stay at USC over the last five years an enjoyable experience.

Ashok. P. Kanjamala

Table of contents

List of figures

List of tables

List of abbreviations

AR : anti-reflection

β : spontaneous emission coupling coefficient

BER : bit error ratio

BG : Bragg grating

BW : 1/e optical bandwidth of the fiber Bragg grating

C : coupling coefficient

cm : centimeters

CMOS : complementary metal oxide semiconductor transistor

D_{ns} : change in refractive index of the semiconductor with carrier density

DBR : Distributed Bragg reflector

DFB : Distributed feedback

f : frequency of RF signal

FBG : fiber bragg grating

GHz : gigahertz

I : current

IC : integrated circuit

kHz : kilohertz

L : light

L-I : light versus current

λ : wavelength

mA : milli amperes

MCL : multi-cavity laser

MHz : megahertz

μm : micrometeres

MSL : mode suppression ratio

mW : milli watts

n : carrier density in the laser gain medium

ns : nanoseconds

nm : nanometeres

ps : picoseconds

r : reflection coefficient of the electric field

RF : radio frequency

SMF : single-mode fiber

SR : set-reset

t : electric field transmission coefficient or time as the case may be.

WDM : wavelength division multiplexing

Chapter 1 : Introduction

1.1 Enabling technologies

1.1.1 Semiconductor lasers

Lasers were first proposed in the seminal paper [1.1] of Schawlow and Townes. This was followed by the successful operation of the solid-state ruby laser in May 1960 [1.2] and the He-Ne gas laser in December 1960 [1.3]. Bernard and Duraffourg first stated in 1961 that for lasing to occur in semiconductors the separation between the quasi-Fermi levels corresponding to the non-equilibrium concentration of electron and holes should exceed the energy of the emitted radiation [1.4]. The early forward biased GaAs p-n junction lasers had threshold current densities greater than 50,000 A/ cm^2 at room temperature. In 1963 it was proposed that semiconductor laser would improve by sandwiching a layer of a semiconductor with a relatively narrow energy gap between two semiconductor layers of a wider energy gap [1.5][1.6]. This structure is called a heterostructure. In 1970 [1.7] the first room temperature continuously operating heterostructure (AlGaAs/GaAs) lasers were reported. Since then the rapid progress in the field has lead to threshold current densities as low as 56 A/cm^2 [1.8] for InGaAs/GaAs/AlGaAs lasers. Currently by using different material systems room temperature operation of semiconductor lasers is possible from 300 nm to 3000 nm [1.9].

1.1.2 Optical fibers

The basic principle of optical communications as practised today was first demonstrated by Alexander Graham Bell [1.10] over a century ago when he transmitted a telephone signal over a distance of 200 m using a beam of sunlight. The lack of an intense reliable light source hampered progress for 8 decades. The advent of lasers in the 1960s rekindled the interest in optical fiber communications. After extensive theoretical work in the early 1960's the first serious proposal to use a clad glass fibers as

a waveguide for optical frequencies appeared in 1966 [1.11]. Optical fiber attenuation of 20 dB/km regarded in the 60's as the threshold for usefulness in telecommunications was announced in 1970 [1.12]. Over the next decade the fiber attenuation continuously dropped with attenuation as low as 0.16 dB/km at λ = 1550 nm reported in 1982 [1.13]. The bandwidth of a single mode fiber (SMF) is limited by chromatic dispersion. Standard Germania doped single mode fiber has zero dispersion at 1300 nm [1.14]. Dispersion shifted fibers allow for zero chromatic at one or more than one wavelengths [1.14]. Zero chromatic dispersion would result in extremely high transmission bandwidths. A study which considered the practical versus theoretical maximum transmission bandwidth concluded that under optimal conditions ultra-high-speed transmission at 100 Gb/s over 100 km is possible [1.15]. The rapid progress in optical fiber technology have made optical fiber components cheap, reliable and readily available. As fiber optic technology becomes established it enables us to design and build all fiber or hybrid optical systems for diverse applications as communications, gyroscopes [1.16] , sensors [1.17] [1.18] and actuators [1.19].

1.1.3 Fiber Bragg gratings

Since 1978 when the fiber Bragg gratings (FBGs) [1.20] were written by exposing the core of the fiber to an intense optical interference pattern generated by launching intense Argon-ion laser radiation into a cleaved germania-doped fiber, there has been a great deal of research in this subject. These initial gratings were narrow band (200 MHz) and centered at the Argon lasers writing wavelength. In 1989 Meltz et al. showed that ultraviolet light at 244 nm could be used to write gratings that would reflect at any wavelength by illuminating the fiber through the side of the cladding with two intersecting beams of UV light. The period of the gratings and the index change induced are controlled by the angle between the beams and the UV wavelength used. This is possible as the fiber cladding is transparent to the UV light whereas the fiber core is highly absorbing to the UV light. FBGs are relatively inexpensive and commercially available [1.21]. Bragg gratings with full width -3 dB opti-

cal bandwidths from less than 0.1 nm to greater than 30 nm and reflectivities from 3% up to 100% are readily available. The excess loss due to the FBGs have been measured to be as low as 0.001%.

1.1.4 Laser to fiber coupling

The coupling efficiency between a cleaved SMF and an edge emitting semiconductor laser is about 10% due to the mismatch between the optical modes of the semiconductor laser and the SMF. Considerable work has been done to improve the optical coupling efficiency between edge emitting lasers and SMFs. GRIN rod lenses or other bulk optic lenses are used to improve the mode matching and thereby improve coupling efficiency. A more compact method to improve coupling efficiency is to modify the optical mode in the semiconductor by tapering the semiconductor waveguide [1.22] and/or in the SMF by lensing it. We use commercially available [1.23] lensed SMF with a coupling efficiency of 40% for our experiments. Microlenses micromachined to the end of SMFs with coupling efficiencies of up to 90% have been reported [1.24].

1.1.5 Need for increased bandwidth

Over the last decade ICs made from submicron CMOS technology have pushed digital circuit speeds into the multi-gigabit range [1.25] [1.26]. This increase in circuit speed will continue in the future as outlined in the Industry Association's National Technology Roadmap for Semiconductors better known as the SIA Roadmap [1.27]. The increase in IC speed and the concomitant increase in computer/microprocessor speeds along with the rapid increase in demand for bandwidth from new services and users have created a need for reliable, inexpensive, high bandwidth, robust and compact medium for data transmission over distances from less than a centimeter to thousands of kilometers. The progress made in fields of semiconductor lasers and fiber optic components over the last three decades has placed optical data links in an unique position to meet this demand.

1.2 Motivation

The progress in SMFs, FBGs, semiconductor lasers and laser to fiber coupling efficiency opens up the possibility of building novel hybrid optoelectronic devices. Edge emitting semiconductor lasers with emission wavelength at 1300 nm or 1550 nm are ideal candidates as components for such hybrid devices since these lasers are already of interest for lightwave communication systems. Novel hybrid devices are needed to add functionality to optical systems and to help in achieving the goal of all-optical signal processing. Key missing components are optical switching and logic devices. Hybrid devices offer the opportunity to build these missing elements cheaply and in a relatively short time. This motivated us to develop a novel hybrid device called the MCL diode.

1.2.1 Multi-cavity laser

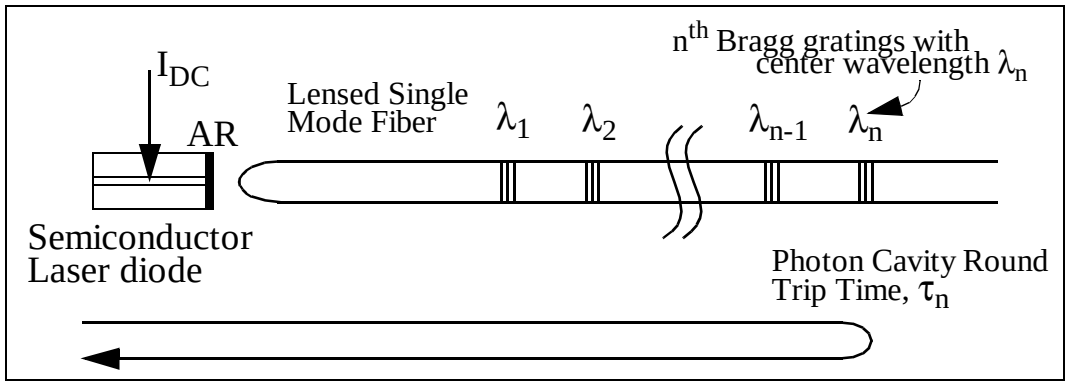

Fig. 1.1 Shows a schematic diagram of the multi-cavity laser diode.
One facet of the semiconductor laser diode is AR coated. The light output from this facet is coupled into a lensed SM fiber. The SM fiber has a series of BG along its length with center wavelengths λ_1, λ_2, ..., λ_{n-1} , and λ_n. Each of the BG mirrors may be regarded as one mirror of an external cavity laser with the uncoated facet of the semiconductor laser as the other facet. All the BG defined laser cavities share the same gain medium and have different photon cavity round trip times. The photon cavity round trip time of the n^{th} cavity is τ_n.

An external cavity semiconductor laser is built by coupling light emitted from the anti-reflection (AR) coated facet of a semiconductor laser to a SMF in which is embedded a BG. The device lases at the center wavelength of the FBG. The fiber BG

efficiently transmits light at non BG wavelengths. Hence, BGs with distinct center wavelengths placed one after another along the SMF provide many distinct wavelength selective mirrors. A multi-cavity laser, as shown in Fig. 1.1, is made by coupling light from the AR coated facet of the semiconductor laser to a SMF in which is embedded a series of BGs with distinct center wavelengths. The BGs form one of the mirrors of the multi-cavity laser cavity. The uncoated facet of the semiconductor laser diode forms the second mirror common to all the cavities of the multi-cavity laser. Each of the laser cavities lase at a distinct BG defined wavelength. There are a number of methods by which the lasing cavity can be selected to allow switching of the lasing light output to precisely defined wavelengths. We study three such methods in particular. They are as follows :

1) The wavelength of light output of an AR coated two section semiconductor laser placed in a BG defined multi-cavity is switched by changing the electrical bias on one of the sections. Wavelength switching is due to coupled cavity effects. This method is discussed in chapter two.

2) Light injected into the multi-cavity from the non-coated facet of the AR coated semiconductor laser is used to switch the lasing cavity. Tuning the wavelength of the light input to a BG grating defined wavelength selects that BG grating defined cavity as the lasing cavity. This method is discussed in chapter three.

3) A laser has a resonance at the photon cavity round trip time. Each of the BG defined cavities in the MCL has a distinct photon cavity round trip time due to their different cavity lengths. A cavity of the MCL is selected as the lasing cavity by modulating the DC biased laser with an RF signal tuned to the photon cavity round trip time of that cavity. The laser light output is in the form of pulses. This method is discussed in chapter four.

1.2.2 Characteristics of the MCL studied in this thesis

The MCL is a device with a number of interacting optical cavities. The MCL has optical cavities, between the cleaved semiconductor facet of the AR coated semiconductor laser and the FBGs, which can lase at BG defined optical wavelengths. The semiconductor laser cavity of the MCL between the AR coated semiconductor facet and the cleaved semiconductor facet interacts with all the FBG defined cavities. In MCL besides the interference effects of the composite cavity, the reflection spectrum of the BG also plays a crucial role in determining the lasing characteristics of the device. In this thesis we take a close look at factors which determine the static characteristics of MCL.

As described earlier, three methods used to switch the lasing cavity of the MCL are studied. The MCL can be easily scaled. Hence a careful study of the device switching dynamics using the three methods is performed, to improve the understanding of the factors limiting the cavity switching speed and underlying device physics, as a part of this thesis. The increased understanding of the MCL can be used to assist in the design of novel functional opto-electronic devices. Ultimately, these ideas could be incorporated in monolithic devices which are scaled to very small (mesoscopic) dimensions.

1.3 Switching dynamics

Over the last decade there have been a number of experimental studies on pulse buildup of actively and passively mode-locked lasers. The optical pulses in passive mode-locking reach their final pulse shape and spectrum after about 170 round-trips [1.28] in monolithic devices, while it takes the pulses approximately 500 round-trips in external cavity devices [1.29]. In active mode-locking, 300-400 round-trips are found to be necessary for the optical pulses to reach steady state conditions [1.30]. Pulses in self-seeded Fabry-Perot lasers take 5-10 round trips to build up [1.31]. As part of our work to study dynamics of multi-cavity lasers, we have measured the pulse

build-up when selecting the lasing cavity using an RF signal as described in method 3 above. We then compare the experimental results with numerical results obtained by simulations.

The need for fast wavelength switching in wavelength division multiplexing (WDM) systems [1.32] have stimulated a number of experimental studies of the dynamics of wavelength switching in monolithic semiconductor lasers in the 90's. Distributed feedback laser (DFB) lasers exhibit a continuous but narrow tuning range. Wavelength switching of 0.56 nm in 400 ps for a two section DFB laser [1.33] and 0.16 nm in 100 ps for a three section DFB laser [1.34] have been reported. The steady state tuning curve of a broadband tunable laser, such as the distributed Bragg reflector (DBR) laser, exhibit discontinuities as a function of tuning current. These discontinuities occur each time the dominant lasing mode switches between longitudinal cavity modes. Intramodal wavelength switching (same longitudinal cavity mode) of 1.25 nm in 1.8 ns [1.35] and 2.22 nm in 15 ns [1.51] have been measured. Intermodal switching (between two different longitudinal modes) of 0.5 nm in 0.5 ns [1.36] and 7.4 nm in 8 ns [1.37] have been demonstrated. Recently, fast wavelength switching in 56 ps between modes 3 nm apart of a DFB laser using voltage-controlled tuning via the Franz-Keldysh and quantum confined Stark effects, has been reported [1.38].

Despite the number of experimental studies of wavelength switching speeds reported in the 90's there is no clear understanding as to why wavelength switching times in monolithic devices range from tens of picoseconds to 10 ns. A systematic study of wavelength switching speed is hampered by the fact that factors influencing switching speed in these devices such as the spontaneous emission coupling factor (β), the single pass net gain (gain - loss) of the lasing modes involved in the switching, and the absolute value of gain at the two modes are difficult to measure. It has been shown [1.39] [1.40] that the temporal development of both lasing light intensity as well as the spectral content are fundamentally influenced by the average number of round-

trips made by the photons inside an optical resonator. This important and basic effect has not been explored in depth. The coupling of the photon and the carrier dynamics complicates matters even further.

In contrast to previous work, our experimental arrangement is suited to studying the physics underlying the transient dynamics when switching the lasing cavity. The carrier dynamics can be decoupled from the photon dynamics by increasing the cavity length allowing a controlled study of switching dynamics. Decreasing the cavity length permits a study of the influence of carrier-photon interaction in cavity/wavelength switching. The transient dynamics when switching the lasing wavelength are studied as a part of this thesis.

1.4 Fiber Bragg Gratings

As FBG is an essential component of the MCL, it is pertinent to briefly describe their characteristics. This section discusses the reflection characteristics as well as temperature characteristics of the FBG.

1.4.1 Reflection characteristics

A FBG is a periodic index perturbation in the core of a SMF. Successive reflections from each period in the index perturbation at optical wavelength, $\lambda_B = 2\varepsilon_{eff}\Lambda$ (where ε_{eff} is the modal index and Λ is the grating period) interferes constructively giving a maxima in the grating reflectivity as seen in Fig. 1.2. Any change in the fiber properties caused by factors such as strain, temperature or polarization which varies the modal index or grating pitch will change λ_B. This property of FBGs is exploited in FBG sensors.

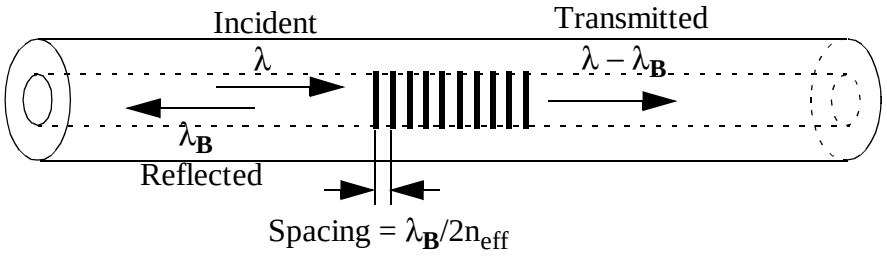

Fig. 1.2 Schematic diagram of a FBG. Reflection of the incident light occurs at wavelength at which the grating pitch along the fiber axis is equal to one-half of the modal wavelength within the fiber core.

The basic parameters which determine the reflection characteristics of FBGs are the magnitude of the induced refractive-index change, $\Delta\varepsilon_{eff}$ in the fiber core and the length of the grating, L_{BG}. Coupled mode theory is widely used to characterize FBGs. Fig. 1.3 taken from Ref. [1.41] summarizes the characteristics for a FBG at λ_B = 514.5 nm as a function of $\Delta\varepsilon_{eff}$, and L_{BG}. From Fig. 1.3 (a) and (c) it is clear that the length of the FBG needed for a fixed reflectivity at λ_B increases with decrease in $\Delta\varepsilon_{eff}$. Fig. 1.3 (b) shows that the grating bandwidth, $\Delta\lambda_{BG}$, decreases with a decrease in $\Delta\varepsilon_{eff}$.

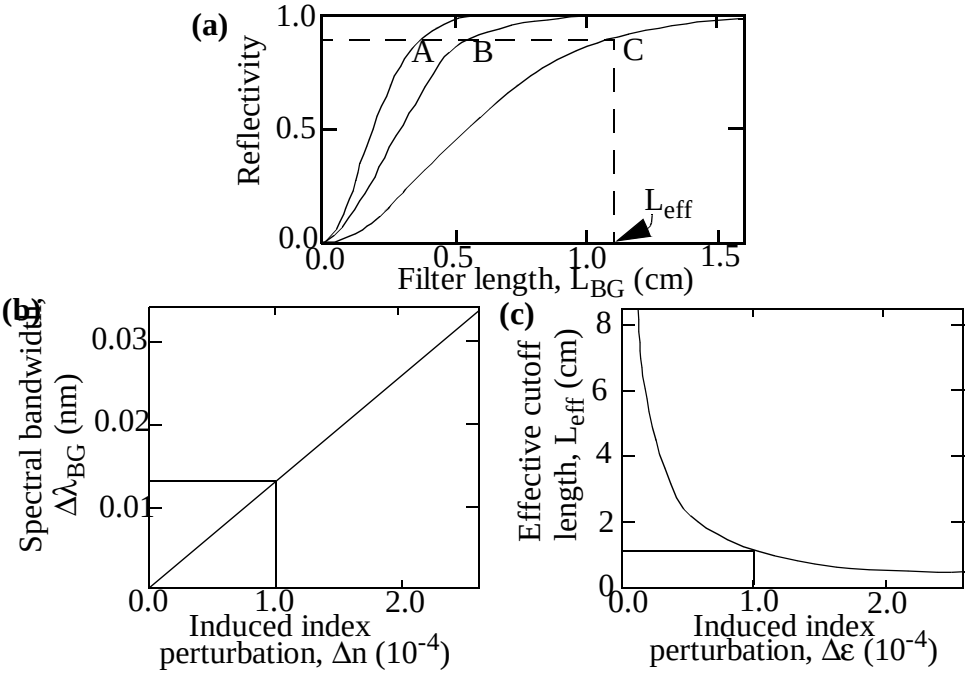

Fig. 1.3 BG reflectivity as a function of induced index perturbation, $\Delta\varepsilon$ and grating length, L_{BG}. **(a)**Theoretical reflectance as a function of filter length at Bragg wavelength, λ_B = 514.5 nm , for different values of induced index perturbation, $\Delta\varepsilon$. Curves A, B, and C correspond to $\Delta\varepsilon$ of $3.0x10^{-4}$, $2x10^{-4}$ and $1.0x10^{-4}$ respectively, and have effective cutoff lengths, L_{eff} , of 0.376, 0.565 and 1.129 respectively. **(b)** Theoretical effective cutoff length of the optical filters as a function of the induced index perturbation. **(c)** Theoretical spectral bandwidth of the optical fiber filters as a function of the induced index perturbation (Taken from Ref. [1.41]).

1.4.2 Temperature characteristics

In contrast to previous work (for example Refs. [1.42] to [1.48]) wavelength selection in the multi-cavity laser is digital in nature as narrow FBG (less than 0.2 nm in our experiments) decide the possible lasing wavelengths. Temperature dependence of emission wavelength under steady-state conditions is better than that of DFB lasers. In monolithic devices changes in current through the device when tuning cause the operating temperature of the device to vary. Typical DFB laser lasing at 1.55 μm has a wavelength tuning of 0.1nm/°C at 20 °C [1.49] and a current tuning of 0.007 nm/ mA at 20 °C [1.50]. Changes in device current when switching between widely spaced wavelengths in DBR lasers cause the device temperature to drift. Thermal effects have been observed to produce wavelengths drifts if the switched wavelength

residency time is greater than about 1 μs [1.51]. This sets an upper bound on the packet lengths that can be transmitted using these lasers. The use of FBGs to define the operating wavelengths make the multi-cavity laser intrinsically temperature insensitive as no current is passed through the FBG . Besides, at 1300 nm for a typical FBG the wavelength changes with temperature at the rate of 0.01 nm/^{o}C [1.52], an order of magnitude less than that for the DFB lasers. It is possible to incorporate a temperature compensating fiber fixture which reduces the temperature sensitivity to 0.001 nm/°C [1.53].

1.5 Grating-stabilized laser diodes

The MCL is an example of a FBG stabilized semiconductor laser. The interactions of laser diodes with FBGs have been studied for many years. In this section a brief survey of work done on FBG stabilized semiconductor lasers is presented. The three main types of FBG stabilized laser diodes reported to date are : 1) Single-mode lasers with optical feedback provided by FBG in close proximity to the output facet of the diode. 2) Mode-locked lasers in which the diode is modulated by a signal whose frequency is a multiple of the characteristic external cavity frequency. 3) Coherence-collapsed lasers where the FBG providing feedback to the laser is beyond the coherence length of the lasing modes.

1.5.1 Single-mode operation

FBGs are used as wavelength references to lock WDM transmitters as FBGs can be reliably manufactured with wavelength tolerance of less than 0.1 nm. The wavelength stability of FBGs can be ensured by packaging that provides temperature compensaton. The wavelength error between a DFB or DBR laser and the FBG reference is used to generate a signal which is fed to the temperature controller of the laser [1.53][1.54].

The light output from an AR coated facet of a laser coupled to a lensed SMF contain-

ing narrow FBG (0.1-0.3 nm) close to the fiber tip is a light source whose wavelength is stable to changes in temperature. Wavelength tuning as low as 0.007 nm/^{o}C have been reported using such a laser [1.55]. The device is very sensitive to the residual facet reflectivity from the AR coated facet. Weak residual facet reflectivity of (~10^{-3}) can result in kinks in the output optical power due to mode hopping. Use of a curved waveguide reduces the reflectivity to less than 10^{-4} [1.56]. Grating stabilized lasers with low linewidth (100-250 kHz), RIN below -135 dB/Hz in the range from 20 MHz to 10 GHz have been used for digital data transmission at 2.48 Gb/s [1.57].

In a novel experiment the section of regular SMF between the FBG and the AR coated facet of the laser is replaced by a length of unpumped erbium-doped fiber [1.58]. At high lasing powers, the erbium absorption saturates at the maxima of the standing wave pattern set up in the fiber. This minimizes the loss experienced by the lasing mode in comparison to other modes which have different spatial intensity profiles along the fiber. Sub-kilohertz bandwidth stable single-mode operation of this device has been reported.

1.5.2 Mode-locked operation

Actively mode locked pulses are obtained from an AR coated semiconductor laser with optical feedback from FBGs when modulated at a frequency corresponding to the cavity round-trip frequency. When a chirped FBG provides feedback to the AR coated laser the optical wavelength as well as the period of the mode locked pulses is tuned by varying the modulating frequency. The device adjusts its output wavelength to ensure that the cavity length corresponds to the modulating frequency [1.59]. This is similar to the method we use to select the lasing cavity of the MCL by modulating the semiconductor gain section with an RF signal.

Self seeding a gain switched non AR coated semiconductor with 0.2 % to 6 % optical feedback from a FBG is a method used to generate wavelength tunable pulses. The

laser is gain switched at a harmonic of the cavity round trip frequency. Wavelength selective light is fed back from the FBG to the laser gain medium biased below threshold when it is driven by the modulating signal above threshold. The optical field in the laser is still dominated by the spontaneous emission and a small amount of additional wavelength selective optical feedback is sufficient to control the light output. Optical MSRs as high as -30 dB have been reported using self seeded laser diodes [1.31].

1.5.3 Coherence-collapse operation

One of the modes of operation of a semiconductor laser with external feedback is known as "coherence collapse" [1.60]. Coherence collapse regime is observed when sufficiently strong feedback (a few percent) is provided to a semiconductor laser from a FBG placed beyond the coherence length of the laser diode. Although the laser operates at the FBG wavelength the optical spectrum of the light output is broadened and the laser operates in a multitude of external cavity modes. While the high frequency noise of the laser is greatly increased, the large number of modes and their lack of coherence averages out the low frequency noise.

Grating stabilized 980 nm semiconductor lasers operating in the coherence collapse are widely used as pump lasers in commercial EDFA's as the high frequency noise does not adversely affect the slow responding erbium ions [1.61], [1.62]. These pump lasers are not affected by optical feedback of upto -20 dB as compared to the conventional pump laser which becomes unstable at -40 dB optical feedback levels [1.62].

1.6 Brief survey of methods of wavelength tuning

Tunable semiconductor lasers are essential components in applications such as wavelength division multiplexing systems (WDM) [1.32], packet switching [1.63] and optically controlled phase array antennas [1.64]. There is ongoing research to increase the tuning range of semiconductor lasers using fast electronic effects as opposed to

slow thermal ones while retaining ease of tuning controls. It is pertinent to make a short survey of the methods used to perform wavelength tuning of semiconductor laser light output as the multi-cavity laser is capable of wavelength selection of the light output.

External cavity lasers were first used to tune the wavelength of the light output from a semiconductor laser. The light from the AR coated facet of a semiconductor laser is collected using a bulk optical lens. A conventional planar grating placed behind the lens is used to provide wavelength selective feedback to the laser. A tuning range of 200 nm [1.65] has been achieved using a multiple quantum-well laser in the external cavity described above. The wavelength in these external cavity systems is mechanically tuned by rotating the grating.

Monolithic semiconductor laser devices with inbuilt semiconductor BGs have been fabricated for wavelength selection. Until the early 1990's semiconductor grating based structures used for fast wavelength tuning had a fractional bandwidth, $\Delta\lambda/\lambda$, less than or equal to the maximum achievable refractive index change, $\Delta\mu/\mu_g$, in the grating section. This limits the tuning range to about 10 nm [1.42] at 1.55 μm. Over the last few years, several groups have developed schemes where $\Delta\mu/\mu_g$ does not limit the wavelength tuning range.

Fig. 1.4 shows the Y-cavity laser [1.43], [1.44] which uses Mach-Zehnder interferometry to extend the tuning range of the laser. The Y-laser can be regarded as two Fabry Perot lasers that share a common gain section. Due to interference of the FP modes the emission spectra of the Y-laser is single-mode. The device has exhibited a tuning range of 51 nm [1.44]. It is relatively easy to fabricate as it has no gratings but suffers from low mode suppression ratio (MSR) on the order of -20 dB.

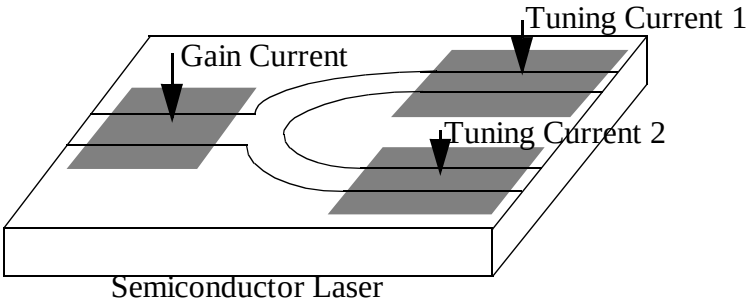

Fig. 1.4 Schematic diagram of a coupled Y-cavity laser.

The second device relies on a grating assisted codirectional coupler (GACC) filter as illustrated in Fig. 1.5. The tuning range in this device depends on $\Delta\mu/(\mu_{1g} - \mu_{2g})$. Reducing $(\mu_{1g} - \mu_{2g})$ would increase the filter bandwidth but would compromise the MSR. With careful design, a tuning range of 57 nm [1.45] has been demonstrated. Increasing the tuning range while maintaining a good MSR is difficult using the GACC.

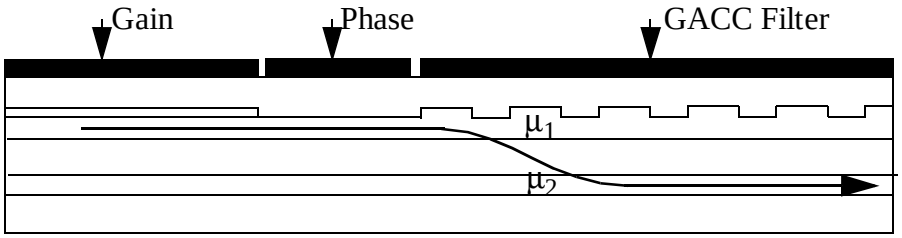

Fig. 1.5 Schematic of the Grating-assisted co-directional coupler.

Another scheme using two "sampled gratings" at the ends of the gain and phase shifter section to achieve wavelength tuning [1.46] is shown in Fig. 1.6. The reflection spectra of the two sampled gratings have periodic maxima that are slightly mismatched. Lasing occurs at that pair of maxima that are aligned with the bias point of the phase shifter adjusted to place this mode at a cavity resonance. Continuous complete wavelength coverage of 40 nm [1.47] and up to 100 nm of tuning with partial coverage [1.48] has been demonstrated using superstructure gratings which uses the same basic idea as the sampled gratings.

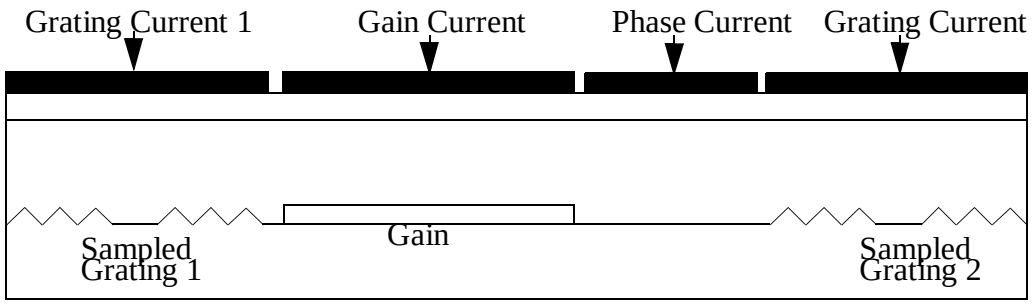

Fig. 1.6 Schematic diagram of Sampled Grating DBR laser.

1.7 Rest of the thesis

Chapter two of this thesis discusses cavity switching using coupled cavity effects. The role of the BG bandwidth on the light versus current (L-I) characteristic of the MCL is also discussed. The transient dynamics of the MCL when switching between are discussed in chapter three. Results presented in chapter three indicate that the MCL can be used as a SR flip-flop. Results of cavity switching done by injecting light into the laser gain section are also discussed in chapter three. Chapter four presents experimental results of wavelength switching by applying an RF signal to the laser gain section. The cavity switching transients when an RF signal is used to select the lasing cavity are discussed in this chapter. A brief conclusion to this thesis is presented in chapter five along with some suggestions for future work.

1.8 References

1.1 A. L. Schawlow, and C H. Townes, “Infrared and optical masers,” Phys. Rev., **112**, pp. 1940-1949 (1958).

1.2 T. H. Maiman, “Stimulated optical radiation in ruby,” Nature, **187**, pp. 493-494 (1960).

1.3 A. Javan, W. R. Bennett Jr. and D. R. Herriot, “Population inversion and continuous optical maser oscillation in a gas discharge containing a He-Ne mixture,” Phys. Rev. Lett., **6**, pp. 106-110 (1961).

1.4 M. G. A. Bernard and G. Duraffourg, "Laser condition in semiconductors," Phys. Status Solidi, **1**, pp. 699-703 (1961).

1.5 H. Kroemer, "A proposed class of hetero-junction injection lasers," Proc. IEEE, **51**, pp. 1782-1783 (1963).

1.6 I. Zh. Alferov, and R. F. Kazarinov, autor certificate 181737 (U.S.S.R), 1963.

1.7 I. Hayashi, M. B. Panish, P. W. Foy and S. Sumski, "Junction lasers which operate continuously at room temperature," Appl. Phys. Lett., **17**, pp. 109-111 (1970).

1.8 R. L. Williams, M. Dion, F. Chatenound, and K. Dzurko, "Extremely low threshold current strained InGaAs/GaAs lasers by molecular beam epitaxy," Appl. Phys. Lett., **58**, pp. 1816-1818 (1991).

1.9 G. P. Agrawal and N. K. Dutta, "Long-wavelength semiconductor lasers," New York : Van Nostrand Reinhold, 6, 1993.

1.10 A. G. Bell, "Apparatus for signalling and communicating, called Photophone," U. S. patent 235 199, filed Aug. 20, 1880, issued Dec. 7, 1880; see also Nature, **23**, pp. 15-19, 1880.

1.11 K. C. Kao and G. A. Hockham, "Dielectric-fiber surface waveguides for optical frequencies," Proc. IEE, **113**, pp. 1151-1158, 1966.

1.12 F. P. Kapron, D. B. Keck, and R. D. Maurer, "Radiation losses in glass optical waveguides," Appl. Phys. Lett., **17**, pp. 423-425 (1970).

1.13 M. G. Blankenship, and C. W. Deneka, "The outside vapor deposition method of fabricating optical waveguide fibers," IEEE J. Quantum Electron., **18**, pp. 459-476 (1982).

1.14 Hewlett Packard, "Fiber optic handbook," Hewlett-Packard GmbH, Boeblingen Instruments Division, Federal Republic of Germany, pp. 25-29, 1989.

1.15 D. Marcuse and C. Lin, "Low dispersion single-mode fiber transmission - The question of practical versus theoretical maximum transmission bandwidth," IEEE J. Quantum. Electron., **17**, pp. 869-877 (1981).

1.16 H. C. Lefevre, "Fundamentals of the interferometric fiberoptic gyroscope," Optical Review, **4**, pp. 20-27 (1997).

1.17 S. M. Klainer, J. R. Thomas, and J. C. Francis, “Fiberoptic chemical sensors offer a realistic solution to environmental monitoring needs,” Sensors and Actuators B-Chemical, **11**, pp. 81-86 (1993).

1.18 X. Fang, R. G. May, A. Wang, R. O. Claus, “ A fiberoptic high temperature sensor,” Sensors and Actuators A-Physical, **44**, pp. 19-24 (1994).

1.19 A. D. Fienerman and S. R. Thodati, “Millimeter-scale actuator with fiberoptic roller-bearings,” J. Microelectromechanical Systems, **4**, pp. 28-33 (1995).

1.20 K. O. Hill, Y. Fujii, D. C. Johnson, and B. S. Kawasaki, “Photosensitivity in optical fiber waveguides : Application to reflection filter fabrication,” Appl. Phys. Lett., **32**, pp. 647-649 (1978).

1.21 Innovative Fibers, Inc., 45 DeVillebois, Suite 200, Gatineau, Canada J8T 8J7, Phone 819-273-3755 and FAX 819-243-3354.

1.22 K. Uppal, D. Tishinin, I. Kim and P. D. Dapkus, “Study of 1.3 mm tapered wave-guide spot size transformers,” IEEE J. Selected Topics in Quantum Electron., **3**, pp. 975-979 (1997).

1.23 Photonic Packaging Technology, 9795 Southwest Gimini Drive, Beaverton, Oregon 97008, Phone 503-641-4219, and FAX 503-643-1703.

1.24 C. Edwards, H. M. Presby, and C. Dragone, “Ideal microlenses for laser to fiber coupling,” J. Lightwave Technol., **11**, pp. 252-257 (1993).

1.25 A. Tanabi, M. Soda, Y. Nakahara, A. Furukawa, T. Tamura, K. Yoshida, “ A single chip 2.4 Gb/s CMOS optical receiver IC with low substrate crosstalk preamplifer,” session **SA 19**, talk 19.2 at IEEE International solid-state circuits conference at San Francisco, Feb. 1998.

1.26 B. Sano, B. Madhavan and A. F. J. Levi, “8 Gbit/s CMOS interface for parallel fiber-optic interconnects,” Electron. Lett., **32**, pp. 2262-2263 (1996).

1.27 R. M. Burger, J. A. Glaze, T. Seidel, O. Williams, “The SIAs Roadmap - Consensus for coorleration,” Solid State Technology, **38**, pp. 38-40 (1995).

1.28 O. Solgaard, M. H. Kiang, and K. Y. Lau, “Pulse buildup in passively mode-locked monolithic quantum-well semiconductor-lasers,” Appl. Phy. Lett., **63**, pp. 2021-20231 (1993).

1.29 N. Stelmakh, D. Pascal, and J. M. Lourtinez, Conf. Dig. 13th IEEE Laser Conf., Takamatsu, Sept. 1992, paper N-2.

1.30 P. Blixt, and A. Krotkus, "Simulations and experiments of mode-locking of semiconductor lasers : pulse evolution, frequency detuning, and bias dependence," Opt. Quantum Electron., 22, pp. 561-570 (1990).

1.31 M. Schell, D. Huhse, W. Utz, J. Kaessner, and D. Bimberg, "Jitter and dynamics of self-seeded Fabry-Perot laser-diodes," IEEE J. Selected Topics Quantum Electron., **1**, pp. 528-534 (1995).

1.32 C. A. Brackett, "Dense wavelength division multiplexing networks : Principles and applications," IEEE J. Select. Areas Commun., **8**, pp. 948-964 (1990).

1.33 R. S. Vodhanel, M. Okai, and S. Sasaki, Conf. Optical Fiber Commun., San Diego, CA, paper PD19 CA, Feb., pp. 18-22, 1991.

1.34 S. Kuwano, Y. Tada, and N. Shibata, "100 ps frequency switching without bit loss for a 10 Gb/s ASK modulated signal," IEEE Photon. Technol. Lett., **5**, pp. 354-356 (1993).

1.35 N. Shimosaka, M. Fujiwara, S. Murata, N. Hemni, K. Emura, and S. Suzuki, "Photonic wavelength-division and time-division hybrid switching system utilizing coherent optical detection," IEEE Photon. Technol. Lett., **2**, pp. 301-303 (1990).

1.36 F. Delorme, P. Gambini, M. Puleo, and S. Slempkes, "Fast tunable 1.5 μm distributed Bragg reflector laser for optical switching applications," Electron. Lett., **29**, pp. 41-43 (1993).

1.37 B. Glance, U. Koren, R. W. Wilson, D. Chen, and A. Jourdan, "Fast optical packet switching based on WDM," IEEE Photon. Technol. Lett., **4**, pp. 1186-1188 (1992).

1.38 L. E. Adams, G. Nykolak, C. G. Bethea, T. Tunbun-ek, R. People, A. M. Sergent, P. F. Sciortino, Jr., and T. Fullowan, "System performance of high-speed broadband-tunable laser for wavelength conversion in WDM networks," in Proc. Conf. Optical Fiber Comm. (OFC'97), Dallas, Texas 1997, pp. 412-415, PD11-1.

1.39 J. O'Gorman, A. F. J. Levi, D. Coblentz, T. Tanbun-Ek, and R. A. Logan, "Cavity formation in semiconductor-lasers," Appl. Phys. Lett., **61**, pp. 889-891

(1992).

1.40 N. A. Olsson, and W. T. Tsang, "Transient effects in external cavity semiconductor lasers," J. Quantum Electron., **19**, pp. 1479-1481 (1983).

1.41 D. K. W. Lam and B. K. Garside, "Characterization of single-mode optical fiber filters," Applied Optics, **20**, pp. 440-445 (1981).

1.42 T. Koch, U. Koren, R. Gnall, C. Burrus, and B. Miller, "Continuously tunable 1.5 mm multi-quantum-well GaInAs/GaInAsP Distributed-Bragg-Reflector lasers," Electron. Lett., **24**, pp. 1431-1433 (1988).

1.43 O. Hildebrand, M. Schilling, W. Idler, D. Baums, W. Idler, K. Dutting, G. Laube, and K. Wunstel, "The Y-laser - a multifunctional device for optical communication-systems and switching-networks," J. Lightwave Technol., **11**, pp. 2066-2075 (1993).

1.44 M. Kuznetsov, P. Verlangieri, A. D. Dentai, C. H. Joyner, and C. A. Burrus, "Asymmetric Y-branch tunable semiconductor-laser with 1.0 THz tuning range," IEEE Photon. Technol. Lett., **4**, pp. 1093-1095 (1992).

1.45 R. C. Alferness, U. Koren, L. L. Buhl, B. I. Miller, M. G. Young, T. L. Koch, G. Raybon, and C. A. Burrus, "Broadly tunable InGaAsP/InP laser based on a vertical coupler filter with 57 nm tuning range," Appl. Phys. Lett., **60**, pp. 3209-3211 (1992).

1.46 V. Jayaraman, Z. Chuang, and L. A. Coldren, "Theory, design and performance of extended tuning range semiconductor-lasers with sampled gratings," IEEE J. Quantum Electron., **29**, pp. 1824-1834 (1993).

1.47 M. Oberg, P. Rigole, S. Nilsson, T. Klinga, L. Backbom, K. Streubel, J. Wallin, and T. Kjellberg, "Complete single-mode wavelength coverage over 40 nm with a super structure grating DBR laser," J. Lightwave Technol., **13**, pp. 1892-1898 (1995).

1.48 Y. Tohmori, Y. Yoshikuni, H. Ishii, F. Kano, T. Tamamura, Y. Kondo, and M.Yamamoto, "Broad-range wavelength-tunable superstructure grating (SSG) DBR lasers," IEEE J. Quantum Electron., **29**, pp. 1817-1823 (1993).

1.49 M. Kitamura, M. Yamaguchi, S. Murata, I. Mito, and K. Kobayashi, "Low threshold and high temperature single-longitudinal mode operation of 1.55 mm-band DFB-DC-PBH LDs," Electron. Lett., **20**, pp. 595-596.

1.50 J. O'Gorman, private communication.

1.51 H. Kobrinski, M. P. Vecchi, M. S. Goodman, E. L. Goldstein, T. E. Chapuran, J. M. Cooper, M. Tur, C. E. Zah, and S. G. Menocal, "Fast wavelength-switching of laser transmitters and amplifiers," IEEE J. Select. Areas Commun., **8**, pp. 1190-1201 (1990).

1.52 J. R. Dunphy, G. Meltz, and W. W. Morey, Fiber Optic Smart Structures, edited by E.Udd, John Wiley & Sons, Inc., 1995.

1.53 G. W. Yoffe, P. A. Kurg, F. Ouellete and D. A. Thorncraft, "Passive temperature-Compensating package for optical fiber gratings, "Appl. Opt., **34**, pp. 628-630 (1993).

1.54 S. L. Woodward, V. Mizrahi, T. L. Koch, U. Koren and p. J. Lemaire, "Wavelength stabilization of DBR laser using an in-fiber Bragg filter," IEEE Photon. Tech. Lett., **5**, pp. 628-630, 1993.

1.55 F. N. Timofeev, P. Bayvel, L. Reenkie, J. Tucknott, J. E. Midwinter and D N. Payne, "Spectral characteristics of a reduced cavity single-mode semiconductor fiber grating laser for application is dense WDM systems," in Proc. 21st European Conf. Optic. Commun. (ECOC' 95), Brussels, Belgium, 1995, paper Tu.P.26, pp. 477-480.

1.56 R. J. Campbell, J. R. Armitage, G. Sherlock, D. L. Williams, R. Payne, M. Robertson, and R. Wyatt, "Wavelength stable uncooled fiber grating semiconductor laser for use in all optical WDM acesses network," Electron. Lett., **32**, pp. 119-120 (1996).

1.57 M. Ziari, J. M. Verdiell, J. L. Archambault, A. Mathur, H. Jeon, R. C. Yu, and T. L. Koch, "High speed fiber grating coupled semiconductor WDM laser," in Proc. Conf. Lasers Electro-Opt. (CLEO'97), Baltimore, MD 1997, paper CMG1.

1.58 W. H. Loh, R. I. Laming, M. N. Zervas, M. C. Farries, and U. Koren, "Single frequency erbium fiber external cavity semiconductor laser," Appl. Phys. Lett., **66**, pp. 3422-3424, 1995.

1.59 P. A. Morton, V. Mizrahi, S. G Kosinski, L. F. Mollenauer and T. Tanbunek, "Hybrid soliton pulse source with fiber external cavity and Bragg reflector," Electron. Lett., **28**, pp. 561-562 (1992).

1.60 R. W. Tkach and A. R. Chraplyvy, "Regimes of feedback effects in 1.5 mm distributed feedback laser," J. Lightwave Technol., 4, pp. 1655-1611, (1986).

1.61 C. R. Giles, T. Erdogan, and V. Mizrahi, "Simultaneous wavelength stabilization of 980 nm pump lasers," IEEE Photon. Technol. Lett., **6**, pp. 907-909, 1994.

1.62 B. F. Ventrudo, G. A Rogers, G. S. Lick. D. Hargreaves and T. M. Demayo, "Wavelength and temperature stabilization of 980 nm diode lasers coupled to fiber Bragg gratings," Electron. Lett., **30**, pp. 2147-2148 (1994).

1.63 P. E. Green, Fiber Optic Networks, Prentice Hall, Englewood Cliffs, NJ 1993.

1.64 Y. Chang, B. Tsap, H. R. Fetterman, D. A. Cohen, A. F. J. Levi, and I. Newberg, "Optically controlled serially fed phased-array transmitter," IEEE Microwave Guided Wave Lett., **7**), pp. 69-71 (1997).

1.65 A. Lidgard, T. Tanbun-Ek, R. A. Logan, H.T emkin, K. W. Wecht, and N. A. Olsson, "External-cavity InGaAs/InP graded index multiquantum well laser with a 200 nm tuning range," Appl. Phys. Lett., **56**, pp. 816-217 (1990).

1.66 E. Desurvire, "Study of the complex atomic susceptibility of Erbium-doped fiber amplifiers," J. Lightwave Technol., **8**, pp. 1517-1527 (1990).

Chapter 2 : Cavity switching using coupled cavity effects

2.1 Introduction

The idea of using coupled cavity effects to select the longitudinal mode of gas lasers was demonstrated as early as 1962 [2.1]. Early coupled cavity work using semiconductor lasers involved placing the laser in an external cavity [2.2]. Semiconductor coupled cavity lasers were also used to study optical bistability [2.3], optical amplification [2.5] and mode selectivity. In the early 80s there was considerable interest in two-section coupled cavity semiconductor lasers as a stable narrow-band source [2.6]. Interference effects of the composite cavity are used to select the lasing mode. Coupled cavity effects ensure stable single longitudinal mode behavior under high-speed modulation conditions [2.7]. Wavelength tuning is possible by separately pumping the individual sections [2.8]. Due to progress in growth and fabrication techniques, distributed feedback lasers (DFB) and distributed Bragg reflector (DBR) lasers have replaced coupled cavity semiconductor lasers as the stable narrow-band semiconductor source.

The multi-cavity laser (MCL), consisting of an AR coated semiconductor laser in an external cavity with optical feedback from narrow BGs embedded in a singlemode fiber, is a coupled cavity laser. The optical cavity between the cleaved semiconductor facet of the AR coated semiconductor laser and the FBG is one cavity of the MCL. The semiconductor laser cavity between the AR coated semiconductor facet and the cleaved semiconductor facet forms the second cavity. In addition to the interference effects of the composite cavity, the reflection spectrum of the BG also plays a crucial role in determining the lasing characteristics of the device. In this chapter, we present experimental results of wavelength selection using coupled cavity effects. In section 2.2, we present experimental results of wavelength switching by changing coupling

loss. A simulation of the experiment is presented in section 2.3. Experimental results presented in section 2.4, indicate that coupled cavity effects can be used to select the lasing wavelength in a two-section semiconductor laser getting optical feedback from BGs embedded in a SMF. In section 2.5, we present results of wavelength switching using a two-section semiconductor laser with optical feedback from BGs embedded in a SMF. The effect of the BG bandwidth on the static characteristic of the MCL is presented in section 2.6. Section 2.7 is a brief conclusion.

2.2 Wavelength switching by changing coupling loss

2.2.1 Basic Idea

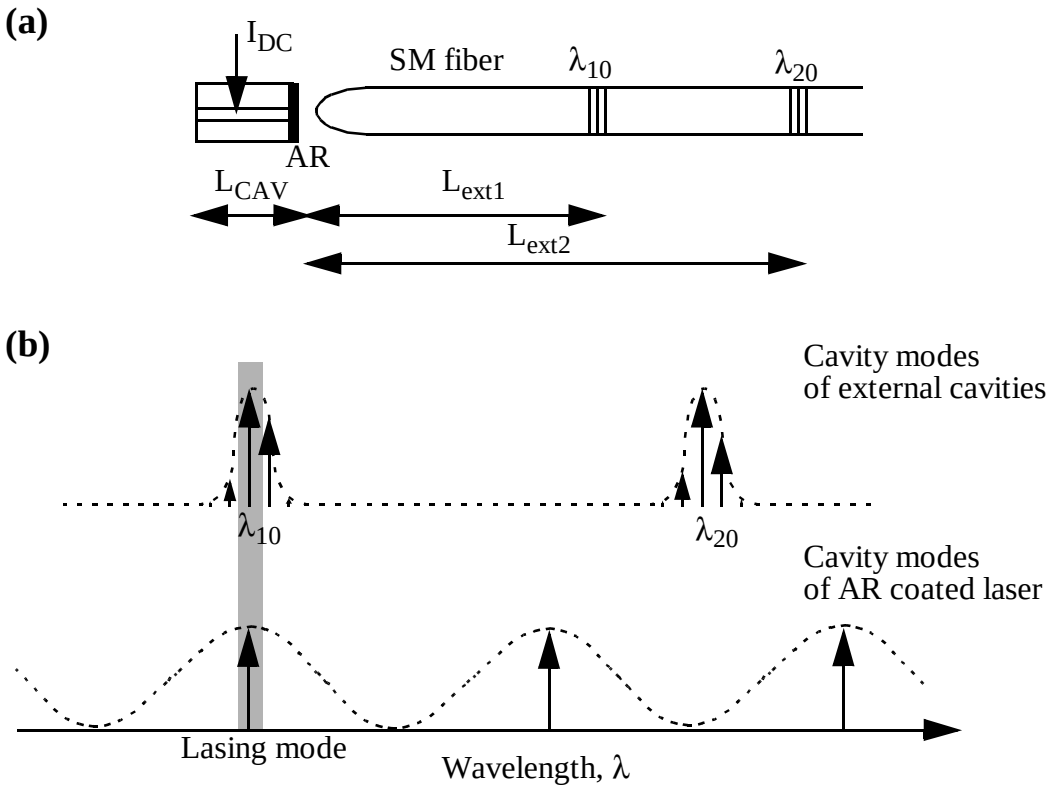

Fig. 2.1 A schematic illustration of the longitudinal mode selectivity of the multi-cavity laser.
(a) is a schematic diagram of the MCL. **(b)** shows the Fabry Perot modes of the laser cavities of the MCL. The number of external cavity FP modes are limited by the reflection spectra of the BGs centered about λ_{10} and λ_{20}. The FP modes of the AR coated semiconductor laser are spaced widely apart compared to the optical bandwidth of the BG. When the wavelength of a FP mode of the AR coated

semiconductor laser cavity is close to the center wavelength of the center wavelength of a BG the device lases at the nominal wavelength defined by that BG. The reflection spectrum of the BG ensures that the laser lases at a single longitudinal mode.

The mechanism of mode selectivity of the MCL is illustrated in Fig. 2.1. Fig. 2.1(a) is a schematic of the MCL consisting of an AR coated semiconductor laser in an external cavity with optical feedback from two BG centered at wavelengths λ_{10} and λ_{20} embedded in an SMF. Coupled cavity effects select an optical wavelength λ_1/λ_2 approximately equal to $\lambda_{10}/\lambda_{20}$ as the lasing wavelength. The cavity modes of the AR coated laser are spaced $\Delta\lambda_{CAV} = \lambda^2/2n_sL_{CAV}$ apart where L_{CAV} is the length of the semiconductor cavity, n_s is the refractive index of the semiconductor medium and λ is the wavelength of the light. The cavity mode spacing of the BG defined external cavity at wavelength λ is $\Delta\lambda_1 = \lambda^2/2(n_gL_{ext1} + n_sL_{CAV})$ and $\Delta\lambda_2 = \lambda^2/2(n_gL_{ext2} + n_sL_{CAV})$ where n_g is the refractive index of glass and L_{ext1} (L_{ext2}) is the effective external cavity length of the cavity formed by the BG centered at wavelength λ_{10} (λ_{20}).

The optical bandwidth of the BG, $\Delta\lambda_{BG}$, and the external cavity mode spacing of the two BG defined cavities, $\Delta\lambda_1$ and $\Delta\lambda_2$, are an order of magnitude smaller than $\Delta\lambda_{CAV}$. As $\Delta\lambda_{BG}$ is comparable to $\Delta\lambda_1$ and $\Delta\lambda_2$ the number of external cavity modes are limited by the reflection spectra of the BGs centered at λ_{10} and λ_{20}. When the wavelength of a FP mode of the AR coated semiconductor laser cavity is close to the center wavelength λ_{10} (λ_{20}) of the BG, the device lases at the nominal wavelength λ_1 (λ_2) approximately equal to λ_{10} (λ_{20}). The reflection spectrum of the BG ensures that a single longitudinal mode of the compound cavity is selected as the lasing wavelength.

Tuning the FP modes of the AR coated semiconductor laser cavity is a method to switch the wavelength of the lasing light emitted by the device between the nominal wavelengths λ_1 and λ_2 defined by the two BGs. Changing the coupling loss is one

method to tune the FP modes of the AR coated semiconductor laser. This method of wavelength tuning is discussed in the next section.

2.2.2 Experimental results and discussion

The inset to Fig. 2.2 shows our experimental arrangement. A 300 μm long multiple quantum well semiconductor laser diode [2.9] has a 0.1% anti-reflection (AR) coated facet on one side and a 32% reflecting mirror on the other. Optical emission at λ = 1300 nm wavelength from the AR coated side of the semiconductor diode is coupled with 40% efficiency into a lensed SMF. The laser experiences optical feedback from two 1 mm long BGs embedded in the SMF with center wavelengths λ_{10} = 1311.7 nm and λ_{20} = 1310.4 nm and a -3 dB optical bandwidth of 0.24 nm and 0.26 nm respectively. Although the reflectivity of the FBG has complex dependence on wavelength [2.10] it can be reasonably approximated by a gaussian. Each BG has 75% reflectivity. The BG at λ_{10} (λ_{20}) defines a distinct laser cavity with photon cavity round-trip time of 112 ps (138 ps).

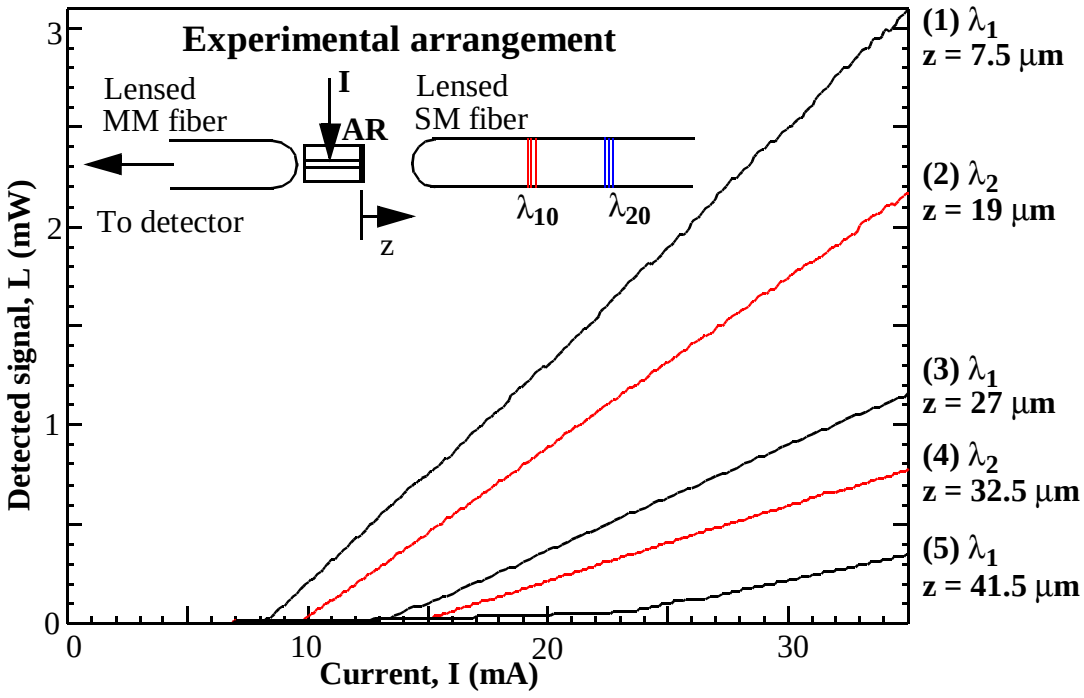

Fig. 2.2 Measured L-I characteristics as optical coupling efficiency between the semiconductor diode and the SMF is decreased by increasing z, the distance from the AR coated facet to the SMF.
The inset shows a schematic of the experimental arrangement. Two BGs embedded in a SMF have center wavelengths λ_1 = 1311.7 nm and λ_2 = 1310.4 nm and a -3 dB optical bandwidth of 0.24 nm and 0.26 nm respectively. The photon cavity round-trip time at λ_1 (λ_2) is 112 ps (138 ps).

When the lensed SMF is aligned to give maximum coupling efficiency, laser threshold current is I_{th} = 8 mA with emission at wavelength, λ_1 (approximately equal to λ_{10}). Increasing the axial distance, z, between the AR coated facet of the semiconductor diode and the SMF decreases optical coupling efficiency and increases threshold current. Fig. 2.2 shows light-current (L-I) characteristics for the indicated values of z. The device lases at optical wavelength λ_1 along the L-I curves labeled 1, 3 and 5 and lases at wavelength λ_2 (approximately equal to λ_{20}) along curves labeled 2 and 4. Longitudinal modes of the external cavity are spaced 9 GHz (7.24 GHz) apart at λ_1 (λ_2). Because the BGs have a -3 dB optical bandwidth of 42.72 GHz (46.28 GHz) at λ_1 (λ_2), a few longitudinal external cavity modes lie within the BG bandwidth at λ_1 (λ_2). The small discontinuities in the L-I characteristic seen in Fig. 2.2 likely occur due to mode hopping between longitudinal external cavity modes that lie within a given BG's optical bandwidth. Fig. 2.3 shows the optical spectrum of light output as z increases for I = 30 mA.

Residual reflectivity of the AR coated semiconductor facet gives rise to peaks in the optical spectrum away from the BG wavelength which correspond to cavity modes of the semiconductor cavity. The cavity mode spacing is $\Delta\lambda_{FP}$ = 0.77 nm. Decreasing optical coupling efficiency between the semiconductor diode and the SMF by pulling back the fiber from the AR coated facet of the laser causes an increase in threshold carrier density. This is due to an increase in optical gain needed to compensate for the increase in optical loss. An increase in carrier density in the semiconductor causes a decrease in the refractive index [2.11] and moves the FP peaks of the semiconductor cavity to shorter wavelengths. Fig. 2.3 shows that FP peaks in the spontaneous emis-

sion spectrum move to shorter wavelengths as z is increased.

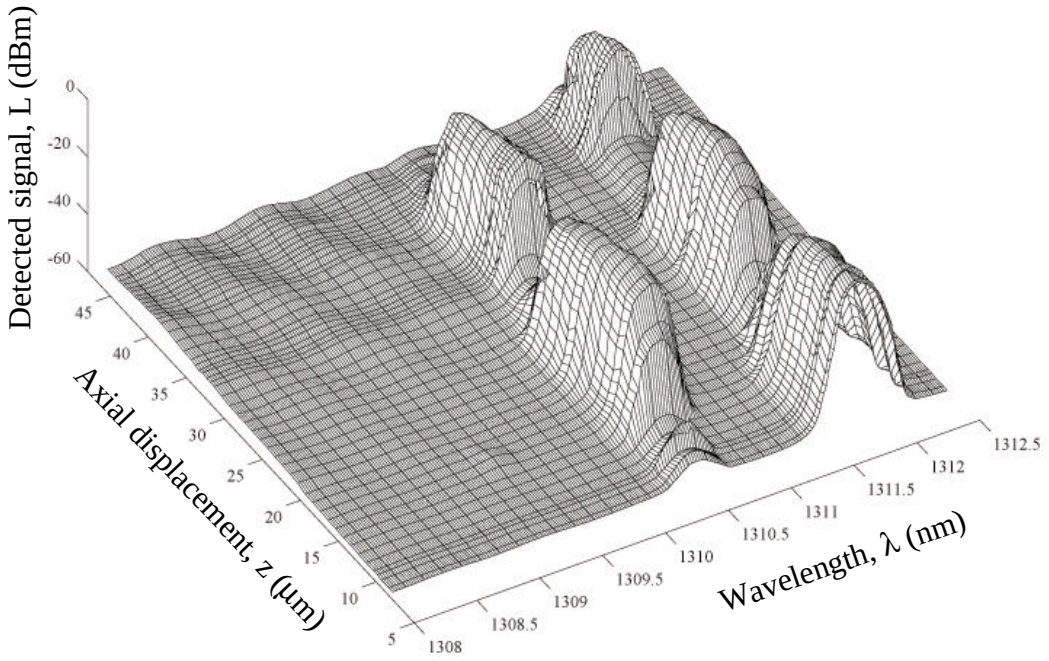

Fig. 2.3 (a) Measured optical spectrum for I = 30 mA as the axial distance from the lensed SMF to the AR coated facet, z, is increased.
With increasing z, peaks in the spontaneous emission background move to shorter wavelength. The optical spectrum analyzer has a resolution of 0.1 nm.

The measured change in detected light intensity at wavelength λ_1 (λ_2) as z is increased is illustrated in Fig. 2.4. This demonstrates that sequential wavelength switching of lasing light output at constant current, I is possible by changing the coupling efficiency between the semiconductor diode and the SMF.

.

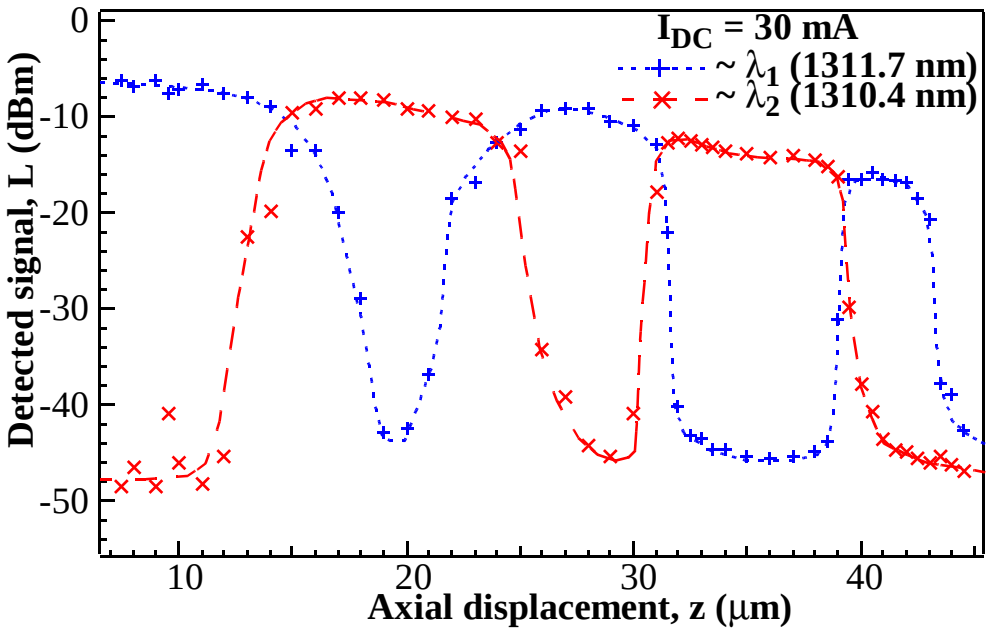

Fig. 2.4 Measured light intensity at λ_1 (λ_2) as z increases illustrating sequential wavelength switching. The optical spectrum analyzer has a resolution of 0.1 nm. The cavity mode spacing is 0.015 nm.

Optical loss is minimized and lasing occurs at wavelength λ_1 (λ_2) when a peak in the spontaneous emission background of the semiconductor cavity coincides with the center wavelength of the BG at λ_{10} (λ_{20}). In this manner the small residual reflectivity of the AR coated facet can cause a large mode suppression ratio (MSR) when selecting lasing wavelengths. In our experiments, the MSR is in excess of -35 dB.

2.3 Simulation

Electric field interference effects play a crucial role in determining the characteristic of a MCL as illustrated by the experiment described in section 2.2. The model used for the simulations is along the lines of the model used in Refs. [2.12] and [2.13], and includes the electric field interference effects.

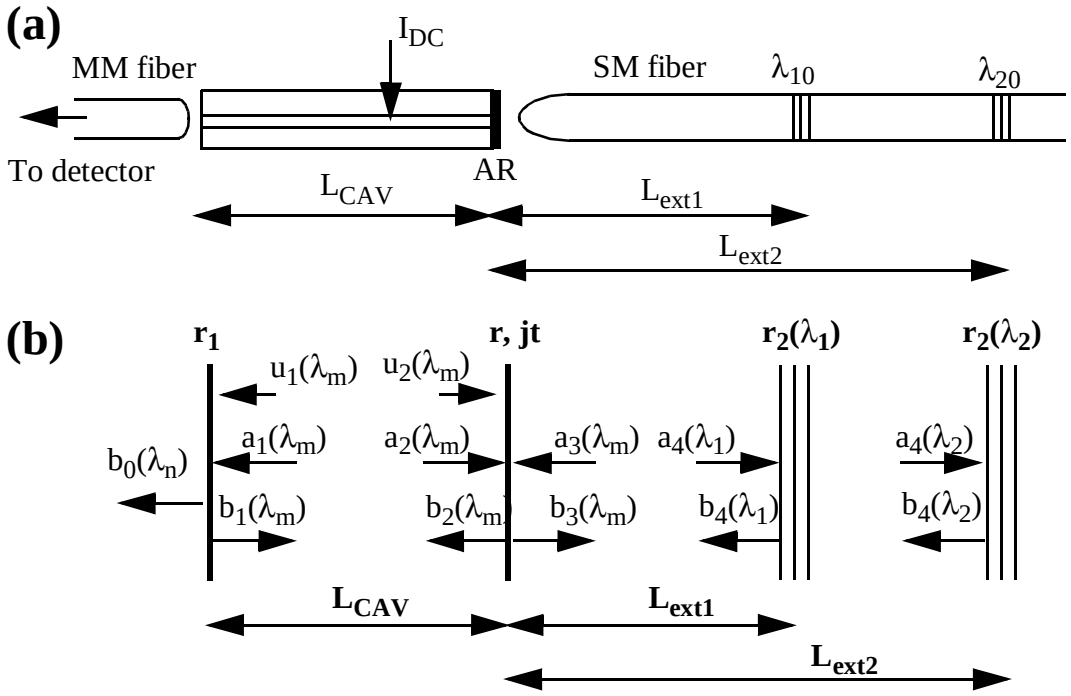

Fig. 2.5 (a) Illustrates a schematic diagram of the experimental arrangement used switch the laser cavity by changing the coupling loss. **(b)** The schematic diagram of the external cavity laser used for the simulation.

A schematic diagram of the two-section laser used for the experiment is shown in Fig. 1(a) and the mathematical model used for the simulation is illustrated in Fig. 1(b). The electric field amplitude incident on the mirror at optical wavelength λ_m, m = 1 or 2, is designated as $a_m(\lambda_m)$ while the electric field amplitude travelling away from the mirror is designated as $b_m(\lambda_m)$. The field amplitudes, a_m, are normalized so that $|a_m|^2$ gives the intensity or power flow in the medium. The electric field amplitude travelling away from the mirror with reflectivity r_1 is given by $B_1(\lambda_m,z,t) = b_1(z,\lambda_m)\exp(-j2\pi\nu_m t)$ where $b_1(z,\lambda_m)$ is the amplitude of the electric field at time t at an axial distance z in the semiconductor cavity from the facet with electric field reflectivity r_1 and $\nu_m = (c/\lambda_m)$. The reflection coefficient of the AR coating is r, while its transmission coefficient is jt where $j = (-1)^{1/2}$ and $|r|^2 + |t|^2 = 1$.

2.3.1 Reflection coefficient of the Bragg gratings

The BG grating with center wavelength λ_{10} (λ_{20}) at a distance L_{ext1} (L_{ext2}) from the AR coated facet of the laser has a reflection coefficient $r_2(\lambda)$ ($r_2(\lambda)$). The reflection coefficient of the BG is a function of the wavelength of the incident light and is assumed to be

$$r_2(\lambda) = r_{20}\exp\left[-((4(\lambda-\lambda_k))/(\Delta\lambda_{BG}))^2\right] \qquad \text{(Eq. 2.1)}$$

where λ is the wavelength of the incident light and λ_k, k = 10 or 20, is the center wavelength of the Bragg grating and $\Delta\lambda_{BG}$ is the optical bandwidth of the BG. In our model $r_{20} = |C|^2 r_0$ where r_0 is the peak electric field reflection coefficient at the center of the two BGs and C is the coupling coefficient of the electric field between the AR coated facet of the semiconductor laser and the lensed SMF at λ. It is assumed that the magnitude of the electric field coupling coefficient, C, is independent of optical wavelength. The BG with a center wavelength λ_{10} (λ_{20}) is assumed to be completely transparent at wavelength λ_2 (λ_1) near the center wavelength of the other grating. By appropriately tailoring the profile of the index modulation along the fiber length unwanted reflections can be supressed by 30-40 dB. It should be noted however that narrowing or broadening of laser spectrum is observed to occur at very low feedback levels (< -50 dB) [2.15] [2.16]. The phase response of the BGs and the phase of the coupling coefficient are ignored for the study of the static characteristics of the MCL.

2.3.2 Spontaneous emission

As in the resonance amplifier model [2.17] the distributed spontaneous emission is replaced by two electric field inputs at the mirrors of the laser gain medium. The equivalent input is given by

$$wd\frac{|u_m|^2}{h\nu_m}\frac{c}{n_s} = \frac{1}{2}\beta Bn^2 wdL \qquad \text{(Eq. 2.2)}$$

where w, d and L are the width, depth and length of the laser active region, h is the

Planck's constant, B is the laser B coefficient, β is the spontaneous emission factor, c is the speed of light in free space, ν_m is the frequency of the electric field ($\nu_m = c/\lambda_m$) and n_s is the refractive index of the laser gain medium whose variation as a function of carrier density is

$$n_s = n_{s0} - D_{ns}(n - n_c) \qquad \text{(Eq. 2.3)}$$

where n_{s0} is the refractive index of the gain medium at a carrier density n_c and D_{ns} is the change of refractive index with carrier density.

Table 2.1 Parameters used for simulations

Parameter	Symbol	Value
Semiconductor laser length	L_s	$3x10^{-2}$ cm
Length of fiber forming the external cavity 1	L_{ext1}	1.339999 cm
Length of fiber forming the external cavity 2	L_{ext2}	1.069994 cm
Width of active region	w	$2x10^{-4}$ cm
Depth of active region	d	$2x10^{-5}$ cm
Confinement Factor	Γ	0.25
Beta	β	10^{-6}
Nonradiative recombination coefficient	A	10^6 /s
Radiative recombination coefficient	B	10^{-8} cm^3/s
coefficient of the n^2 term for recombination	C	$0.6x10^{-26}cm^6$/s
Electric field reflectivity of AR coated facet	r	0.033
Electric field reflectivity of cleaved coated facet	r_1	0.57
Center wavelength of Bragg grating 1	λ_{10}	$1.31000x10^{-4}$ cm
Center wavelength of Bragg grating 2	λ_{20}	$1.31116x10^{-4}$ cm
Refractive index of semiconductor gain medium	n_s	3.7
Change in semiconductor refractive index with carrier density	D_{ns}	$7x10^{-21}$ cm^3
Refractive index of singlemode fiber	n_g	1.5
Speed of light	c	$3x10^{10}$ cm/s
Semiconductor gain coefficient	a	361 /cm
Internal loss	α_i	35 /cm
Transparency carrier density	n_0	$1x10^{18}$ /cm^3
Unit charge	q	$1.6x10^{-19}$ C

The parameter β for the MCL is an order of magnitude smaller than that for monolithic devices because the longer length of the MCL cause the cavity modes of the MCL to be at least an order of magnitude more closer than in monolithic devices. Hence the fraction of the spontaneous emission coupling to the lasing mode drops by an order of magnitude. The electric field amplitude, u_m, m = 1 or 2, at λ_m is normalized such that $|u_m|^2$ gives the energy density stored in the electric field.

2.3.3 Solution

The electric fields in the coupled cavity are related by the following equations

$$\begin{bmatrix} a_1(\lambda_m) \\ a_2(\lambda_m) \end{bmatrix} = \begin{bmatrix} p_1(\lambda_m) & 0 \\ 0 & p_1(\lambda_m) \end{bmatrix} \begin{bmatrix} b_2(\lambda_m) \\ b_1(\lambda_m) \end{bmatrix} \quad \text{(Eq. 2.4)}$$

$$\begin{bmatrix} a_3(\lambda_m) \\ a_4(\lambda_m) \end{bmatrix} = \begin{bmatrix} p_2(\lambda_m) & 0 \\ 0 & p_2(\lambda_m) \end{bmatrix} \begin{bmatrix} b_4(\lambda_m) \\ b_3(\lambda_m) \end{bmatrix} \quad \text{(Eq. 2.5)}$$

$$\begin{bmatrix} b_1(\lambda_m) \\ b_4(\lambda_m) \end{bmatrix} = \begin{bmatrix} r_1 & 0 \\ 0 & r_2(\lambda_m) \end{bmatrix} \begin{bmatrix} a_1(\lambda_m) + u_1(\lambda_m) \\ a_4(\lambda_m) \end{bmatrix} \quad \text{(Eq. 2.6)}$$

$$\begin{bmatrix} b_2(\lambda_m) \\ b_3(\lambda_m) \end{bmatrix} = \begin{bmatrix} r & jt \\ jt & r \end{bmatrix} \begin{bmatrix} a_2(\lambda_m) + u_2(\lambda_m) \\ a_3(\lambda_m) \end{bmatrix} \quad \text{(Eq. 2.7)}$$

where $p_1(\lambda_m)$ and $p_2(\lambda_m)$, m = 1 or 2, are the electric field propagation in the semiconductor cavity and the BG defined external cavities respectively.

$$p_2(\lambda_m) = \exp(-j\theta_m/2) \quad \text{(Eq. 2.8)}$$

where $\theta_m = 4\pi n_g L_{extm}/\lambda_m$, and n_g is the effective refractive index of the SMF at the wavelengths of interest.

$$p_1(\lambda_m) = G^{1/2}\exp(-j\phi_m/2) \quad \text{(Eq. 2.9)}$$

where $\phi_m = 4\pi n_s(n)L_{CAV}/\lambda_m$, and G is the electric field gain for one cavity round-trip. The round-trip electric field gain, $G = \exp((\Gamma a \log(n/n_0)-\alpha_i)L_{CAV})$, where n_0 is the transparency carrier density and α_i is the internal loss coefficient. The optical gain of quantum wells is assumed to have a logarithmic dependence on carrier density [].

Solving the above equations we obtain,

$$a_1(\lambda_m) = \frac{u_1(\lambda_m)M_1 + u_2(\lambda_m)M_2}{\left\{1 - p_1(\lambda_m)^2 rr_1 - p_2(\lambda_m)^2 rr_2 + p_2(\lambda_m)^2 p_1(\lambda_m)^2 r_1 r_2\right\}} \quad \text{(Eq. 2.10)}$$

and

$$a_2(\lambda_m) = p_1(\lambda_m)r_1[a_1(\lambda_m) + u_1(\lambda_m)] \quad \text{(Eq. 2.11)}$$

where

$$M_1 = p_1(\lambda_m)^2 rr_1 - p_1(\lambda_m)^2 p_1(\lambda_m)^2 r_1 r_2 \quad \text{(Eq. 2.12)}$$

and

$$M_2 = p_1(\lambda_m)r - p_1(\lambda_n)p_2(\lambda_m)^2 r_2 \quad \text{(Eq. 2.13)}$$

To simplify the simulations we write

$$a_1(\lambda_m) \cong \frac{u_1(\lambda_m)}{\left\{1 - p_1(\lambda_m)^2 rr_1 - p_2(\lambda_m)^2 rr_2 + p_2(\lambda_m)^2 p_1(\lambda_m)^2 r_1 r_2\right\}} \quad \text{(Eq. 2.14)}$$

The total number of photons, S_m, in the semiconductor cavity is given by

$$S_m = E_m / (h\nu_m) \quad \text{(Eq. 2.15)}$$

where E_m is the energy stored in the electric field. E_m is obtained by integrating the electric field intensity over the semiconductor cavity.

$$E_m \cong wd\left(\frac{1 - |p_1(\lambda_m)|}{\Gamma a \log((n/n_0) - \alpha_i)}\right)\left(2|a_1(\lambda_m)|^2\right) \quad \text{(Eq. 2.16)}$$

The number of photons present in the cavity depend on the carrier density in the semi-

conductor laser gain medium. The carrier density in the laser gain medium is obtained by equating the time derivative of the carrier density in the conventional semiconductor laser rate equation to zero.

$$\frac{dn}{dt} = \frac{I}{qV} - \frac{n}{\tau_e} - a\log\left(\frac{n}{n_0}\right)\frac{(S_1 + S_2)}{V} = 0 \qquad \text{(Eq. 2.17)}$$

where I is the DC bias current applied to the laser, q is the electron charge, $V = wdL_{CAV}$ is the volume of the semiconductor laser gain medium, $\tau_e = 1/(A + Bn + Cn^2)$ is the lifetime of carriers, S_1 and S_2 is the total number of photons at wavelengths λ_1 and λ_2 respectively, in the semiconductor laser gain medium.

2.3.4 Static solution for the coupled cavity

To obtain the static characteristics one has solve the above set of coupled transcendental equations in a self-consistent manner. To find self-consistent solutions we use an iterative procedure. We assume an initial carrier density, n_{in}, and total number of photons in the cavity at nominal wavelengths λ_{1in} and λ_{2in}, S_{1in} and S_{2in} and then solve for the wavelengths of the light output λ_{1out} and λ_{2out}, by requiring that the denominator of Eq. 2.14 be purely real. We then solve for the carrier density, n_{out}, and the number of photons, S_{1out} and S_{2out}, at wavelengths λ_{1out} and λ_{2out}. If n_{out}, S_{1out} and S_{2out} are not approximately equal to n_{in}, S_{1in} and S_{2in} respectively, we then appropriately adjust n_{in}, S_{1in} and S_{2in}. This process is repeated until self consistent values n_{out}, S_{1out} and S_{2out} are obtained.

The laser modeled for the simulation is an AR coated 300 μm long semiconductor laser in an external cavity with optical feedback from two BGs embedded in a single-mode fiber. The two BG have center wavelengths $\lambda_1 = 1310$ nm and $\lambda_2 = 1311.16$ nm with an optical bandwidth, BW = 0.4 nm and are located at a distance of $L_{ext1} = 1.339999$ cm and $L_{ext2} = 1.069994$ cm from the AR coated facet of the laser.

The laser parameters used for the simulations are listed in Table 2.1, "Parameters used for simulations," on page 32.

The shape of the switching characteristic is very sensitive to the phase of the electric field feedback to the laser. Any changes in the semiconductor cavity length, L_s, external cavity length, L_{ext1} and L_{ext2}, and refractive index of the semiconductor laser, n_s, and refractive index of the SMF, n_g, dramatically influence the wavelength switching characteristic. The cavity modes of the semiconductor laser are spaced $\Delta\lambda_{CAV} = 0.7736$ nm, apart. The center wavelengths of the BGs are spaced, $\Delta\lambda_{BG} = 1.5(\Delta\lambda_{CAV})$ apart. Hence, at any operating point of the device the cavity modes of the semiconductor laser will select one of the BG defined wavelengths as the lasing mode. The external cavity lengths, L_{ext1} and L_{ext2}, are carefully selected to give a roundtrip phase that is an integer multiple of 2π in the external cavity at the center wavelength of the BGs, λ_{10} and λ_{20} respectively.

The decrease in coupling efficiency, C, between the lensed SMF with the embedded BG and the semiconductor laser as the fiber is pulled back from the AR coated facet of the laser is modeled by a decrease in the effective BG reflectivity, r_2. The carrier density, n, in the semiconductor laser cavity increases with a decrease in r_2 as seen in Fig. 2.6(a). Wavelength of the lasing light output switches between λ_1 and λ_2 as r_2 decreases. This is accompanied by a rapid increase in semiconductor carrier density, n, to its new equilibrium value. The device has two lasing solutions, one at wavelength λ_1 and the other at λ_2 near values of r_2 when switching occurs. The range of values of r_2 over which the system has multiple lasing solutions when wavelength switching occurs increases as the values of r_2 decreases approaching the electric field reflection coefficient, r = 0.033, of the AR coated semiconductor facet.

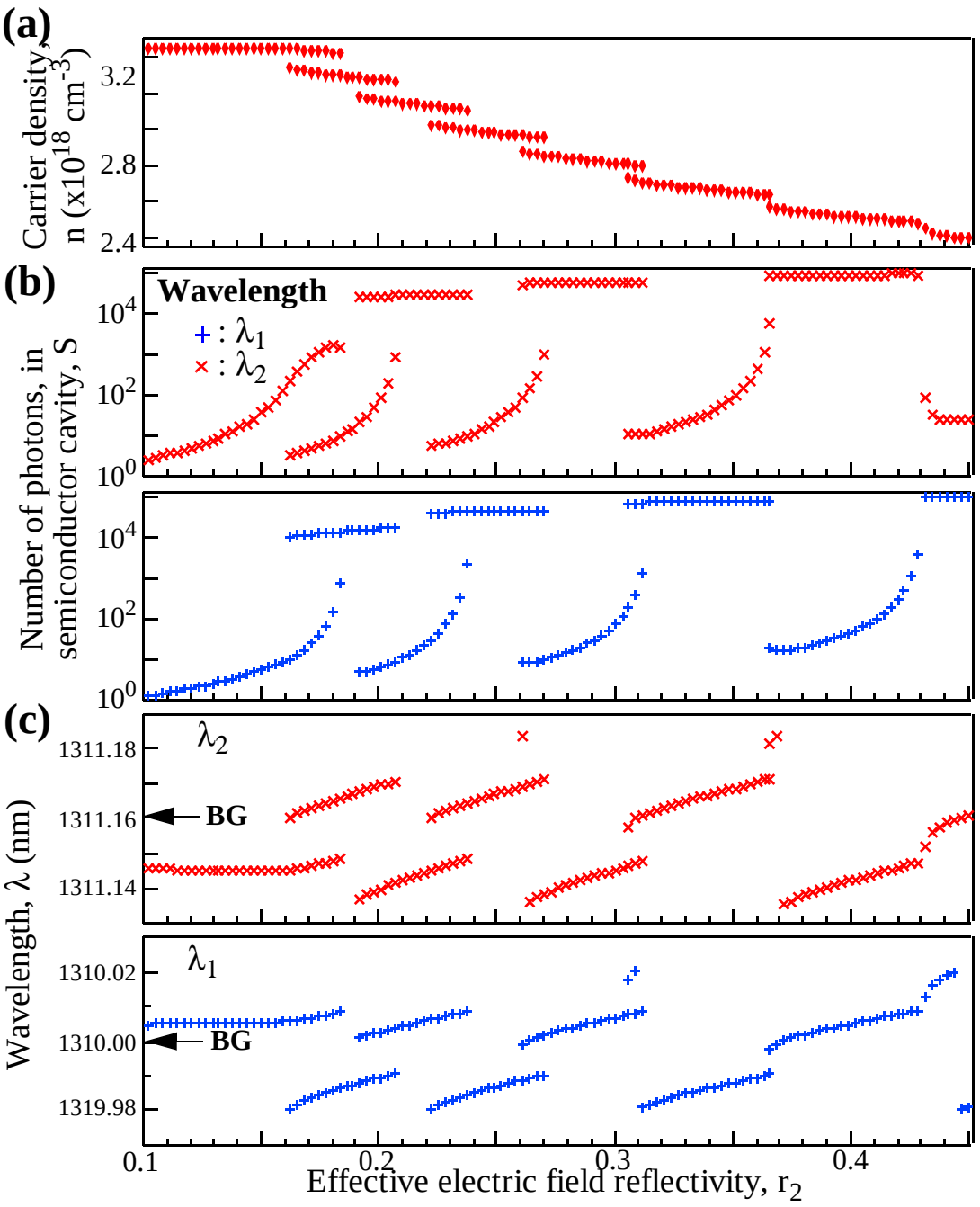

Fig. 2.6 Simulated results when the coupling between the AR coated facet of the laser and the SMF with the embedded BG is decreased. The laser is biased at 40 mA.

Fig. 5 illustrates the results of wavelength switching by decreasing coupling efficiency, C, between the lensed SMF with the embedded BG and the semiconductor

laser assuming a perfect AR coating. The mode suppression ratio between the two wavelengths is drastically reduced as coupled cavity effects no longer select the lasing wavelength. As C decreases the carrier density in the semiconductor laser gain medium increases until the device stops lasing. The wavelengths, λ_1 and λ_2, of lasing modes tune with an increase in carrier density. The mode suppression between the two modes at wavelengths λ_1 and λ_2 is due to the differences in reflectivity of the BGs at the lasing wavelengths. It is interesting to note that there are no discontinuities in the carrier density curve when r = 0.

In the simulations presented in this section the laser is assumed to lase at a single longitudinal mode at wavelengths, λ_1 and λ_2, near the center wavelengths λ_{10} and λ_{20} of the two BG. As the $\Delta\lambda_{BG}$ of the two BGs are broad compared to the cavity mode spacing, $\Delta\lambda_{CEXT}$, of the external cavities this approximation is not valid when (λ_1 (λ_2) - λ_{10} (λ_{20})) ~ $\Delta\lambda_{CEXT}/2$. In this case there is yet another mode within the grating bandwidth that has approximately the same net round-trip gain as the lasing mode.

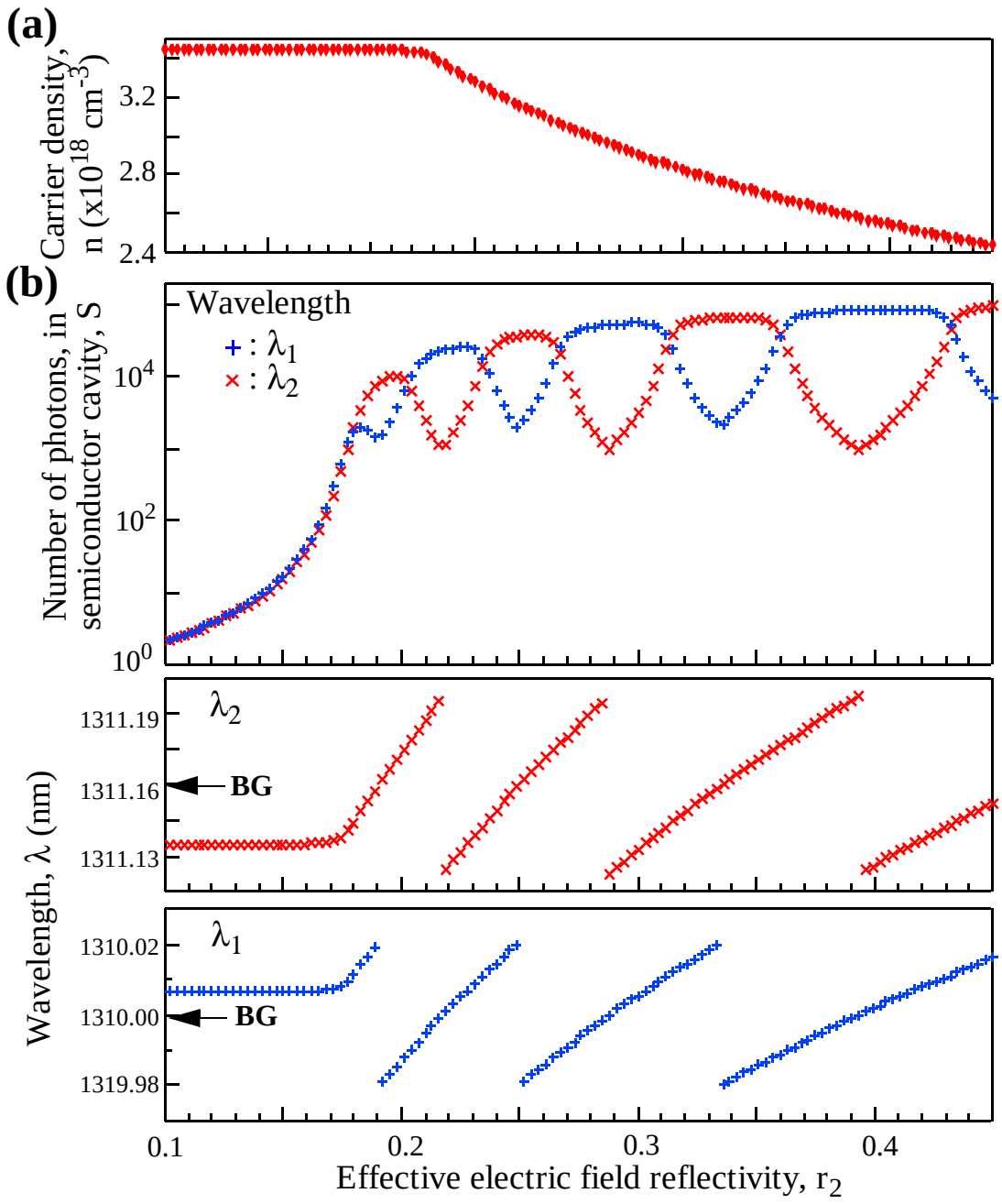

Fig. 2.7 Simulated results when the coupling between the AR coated facet of the laser and the SMF with the embedded BG is decreased. The AR coating is assumed to have no residual facet reflectivity at the lasing wavelengths. The laser is biased at 40 mA.

2.4 Wavelength selective feedback to a two-section laser

In experiments presented in section 2.2, carrier density in the laser gain medium is changed by mechanically moving the lensed SMF thereby controlling optical loss. Clearly, mechanical movement limits wavelength switching speed. High-speed (100 Mb/s) wavelength switching is possible if electronic or optical injection can be used to achieve carrier density changes in the semiconductor gain medium. In a two-section laser the carrier density is not pinned above threshold.

A schematic of a two-section laser is illustrated in Fig. 2.8(a). L is the length of the laser and two sections have fractional lengths of hL and (1-h)L respectively. Gain clamping of the lasing two-section device requires that

$$hg(n_1)L + (1-h)g(n_2)L = g_{th} \qquad \text{(Eq. 2.18)}$$

where g(n) is the quantum well gain per cm. When the current i_1 (i_2) to a section increases, n_1 (n_2) increases while n_2 (n_1) decreases due to the increase in the cavity photon density. The new equilibrium values of n_1 and n_2 still satisfy Eq. 2.18. The average carrier density, $\bar{n}$, in the laser is given by

$$\bar{n} = hn_1 + (1-h)n_2 \qquad \text{(Eq. 2.19)}$$

As g(n) illustrated in Fig. 2.8(b) is a nonlinear function of n, a change in the drive current i_1 causes $\bar{n}$, which depends linearly on n_1 and n_2, to vary.

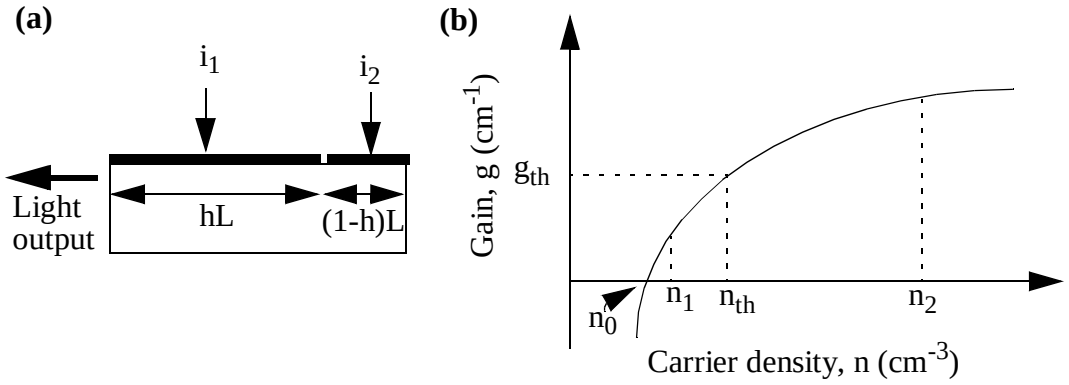

Fig. 2.8 (a) A schematic of a two-section laser. **(b)** Semiconductor gain as a function of carrier density at the lasing wavelength. n_{th} is the carrier density corresponding to threshold gain, g_{th}, and n_0 is the

transparency carrier density.

The next section presents experimental results which show that changing the bias current applied to one of the sections of an AR coated two-section laser in a BG defined external cavity changes the optical loss in the cavity.

2.4.1 Experimental results and discussion

The laser diode used for these experiments is a 500 μm long InGaAs/InP buried heterostructure four quantum well device with an integrated saturable absorber. Ref [2.18] gives details of diode structure and fabrication. The series resistance between the 12 μm long saturable absorber and the laser gain section is 500 Ω. The as-cleaved device lases at λ = 1548 nm wavelength with a threshold current of $I_{gain}(th)$ = 19 mA. The threshold current of the laser after anti-reflection (AR) coating one mirror facet is greater than 100 mA. The peak in the spontaneous emission spectrum after AR coating is around 1520 nm.

As illustrated in the inset to Fig. 2.9, optical feedback is provided by coupling emission from the AR coated facet into a single-mode fiber in which is embedded a single FBG [2.19]. The 2 mm long BG has a peak reflectivity of 80% centered at wavelength λ = 1544.6 nm with a -3 dB optical bandwidth of 0.242 nm. The coupling efficiency between emission from the laser and the single-mode lensed fiber is 0.42.

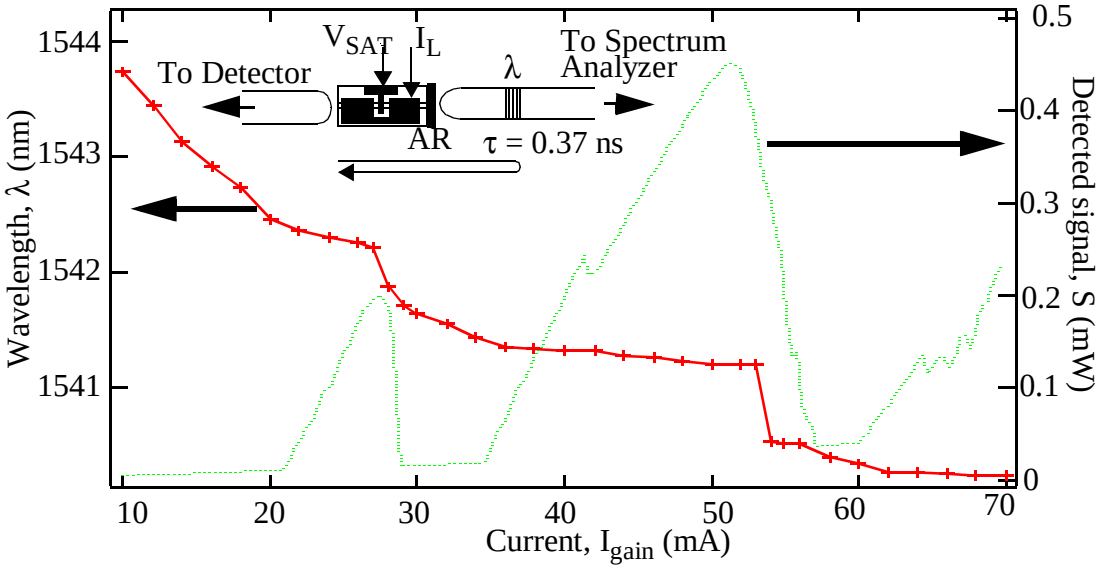

Fig. 2.9 Measured L-I_{gain} characteristic of the AR coated two-section laser in an external cavity with optical feedback from a BG embedded in a SMF.
BG has a peak reflectivity of 80% centered at wavelengths λ = 1544.6 nm with a -3 dB optical band-width of 0.242 nm. The absorber section is biased at a constant voltage of 1 V. The graph also plots the measured wavelength of peak in the spontaneous emission spectrum as the current to the gain section is varied. The inset shows a schematic diagram of the experimental arrangement.

The measured detected light intensity (L) versus gain section current (I_{gain}) LI_{gain}, characteristic of the laser with the absorber section biased at V_{sat} = 1V is shown in Fig. 2.9. The laser starts to lase near 20 mA. L increases with I_{gain} till I_{gain} = 29 mA. Then rapidly decreases with increasing I_{gain} and the lasing stops. The laser starts to lase at I_{gain} = 35 mA and with increase in I_{gain} the same characteristic is repeated.

Fig. 2.9 also shows the wavelength of a peak in the spontaneous emission spectrum as I_{gain} is increased. The measured change in the position of a peak in the spontaneous emission is related to the change in the refractive index in the gain medium. It can be shown that,

$$\Delta\lambda/\lambda = \Delta n_s/n_s \qquad \text{(Eq. 2.20)}$$

where $\Delta\lambda$ is the change in wavelength of a spontaneous emission peak and Δn_s is the

change in refractive index of the semiconductor gain medium. The refractive index of the semiconductor decreases with increase in carrier density. Hence, with increase in carrier density in the semiconductor gain medium the peak in the spontaneous emission spectrum moves to shorter wavelengths. Below threshold the peak in the spontaneous emission spectrum moves to shorter wavelength with increase in I_{gain} due to increase in carrier density with I_{gain}. When the laser starts to lase the rate at which the peak in the spontaneous emission spectrum moves to shorter wavelength decreases indicating that although the carrier density in the laser gain medium continues to increase with I_{gain} it now does so at slower rate.

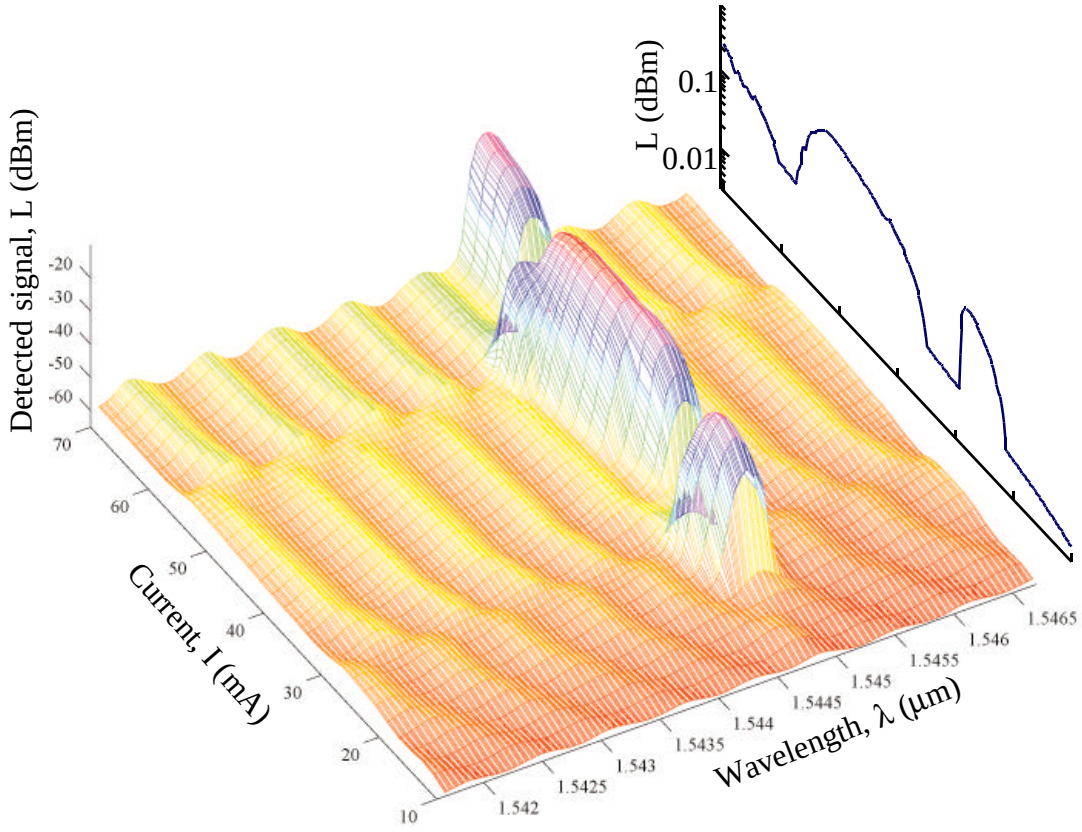

Fig. 2.10 Shows the measured optical spectrum of the laser as a function of I_{gain} with the absorber section biased at a constant voltage of 1 V. The inset to shows the LI_{gain} characteristic of the laser. The laser lases when a peak in the spontaneous emission spectrum matches the BG defined wavelength.

Fig. 2.10 shows the measured optical spectrum of the laser in the external cavity as a function of gain section current with the saturable absorber biased at 1 V. As may be seen, when a peak in the spontaneous emission spectrum lines up with the BG defined wavelength the laser lases. The inset shows the LI_{gain} characteristic of the laser.

2.5 Wavelength switching using two-section laser

For a MCL when a Fabry Perot peak in the spontaneous emission background of the semiconductor cavity coincides with the center wavelength of the BG optical loss is minimized and lasing occurs at that wavelength. Experimental results presented in section 2.4 indicate that the carrier density of a two-section semiconductor laser is not pinned above threshold and so the peaks in the spontaneous emission background move to shorter wavelengths with increase in current. If the AR coated two-section laser obtains optical feedback from two gratings with distinct center wavelengths, it should be possible to switch the wavelength of the light output by tuning the peaks in the spontaneous emission background. This is commonly known as wavelength tuning using the vernier effect. In this section the vernier effect is used to select the lasing wavelength of light output from a two-section laser in an external cavity with feedback from two BG embedded in an SMF.

The semiconductor laser described in section 2.4.1 is used in the following experiments. As illustrated in Fig. 2.11(a), optical feedback is provided by coupling emission from the AR coated facet into a single-mode fiber in which are embedded two discrete BGs. The 2 mm long BGs have a peak reflectivity of 95% and are centered at wavelengths λ_{10} = 1524.6 nm and λ_{20} = 1529.9 nm with a -3 dB full-width optical bandwidth of 0.190 nm and 0.242 nm respectively. The coupling efficiency between emission from the laser and the single-mode lensed fiber is C = 0.42. The device lases at optical wavelength λ_1 (λ_2) nominally equal to λ_{10} (λ_{20}) depending on the DC bias conditions.

Fig. 2.11(a) shows results of measuring the light versus gain-section current ($L\text{-}I_{gain}$) characteristic of the laser in an external cavity for different saturable absorber voltage levels. Note the region of negative slope (dL/dI_{gain}). Fig. 2.11(b) shows the measured optical spectrum of the laser at different bias points of the $L\text{-}I_{gain}$ with the saturable absorber biased at $V_{sat} = 0.80$ V. It is evident from the optical spectra that wavelength switching, between all four binary combinations, with a discrimination of at least -30 dB is possible using this arrangement.

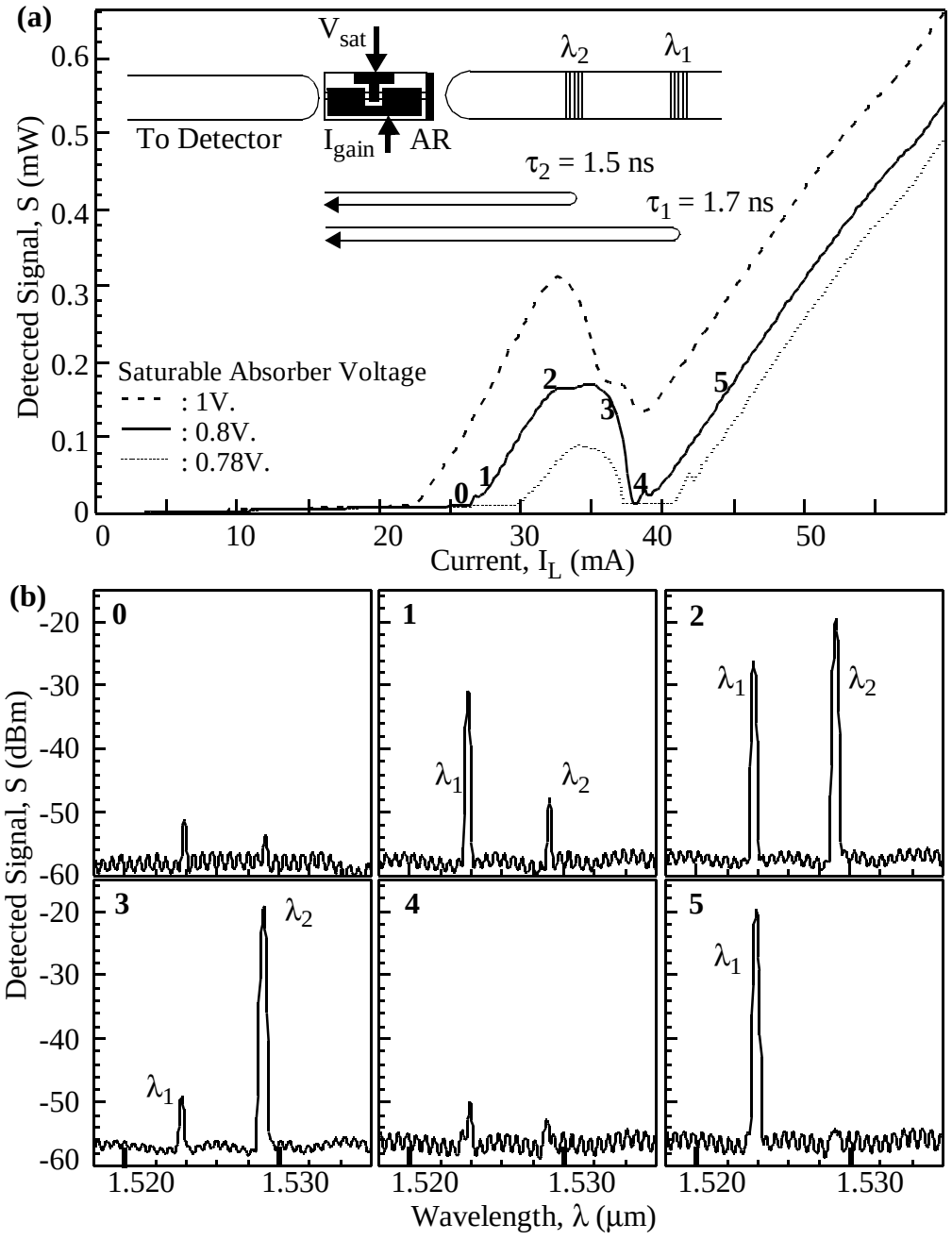

Fig. 2.11 Experimental results demonstrating wavelength coding using a two-section laser.
(a) Measured L-I_{gain} characteristics of the laser with saturable absorber biased at V_{sat} = 1 V, 0.8 V, and 0.78 V. Inset shows a schematic of the laser in an external cavity. Optical feedback is provided by two discrete BGs embedded in a single-mode fiber. The 2 mm long BGs have a peak reflectivity of 95% and are centered at wavelengths λ_{10} = 1524.6 nm and λ_{20} = 1529.9 nm with an -3dB optical bandwidth of 0.190 nm and 0.242 nm respectively. **(b)** Measured optical emission spectra at indicated bias points on the L-I_{gain} curve with V_{sat} = 0.8 V. Spectrometer resolution is 0.1 nm. Lasing occurs at opti-

cal wavelength λ_1 (λ_2) nominally equal to λ_{10} (λ_{20}).

When biased to the peak of the L-I_{gain} characteristic, laser light intensity pulsates at frequencies corresponding to photon cavity round-trip times defined by the two gratings. The cavity round-trip time for photons of wavelength λ_1 is τ_1 = 1.7 ns corresponding to a frequency of f_1 = 580 MHz. The cavity round-trip time for photons of wavelength λ_2 is τ_2 = 1.5 ns corresponding to a frequency of f_2 = 670 MHz. Fig. 2.12(a) shows the measured radio frequency (RF) spectrum of the light output at different bias points on the L-I_{gain} curve shown in Fig. 2.11(a). Wavelength λ_1 = 1524.6 nm has RF spectral content at frequency f_1 = 580 MHz and its higher harmonics. Similarly, wavelength λ_2= 1529.9 nm has RF spectral content at frequency f_2 = 670 MHz and its higher harmonics. A possible reason for the lasing light output to pulsate at the cavity round-trip time is that the effective loss seen by photons decreases if photons travel through the saturable absorber as pulses [2.20]. The attenuation suffered by light passing through a saturable absorber has a non-linear dependence on light intensity. The same energy of light passing through the absorber in the form of narrow pulses with high peak powers will suffer less attenuation than light with lower intensity spread out over time. As shown in Fig. 2.12(b), the measured time-domain emission intensity at wavelengths λ_1 and λ_2 exhibit peaks corresponding to the photon cavity round-trip times for the two wavelengths.

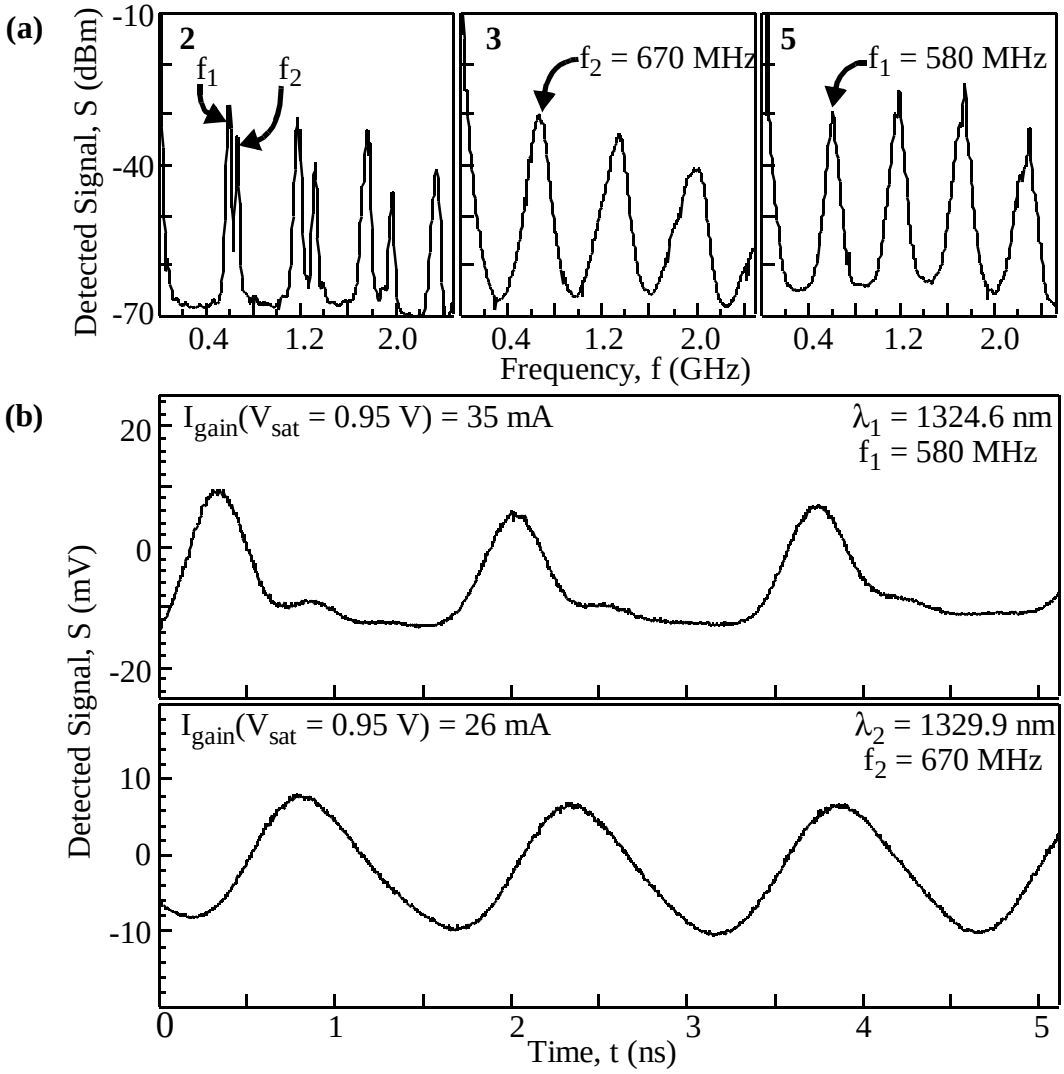

Fig. 2.12 Measured characteristics of pulsed light output from the two-section laser.
(a) Measured RF spectra of light output at various points on the laser's L-I_{gain} (V_{sat} = 0.8V) indicated in Fig. 2.11(a). There is a one-to-one correspondence between the wavelengths present in the light output and the peaks in the RF spectra. **(b)** Measured self-pulsation emission at wavelengths λ_1 and λ_2. The laser gain section is biased at the indicated values and the saturable absorber is biased at V_{sat} = 0.95 V.

2.6 Effect of Bragg grating bandwidth on laser characteristic

There has been considerable interest in using fiber BGs to provide wavelength selective feedback to external cavity semiconductor lasers [2.21] [2.22] [2.23]. Fiber BG act as high-reflectivity mirrors having bandwidths ranging from less than 0.1 nm to

30 nm. The effect of the grating bandwidth on the characteristics of the laser has been ignored. In this section, the dramatic influence of the grating bandwidth on the characteristic of the laser is presented.

2.6.1 Simulation results and discussion

The laser modeled for the simulation is an AR coated 500 μm long semiconductor laser in an external cavity with optical feedback from one BG embedded in a single-mode fiber. The BG has center wavelength $\lambda_{10} = 1520$ nm and a bandwidth, $\Delta\lambda_{BG} = 0.1$ nm. The BG is located at a distance of $L_{ext1} = 0.500029333$ cm from the AR coated facet of the laser. The remaining laser parameters used for the simulations are listed in Table 2.1, "Parameters used for simulations," on page 32.

The model presented in section 2.3 is used for the simulation results presented in this section . The quantum well gain is modeled as

$$g = \text{alog}(n/n_0)/(1+S/S_{Sat})\ \text{cm}^{-1} \qquad \text{(Eq. 2.21)}$$

to include gain saturation effects in the simulation. Here, S is the number of photons in the laser cavity and S_{Sat} is the gain saturation photon number. S_{Sat} is assumed to be 510000 [2.24] corresponding to 10 mW saturation power output of an optical amplifier. The saturation effects are included in the model to allow the carrier density in the semiconductor gain medium to increase with current above the laser threshold.

Fig. 2.13 shows the static characteristic of the laser in an external cavity with optical feedback from a single BG embedded in a singlemode fiber. The cavity modes of the external cavity are spaced 0.134 nm apart. The simulations indicate that when the bandwidth of the BG, $\Delta\lambda_{BG}$, is greater than the external cavity mode spacing, $\Delta\lambda_{FP}$, the laser has a unique solution at all drive currents but when $\Delta\lambda_{BG}$ is comparable to or less than $\Delta\lambda_{FP}$ the laser has multiple lasing wavelength solutions.

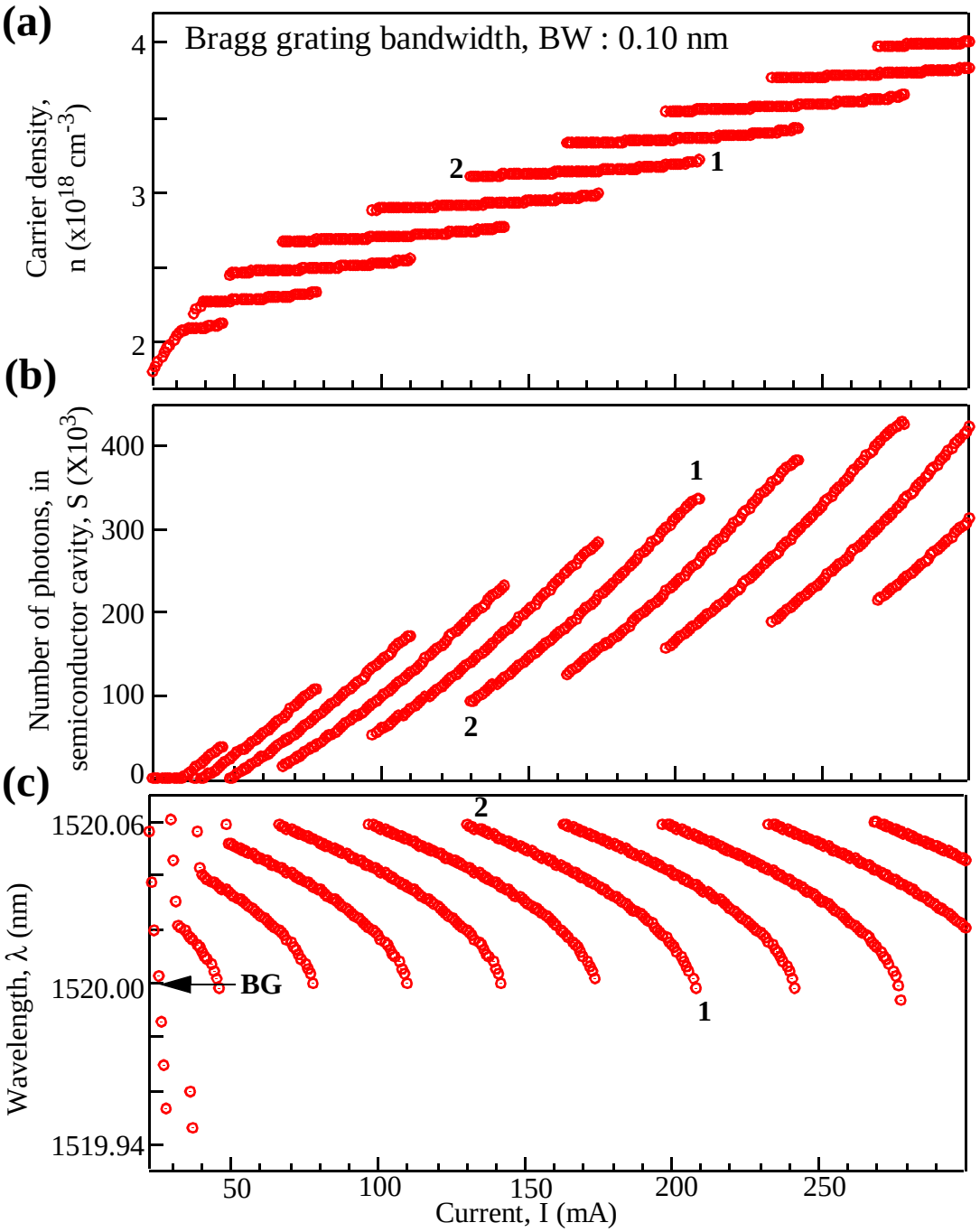

Fig. 2.13 Simulated results of AR coated laser with optical feedback from a BG embedded in an single-mode fiber. The BG bandwidth is 0.10 nm.

To better understand the multiple wavelength solutions when $\Delta\lambda_{BG}$ is comparable to

or less than $\Delta\lambda_{FP}$, consider a perfectly AR coated semiconductor laser in an external cavity with optical feedback from a BG. Neglecting the residual reflectivity of the AR coating in Eq. 2.14, the electric field of the lasing mode can be written as

$$a_1(\lambda_1) \cong \frac{u_1(\lambda_1)}{\{1 + G(n) r_1 r_2(\lambda_1) \exp(-j(\theta(\lambda_1) + \phi(\lambda_1)))\}} \qquad \text{(Eq. 2.22)}$$

For a physical steady state solution the denominator of Eq. 2.22 should be purely real. Hence,

$$\theta(\lambda_1) + \phi(\lambda_1) = (2m+1)\pi \qquad \text{(Eq. 2.23)}$$

where m is a natural number. Eq. 2.23 can be solved for the wavelength, λ_1, of the light output for a given carrier density, n. For any n there exists a wavelength λ_1 within the cavity mode spacing, $\Delta\lambda_{FP}$, given by

$$\Delta\lambda_{FP} = (\lambda_1)^2 / (2(n_g L_{ext1} + n_s L_s)) \qquad \text{(Eq. 2.24)}$$

that satisfies Eq. 2.23.

When the laser is lasing at a wavelength λ_1 denominator of Eq. 2.22 can then be simplified as

$$\{1 + G(n) r_1 r_2(\lambda_1)\} \to 0 \qquad \text{(Eq. 2.25)}$$

For a steady state solution the number of lasing photons obtained by substituting $a_1(\lambda_1)$ into Eq. 2.16 should give a self-consistent solution for the carrier density, n, in the semiconductor gain medium when substituted into Eq. 2.17.

.

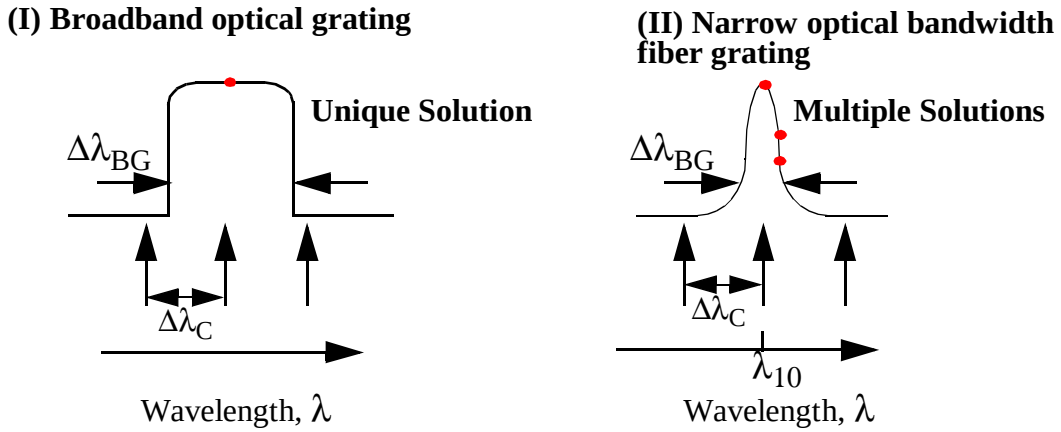

Fig. 2.14 Schematic illustrating (I) unique solution for $\Delta\lambda_{BG} > \Delta\lambda_C$ and (II) multiple solutions obtained for narrow optical bandwidth fiber grating when $\Delta\lambda_{BG} < \Delta\lambda_C$.

Consider a flat top fiber BG as illustrated in Fig. 2.14. If the fiber grating bandwidth, $2x\Delta\lambda_{BG}$ is broad compared to the cavity mode spacing, $\Delta\lambda_{FP}$, as illustrated in Fig. 2.14, then for any carrier density, n, there is a wavelength, λ_1, within the $\Delta\lambda_{BG}$ which satisfy Eq. 2.23. In this case $r_2(\lambda_1) = r_{20}$, and so Eq. 2.25 can be simplified as $1 - G(n)r_1r_{20} \rightarrow 0$. As G(n) increases monotonically with carrier density an unique value of carrier density, n_1, will satisfy the system of equations above laser threshold. For carrier densities, $n < n_1$, no mode will lase and for $n > n_1$, a mode within the grating bandwidth will have round-trip gain greater than 1 which is not a valid physical solution.

When the grating bandwidth is narrow compared to the cavity mode spacing, as illustrated in Fig. 2.14, multiple solutions are possible. The laser can lase at λ_1 and n_1 when $1-G(n_1)r_1r_2(\lambda_1) \rightarrow 0$ and lase at λ_2, and n_2 ($n_2 > n_1$), when $1-G(n_2)r_1r_2(\lambda_2) \rightarrow 0$. The increase in round-trip gain G(n) at the carrier density n_2 compared to n_1 is compensated for by the drop in the mirror reflectivity, $r_2(\lambda)$.

The multiple solutions predicted in this section when the BG bandwidth is narrower

than the FP mode spacing of the external cavity modes is not due to coupled cavity effects. The device will have multiple lasing states at the same bias current even when the residual facet reflectivity of the AR coated is reduced to 0.

2.6.2 Stability of the steady state solution

Fig. 2.16 shows the static characteristic of the laser diode in an external cavity with optical feedback from a single BG embedded in a SMF. It is interesting to note that lasing output is on the long wavelength side of λ_0. As D_{ns} is negative with increase in bias current the carrier density in the laser gain medium increases causing the wavelength of the light output to tune to shorter wavelengths. Because the increase in carrier density tunes the lasing mode closer to λ_{10}, the device is stable. If however the laser is lasing at the shorter side of λ_{10} an increase in current will cause the lasing mode will tune away from λ_{10}. This will decrease the reflectivity of the BG to the lasing mode and may result in a drop in the light intensity at the lasing wavelength. A drop in the light intensity will result in a further increase in the carrier density. Hence, this is potentially an unstable solution.

To simplify the derivation of the condition for stability we assume the device has an AR coating r = 0. Eq. 2.23 which constrains the wavelength of the lasing made may be rewritten as $(n_sL_s + n_gL_{ext1})/\lambda_1 = (2m+1)\pi$. Hence

$$d\lambda_1/dn_s = \lambda_1 L_s/(n_sL_s + n_gL_{ext1}). \qquad \text{(Eq. 2.26)}$$

Using Eq. 2.3 and Eq. 2.25 we obtain

$$\frac{d\lambda_1}{dn} = \frac{-D_{ns}L_s\lambda_1}{n_sL_s + n_gL_{ext1}} \qquad \text{(Eq. 2.27)}$$

Using Eq. 2.15, Eq. 2.16 and Eq. 2.17, photon number in the lasing mode can be written as

$$S_1 = \frac{K(n)}{1 - r_1 r_{20} \exp\left\{\left(a\left(\ln\frac{n}{n_0}\right) - \alpha_i\right)L_s - 4\left(\frac{\lambda_1 - \lambda_{10}}{\Delta\lambda_{BG}}\right)^2\right\}} \qquad \text{(Eq. 2.28)}$$

It should be noted that, to simplify the derivation gain saturation effects are neglected. For the lasing mode to be stable, with increase n there should be a increase in S_1 or $dS_1/dn > 0$. dS_1/dn is dominated by change in the denominator of Eq. 2.28 with carrier density. Hence the condition for the stability of the lasing mode can be written as

$$\frac{d}{dn}\left(r_1 r_{20} \exp\left\{\left(a\left(\ln\frac{n}{n_0}\right) - \alpha_i\right)L_s - 4\left(\frac{\lambda_1 - \lambda_{10}}{\Delta\lambda_{BG}}\right)^2\right\}\right) > 0 \ . \qquad \text{(Eq. 2.29)}$$

This can be simplified to

$$8\{(\lambda_1-\lambda_{10})/(\Delta\lambda_{BG})^2\}d\lambda_1/dn > aL_s/n \qquad \text{(Eq. 2.30)}$$

Combining Eq. 2.26 and Eq. 2.30 we obtain

$$(\lambda_1-\lambda_{10}) > -a(\Delta\lambda_{BG})^2(n_sL_s + n_gL_{ext1})/(8nD_{ns}\lambda_1). \qquad \text{(Eq. 2.31)}$$

Notice that the lasing mode becomes unstable at optical wavelengths shorter than the center wavelength of the grating. This instability of the lasing mode causes the discontinuities in the static characteristic of the device with injection current seen at point 1 and other similiar points in Fig. 2.13.

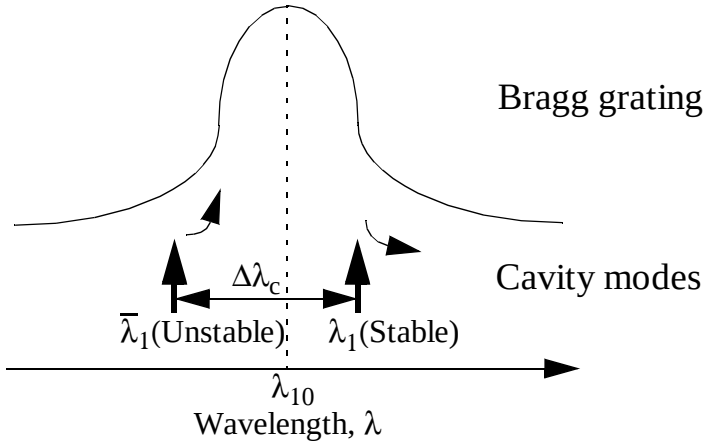

Fig. 2.15 Schematic of the cavity modes of the AR coated laser in an external cavity with feedback from a narrow FBG. λ_1 is the wavelength of the lasing mode while λ_1 is the next wavelength of the

next cavity mode. λ_{10} is the center wavelength of the BG.

To understand the discontinunities seen at point 2 and other such points seen in Fig. 2.13 consider the schematic of the cavity modes presented in Fig. 2.15. Wavelength solutions to Eq. 2.23 are spaced $\Delta\lambda_C$ apart. From the above derivation we see that for a narrow BG the optical wavelength, λ_1, corresponds to a stable lasing mode on the longer wavelength side of the BG center wavelength λ_{10}. With decrease in bias current the mode lasing at wavelength λ_1 tunes to longer wavelengths away from λ_{10}. If $(\lambda_1 - \lambda_{10}) > \Delta\lambda_C/2$ then there is a cavity mode at wavelength, $\overline{\lambda}_1$, on the shorter wavelength side of λ_{10} which has lower cavity loss due to the larger reflectivity of the BG at $\overline{\lambda}_1$ compared to λ_1. The device should then lase at $\overline{\lambda}_1$. As the cavity mode at wavelength $\overline{\lambda}_1$ is unstable this situation is not physically possible. Hence, the wavelength of the lasing mode λ_1 cannot tune to longer wavelengths away from λ_{10} beyond ($\lambda_{10} + \Delta\lambda_C/2$) as the device will become unstable.

2.6.3 Multiple lasing solutions due to coupled cavity effects

Bistability has been predicted [2.3] and observed [2.25] [2.26] [2.27] in coupled-cavity semiconductor lasers in the early 80s. The bistability in these lasers is due to the coupling between the modes of the two Fabry Perot cavities of the coupled-cavity laser. A similar bistability is seen in the device discussed in this paper when the AR coated facet of the laser is assumed to have a finite residual facet reflectivity and the bandwidth of the BG is greater than the cavity mode spacing.

Fig. 2.16 shows the simulation of a semiconductor laser in an external cavity with optical feedback from a FBG centered at wavelength 1520 nm and a bandwidth of BW = 0.4 nm. The cavity mode spacing is 0.12 nm. If the AR facet of the MCL is assumed to have a reflectivity of 0.25% the device exhibits bistability. To simplify the simulation gain saturation effects are neglected. The remaining parameters used in the simulation are the same as in section 2.6.1.

As gain saturation effects are neglected the carrier density, n, in the laser gain medium is pinned compared to the results presented in section 2.6.1. The wavelength of the light output when lasing is on the shorter wavelength of the BG center wavelength. As the facet reflectivity of the AR coated facet or the bandwidth of the BG is increased this is no longer the case.

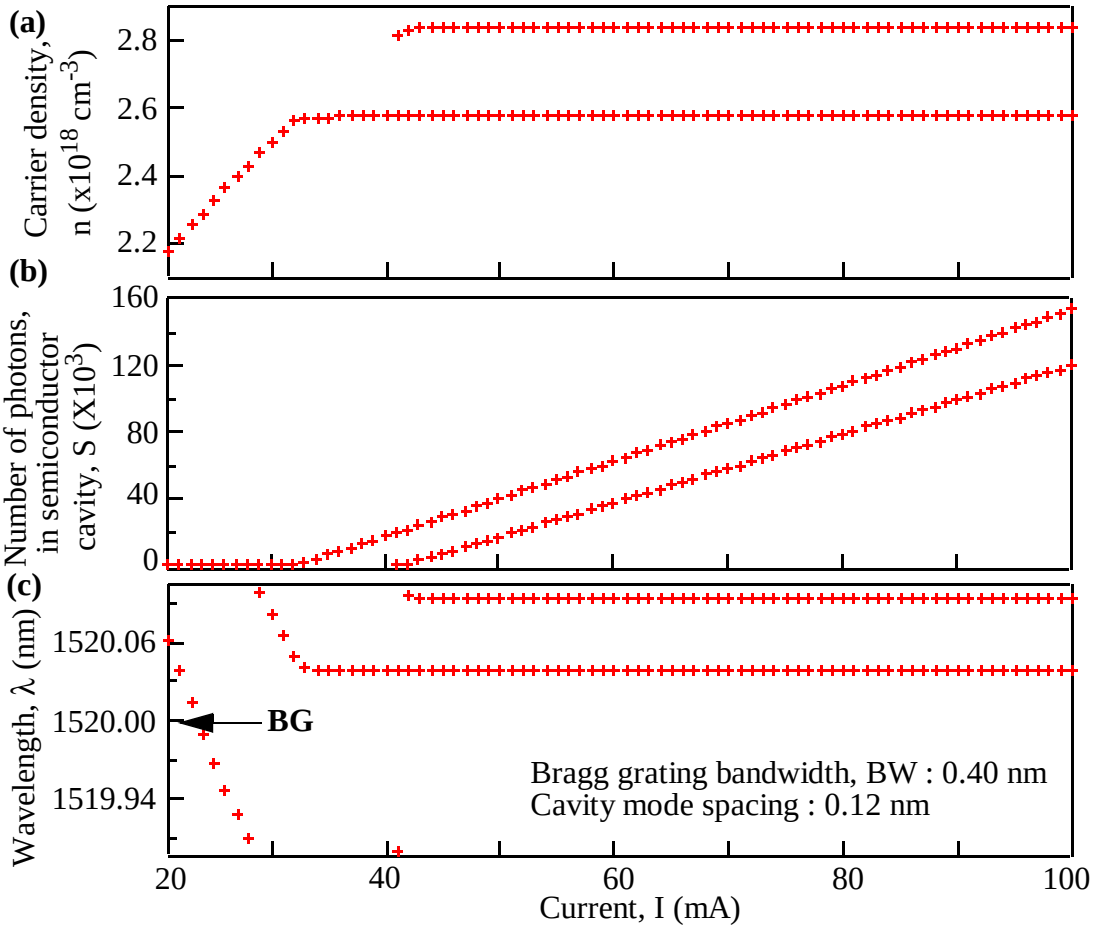

Fig. 2.16 Shows the simulation of a semiconductor laser in an external cavity with optical feedback from a FBG centered at 1520 nm and an bandwidth of 0.4 nm. The cavity mode spacing is 0.12 nm. If the AR facet of the MCL is assumed to have a reflectivity of 0.25% the device exhibits bistability.

The semiconductor laser described in section 2.4.1 is used in the following experiment. Optical feedback is provided by coupling emission from the AR coated facet into a SMF in which is embedded a BG. The 2 mm long BG has a peak reflectivity of

95% centered at wavelengths λ = 1537.55 nm with a -3 dB full-width optical bandwidth of 0.33 nm. The cavity mode spacing is 0.02 nm. The coupling efficiency between emission from the laser and the single-mode lensed fiber is C = 0.42.

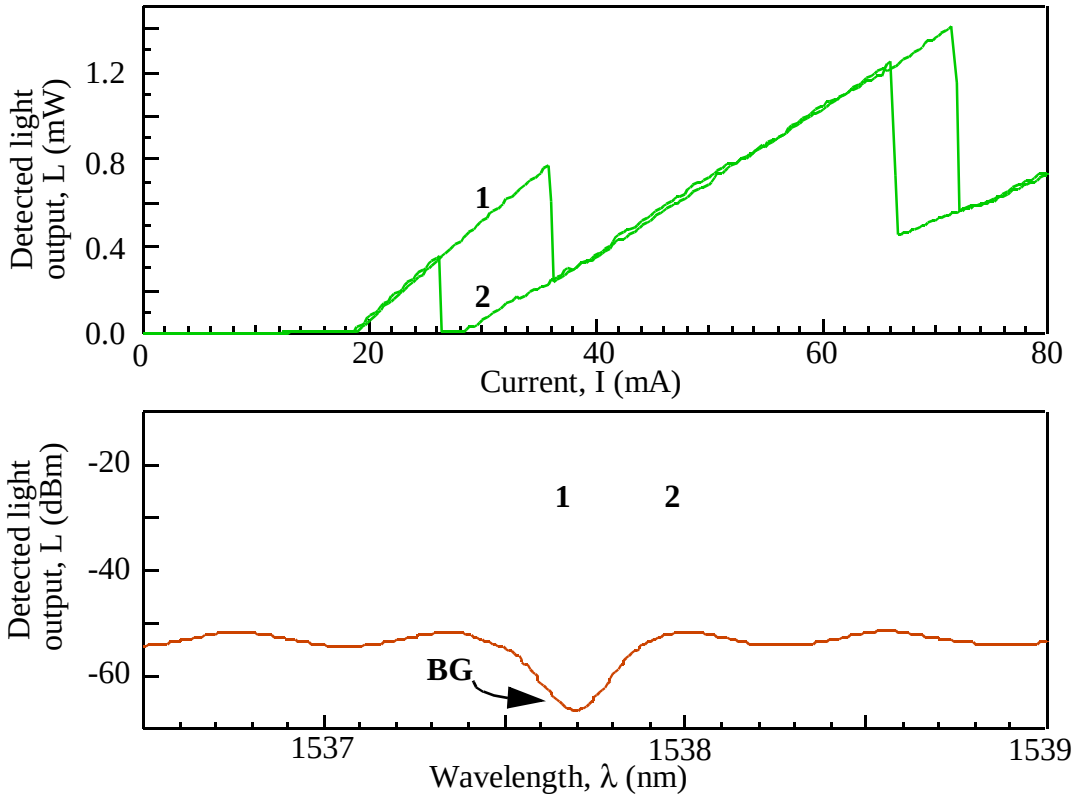

Fig. 2.17 Experimental results demonstrating multiple stable lasing states of the MCL due to coupled cavity effects.
(a) Measured L-I_{gain} characteristic of the AR coated two-section laser in an external cavity with optical feedback from a BG embedded in a SMF. BG has a peak reflectivity of 95% centered at wavelengths λ = 1537.55 nm with a -3 dB optical bandwidth of 0.33 nm. The absorber section is biased at a constant voltage of 1 V. **(b)** The measured optical spectrum of the laser at operating points 1 and 2 on LI_{gain} characteristic shown in Fig. 2.17(a). The measured transmission of the FBG as a function of wavelength is also shown for reference.

The measured L-I_{gain} characteristic of the device is shown in Fig. 2.17 with the absorber biased at 1 V. The device exhibits optical bistability. It is interesting to note that the bistability is seen at relatively high light output levels indicating that gain saturation effects cause the device to switch between stable solutions.

2.7 Conclusions

Results presented in this chapter show that the MCL described in behaves as a coupled cavity laser. The optical cavity between the cleaved semiconductor facet of the AR coated semiconductor laser and the fiber BG is one cavity of the MCL. The semiconductor laser cavity between the AR coated semiconductor facet and the cleaved semiconductor facet forms the second cavity. The device has multiple lasing solutions at the same DC bias conditions if the effective reflectivity of the BG approaches that of the AR coated facet of the laser. If the semiconductor laser gain medium of the MCL is a two-section laser then wavelength coding is possible by changing the DC bias current applied to one section of the to section laser. In MCL besides the interference effects of the composite cavity, the reflection spectrum of the BG also plays a crucial role in determining the lasing characteristics. The device has multiple lasing solutions at the same bias current even when the residual facet reflectivity of the AR coated is reduced to zero if the bandwidth of the BG is comparable to the FP mode spacing of the external cavity modes.

2.8 References

2.1 H. Kogelnik, and C. K. N. Patel, "Mode suppression and single frequency operation in gaseous optical masers," Proc. IEEE, **50** (11), pp. 2365 (1962).

2.2 R. P. Salathe, 'Diode coupled to external resonators,' Appl. Phys., **20**, pp. 1-18 (1979).

2.3 G. J. Lasher, "Analysis of a proposed bistable injection laser," Solid-State Electron. **7**, pp. 707-716 (1964).

2.4 W. F. Kosonocky, and R. H. Connely, "GaAs laser amplifiers," IEEE J. Quantum Electron., **4** (4), pp. 125-131 (1968).

2.5 M. B. Chang, and E. Garmire, 'Amplification in cleaved-substrate lasers,' IEEE J. Quantum Electron., **16** (9), pp. 997-1001 (1980).

2.6 L. A. Coldren, K. Furuya, B. I. Miller, and J. A. Rentschler, ' Etched mirror and groove-coupled GaInAsP/InP laser devices for integrated optics,' IEEE J. Quantum Electron., **18** (10), pp. 1679-1688 (1982).

2.7 W. T. Tsang, N. A. Olsson, and R. A. Logan, ' Transient single longitudinal mode stabilization in double active layer GaInAsP/InP laser under high-bit rate modulation,' Appl. Phys. Lett., **42** (12), pp. 1003-1005 (1983).

2.8 W. T. Tsang, N. A. Olsson, and R. A. Logan, ' High-speed direct single-frequency modulation with large tuning rate and frequency excursion in cleaved-coupled-cavity semiconductor lasers,' Appl. Phys. Lett., **42** (8), pp. 650-652 (1983).

2.9 K. Kojima, *Optical Fiber Communications Conference*, "High-power, high - efficiency, highly uniform 1.3 mm InGaAsP/InP strained MQW lasers," OSA Technical Digest Series (ISBN 1-55752-368-1), **8**, 253 (1995).

2.10 D. K. W. Lam and B. K. Garside, "Characterization of single-mode optical fiber filters," Applied Optics, **20**, pp. 440-445 (1981).

2.11 K. Stubkjaer, Y. Suematsu, M. Asada, S. Arai, and A. R. Adams, "Measurements of refractive-index variation with free carrier density and temperature of 1.6 mm GaInAsP/InP lasers," Electron. Lett., **16** (23), pp. 895-896 (1980).

2.12 H. K. Choi, K. -L. Chen, and Shyh Wang, "Analysis of two-section couple-cav-

ity semiconductor lasers," IEEE J. Quantum Electron., **20** (4), pp. 385-393 (1984).

2.13 L. A. Coldren and T. L. Koch, "Analysis and design of coupled-cavity lasers-Part1: Threshold gain analysis and design guidelines," IEEE J. Quantum Electron., **20**, (6), pp. 662-670 (1984).

2.14 B. Malo, S. Theriault, D. C. Johnson, F. Bilodeau, J. Albert and K. O. Hill, "Apodised in-fiber Bragg grating reflectors photoimprinted using a phase mask," Electron. Lett., **31**, pp. 223-224 (1995).

2.15 K. Kikuchi and T. Okoshi, "Simple formula giving spectrum-narrowing ratio of semiconductor laser output obtained by optical feedback," Electron. Lett., **18**, pp. 10-12 (1982).

2.16 F. Farve, D. LeGuen and J. C. Simon, "Optical feedback effects upon laser diode oscillation field spectrum," IEEE J. Quantum Electron., **18**, pp. 1712-1717 (1982).

2.17 J. A. Fleck, Jr., "Linewidth and conditions for steady oscillation in single and multiple element lasers," J. Appl. Phys., **34** (10), pp. 2997-3003 (1963).

2.18 K. Berthold, A. F. J. Levi, T. Tanbun-Ek, and R. A. Logan, "Wavelength switching in InGaAs/InP quantum well lasers," Appl. Phys. Lett., **56** (2), pp. 122-124 (1990).

2.19 I. Bennion, D. C. Reid, C. J. Rowe and W. J. Steward, "High-reflectivity monomode-fiber grating filters," Electron. Lett., **22** (16), pp. 341-343 (1986).

2.20 E. M. Garmire and A. Yariv, "Laser mode-locking with saturable absorber," IEEE J. Quantum Electron., **3** (6), pp. 222-226 (1967).

2.21 M. Ziari, J. -M. Verdiell, J. -L. Archambault, A. Mathur, H. Jeom, R. C. Yu, and T. L. Koch, "High speed fiber grating coupled semiconductor WDM laser," in Proc. Conf. Lasers Electro-Opt. (CLEO'97), Baltimore, MD, 1997, paper CMG1.

2.22 P. A. Morton, V. Mizrahi, S. G. Kosinski, L. F. Mollenauer, and T. Tanbun-ek, "Hybrid soliton pulse source with fiber external cavity and Bragg reflector," Electron. Lett., **28** (6), pp. 561-562 (1992).

2.23 B. F. Ventrudo, G. A. Rogers, G. S. Lick, D. Hargreaves, and T M. Demayo,

"Wavelength and intensity stabilization of 980 nm diode laser coupled to fiber Bragg grating," Electron. Lett., **30** (25), pp. 2147-2148 (1994).

2.24 D. Tishinin, K. Uppal, I. Kin, and P. D. Dapkus, "1.3 polarization insensitive amplifiers with integrated-mode transformers," IEEE Photonics Technol. Lett., **9** (10), pp. 1337-1339 (1997).

2.25 T. Lee, C. A. Burrus, P. Liu, W. B,. Sessa, and R. A. Logan, "An investigation of frequency stability and temperature characteristics of 1.5 μm coupled-cavity injection lasers," IEEE J. Quantum Electron., **20**, pp. 374-384 (1984).

2.26 C. H. Henry, and R. F. Kazarinov, "Stabilization of single frequency operation of coupled-cavity lasers," **20** (7), pp. 733-744 (1984).

2.27 R. J. Lang, and A. Yariv, "Intermodal stability of a coupled-cavity semiconductor laser," IEEE J. Quantum Electron., **22** (5), pp. 631-636 (1986).

Chapter 3 : Switching dynamics of the multi-cavity laser diode

3.1 Introduction

To realize the promise of Wavelength Division Multiplexing (WDM) it will be necessary to develop new components to enhance the functionality of these systems to include electro-optic as well as all-optical switching and routing capability. Key components which must be developed are optical switching and logic devices. Results presented in the last chapter show that a MCL with optical feedback from a narrow BG can lase at more than one stable state at the same bias current. If it is possible to rapidly switch between the stable states, the MCL can be used to build latches and flip-flops. The operation of the MCL as a wavelength selective electro-optic flip-flop is demonstrated in this chapter.

The measured transient dynamics when switching between the stable lasing states of the MCL at the same bias conditions are presented in this chapter. Initial experiments use electrical signals to set and reset the flip-flop. Factors limiting the switching speed are discussed. In an effort to increase the switching speed an optical pulse is used to reset the flip-flop. Measured transient dynamics when switching between multiple lasing states at the same bias current and nominal optical wavelength are also presented in this chapter. To study cavity switching a new method to switch the lasing cavity of the multi-cavity laser using an optical input which lends itself to dynamical analysis is presented. A travelling wave model of the laser is used to understand the cavity switching dynamics. Limits to cavity switching speed using optical injection are briefly discussed.

The operation of the MCL as an optoelectronic flip-flop is discussed in section 3.2. The transients when switching between the states of the flip-flop are presented. The measured cavity switching transients of the multi-cavity laser using an optical input is

also described in this section. Measured transient dynamics when switching between multiple lasing states at the same bias current and nominal optical wavelength are presented in section 3.3. Section 3.4 presents experimental results of cavity switching by injecting light into the MCL at a BG grating defined wavelength. A travelling wave model of the laser is used to simulate the cavity switching experiment. Section 3.5 is a brief conclusion.

3.2 Operation of electro-optic flip-flop

3.2.1 Experimental arrangement

Fig. 3.1 shows a schematic diagram of the experimental arrangement. The laser diode used for these experiments is a 500 μm long InGaAs / InP buried heterostructure four quantum well device with an integrated saturable absorber. Details of the diode structure and fabrication are given in [3.1]. The series resistance between the 12 μm long saturable absorber and the laser gain section is 500 Ω . The as-cleaved device lases at wavelength λ = 1548 nm with a threshold current of 20 mA. The threshold current of the laser after anti-reflection (AR) coating one mirror facet is greater than 100 mA. As illustrated in Fig. 3.1, optical feedback is provided by coupling emission from the AR coated facet into a single-mode fiber (SMF) in which is embedded a dual reflection peaked BG. The 10.5 mm long BG has peaks in reflectivity of greater than 90% centered at wavelengths λ_{10} = 1519.03 nm and λ_{20} = 1519.91 nm with a -3 dB full-width optical bandwidth of 0.13 nm (16.9 GHz) and 0.12 nm (15.6 GHz) respectively.

The center wavelengths of the BGs are $\Delta\lambda_{BG}$ = 0.89 nm apart. As cavity modes of the AR coated semiconductor laser are spaced $\Delta\lambda_{cav}$ = 0.59 nm apart, $\Delta\lambda_{BG} = 1.5(\Delta\lambda_{cav})$. Hence, coupled cavity effects should select one of the BG defined wavelengths as the lasing wavelength under any bias conditions [3.2].

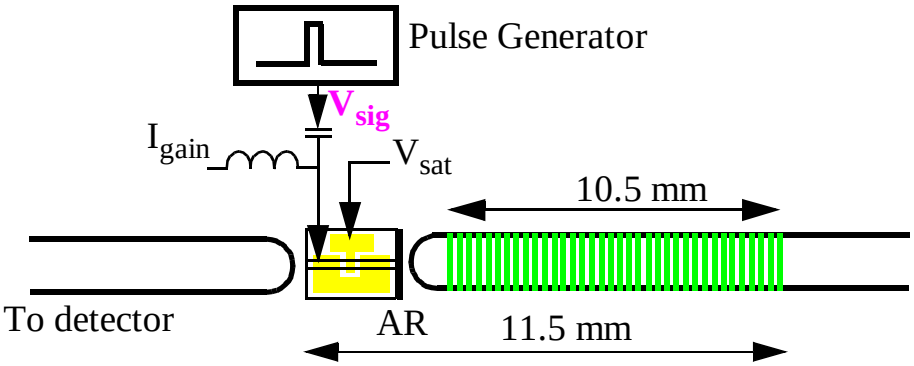

Fig. 3.1 Schematic diagram of the experimental arrangement.
The laser diode used for these experiments is a 500 μm long InGaAs/InP buried heterostructure four quantum well device with an integrated saturable absorber. Optical feedback is provided by coupling emission from the AR coated facet into a single-mode fiber in which is embedded a dual reflection peaked BG. The 10.5 mm long Bragg grating has peaks in reflectivity of greater than 90% and are centered at wavelengths λ_{10} = 1519.03 nm and λ_{20} = 1519.91 nm with a -3 dB full-width optical bandwidth of 0.13 nm and 0.12 nm respectively. The coupling efficiency between emission from the laser and the single-mode lensed fiber is 0.42.

The frequency response of the laser is shown in Fig. 3.2. The laser is biased at current I_{gain} = 45 mA with the saturable absorber biased at a constant voltage of 1 V. A -27 dBm RF signal is applied to the gain section. The frequency shows a peak at 14.7 GHz corresponding to the photon cavity round-trip time in the external cavity and lasing at wavelength λ_1 (nominally equal to λ_{10}). The cavity mode spacing for the external cavity is 14.7 GHz, which corresponds to a mode separation of 0.11 nm. As the mode spacing of the external cavity laser is comparable to the -3 dB optical bandwidth of the BGs this device is capable of lasing in a single longitudinal mode. Because the external cavity mode spacing is comparable to the Bragg grating bandwidth this system is capable of multiple lasing states at the same nominal center wavelength for the same drive conditions as shown in section chapter 2 section 6.

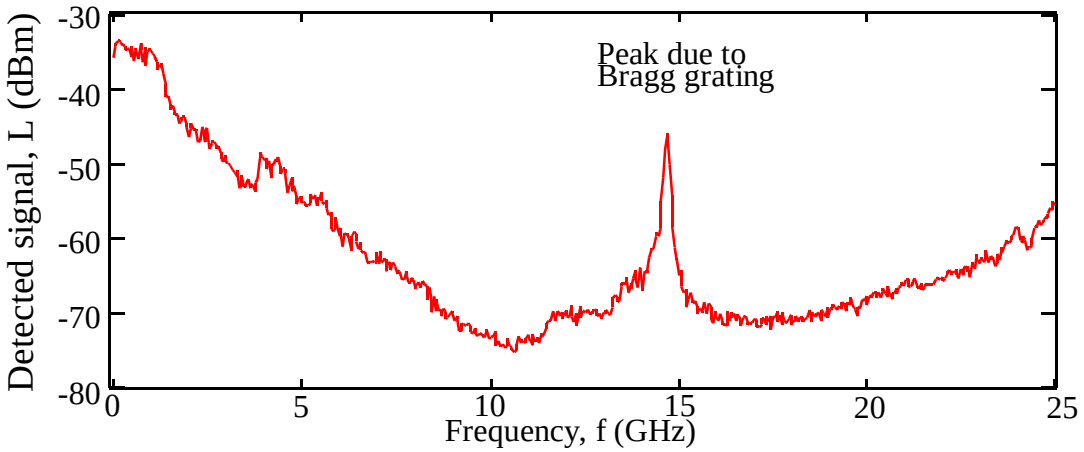

Fig. 3.2 Shows the measured frequency response of the laser in the external cavity. The laser is biased at 45 mA with the saturable absorber biased at a constant voltage of 1 V. A -27 dBm RF signal is applied to the gain section.

3.2.2 Device operation

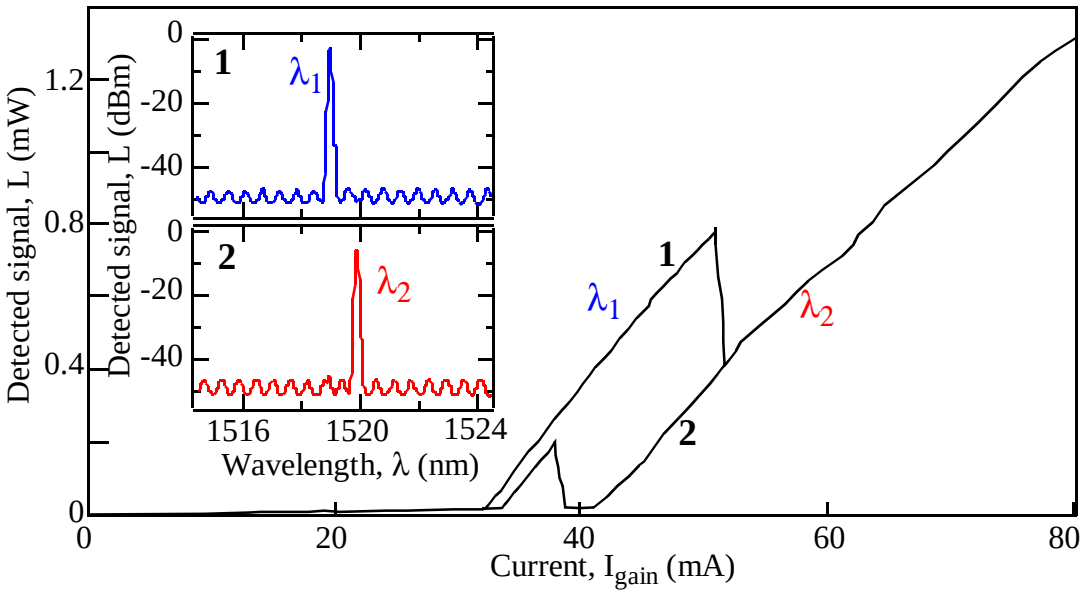

Fig. 3.3 Shows results of measuring the light versus gain-section current (L-I_{gain}) characteristic of the laser in an external cavity for saturable absorber voltage, V_{sat} = 0.9 V. The measured optical spectrum of the light output at points 1 and 2 along the L-I_{gain} curve are also seen as an inset.

Fig. 3.3 shows results of measuring output light intensity versus gain-section current (L-I_{gain}) characteristic of the device for saturable absorber voltage, V_{sat} = 0.9 V.

When I_{gain} = 50 mA and V_{sat} = 0.9 V, lasing occurs at wavelength λ_1 at operating point 1 and at wavelength λ_2 (nominally equal to λ_{20}) at point 2 on the L-I_{gain} curve. The optical spectrum of the device at operating points 1 and 2 is shown as insets to Fig. 3.3.

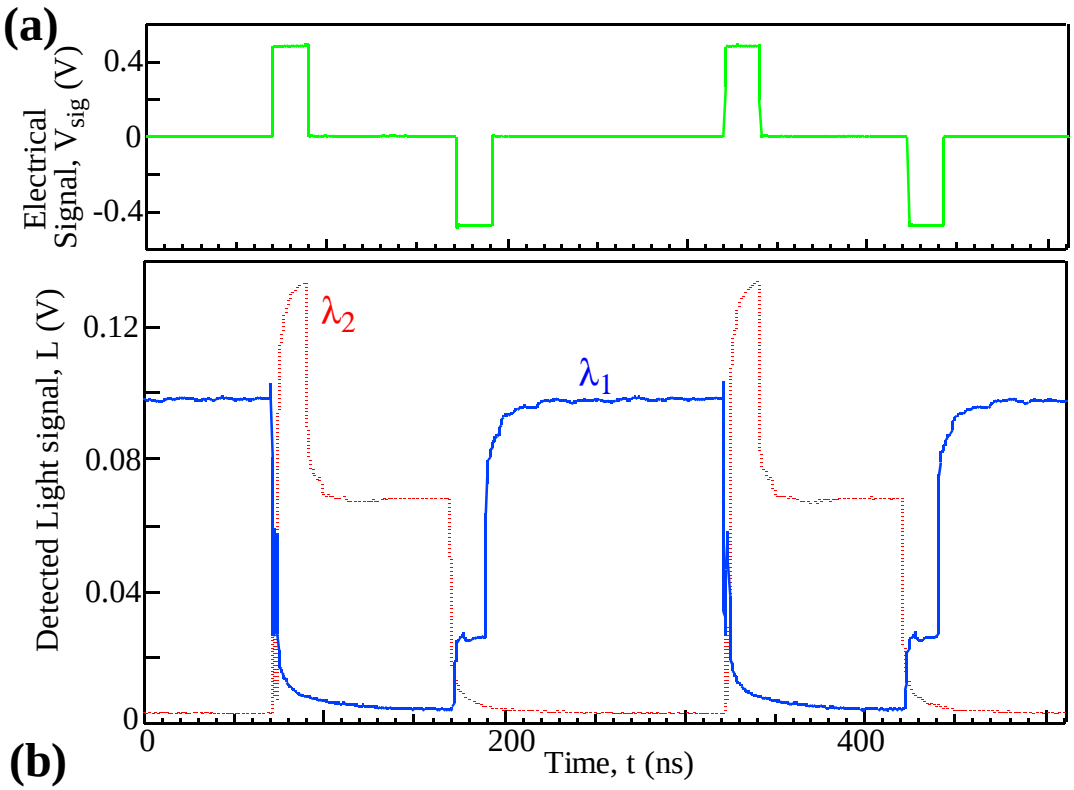

(b)

Truth table of SR Flip Flop

Inputs		Output	
S	**R**	**Q**	**$\overline{Q}$**
0	1	0	1
1	0	1	0
0	0	Q	$\overline{Q}$
1	1	undefined	

Truth table of opto-electronic Flip Flop

Inputs		Output	
S	**R**	**λ_2**	**λ_1**
0	1	0	1
1	0	1	0
0	0	λ_2	λ_1
1	1	undefined	

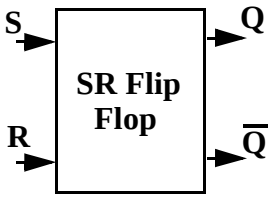

Positive going pulse is S = 1, R = 0.

Negative going pulse is S = 0, R = 1.

Fig. 3.4 shows the device acting as an electro-optical SR flip flop. The laser is biased at a DC bias current of I_{gain} = 55 mA with the absorber biased at V_{sat} = 0.9 V. A 9 mA positive going electrical pulse is applied to the device sets the lasing wavelength to λ_2. The device

stays in that state until a 9 mA negative going electrical pulse resets the device to lase at λ_1. (b) Shows the truth table of a regular SR flip flop and the electro-optical SR flip flop. The positive (negative) going pulse mimics S = 1, R =0, input (S = 0, R =1). The S = 0, R = 0 input equivalent to having no electrical pulse input to the electro-optical SR flip flop.

Along the L-I_{gain} curve from I_{gain} = 40 mA to 55 mA lasing emission occurs at wavelength λ_1 at a relatively lower carrier density, n, in the laser gain medium. At a relatively larger value of n, lasing occurs at wavelength λ_2. When operating at point 1 on the L-I_{gain} curve shown in Fig. 3.3 increase in current will tune λ_1 shorter wavelengths. When λ_1 is shorter than center wavelength of the FBG the device becomes unstable and switches to a state with lasing at λ_2 as described in chapter 2 section 2.6.2. When operating at point 2 on the L-I_{gain} curve shown in Fig. 3.3 decrease in current will tune the lasing optical wavelength λ_2 longer wavelengths. As described in chapter 2 section 2.6.2 when $\lambda_2 - \lambda_{20} > \lambda_{cav}$ the device becomes unstable and switches to a state with lasing at λ_1 . This results in hysteresis in the L-I_{gain} characteristic and can be exploited to build a wavelength selective electro-optic SR flip-flop.

The optical output of the laser is stable at both operating points 1 and 2 on the L-I_{gain} shown in Fig. 3.3. Fig. 3.4 shows the device acting as an electro-optical SR flip-flop. The light output of the device is measured after passing through a monochromator using a detector with a -3 dB bandwidth of 2 GHz. When the laser is operating at point 1 and lasing at wavelength λ_1, a 9 mA 'set' electrical pulse applied to the laser for 20 ns switches the laser operating point to 2 and lasing occurs at wavelength λ_2. The laser continues to operate at point 2 with lasing at λ_2 until a 20 ns -9 mA 'reset' electrical pulse switches the operating point to 1 with lasing at λ_1. Our measurements indicate that the temporal response to set and reset signals can be as short as 2 ns. The optical emission at wavelength λ_2 serves as Q output of the flip-flop while emission at wavelength λ_1 serves as the $\overline{Q}$ output. The measured optical mode suppression ratio between the two lasing states is greater than -35 dB.

3.2.3 Switching transients

On switching the laser from state 2 to state 1 of the L-I_{gain} characteristic shown in Fig. 3.3, the steady state carrier density, n, in the laser gain medium decreases due to a increase in the photon density at state 1 compared to that in state 2 whereas while switching the laser from state 1 to state 2, n increases. Switching transients show oscillations as seen in Fig. 3.5(a) when switching from a state with lower n to a state with higher n. The 9 mA current pulse causes a rapid drop in the photon number at wavelength λ_1 when switching from state 1 to state 2. Accompanying this is a rapid increase in carrier density, n, as the carrier lifetime is in the ps range due to stimulated recombination. The build up of photons at optical wavelength λ_2 from the spontaneous emission noise is relatively slow compared to the rate of change of carriers. The coupling between the carrier and photon dynamics cause the device to oscillate during the switching transient causing a pulse at wavelength λ_2 followed by a pulse at λ_1 during the switching transient. The timing jitter associated with these pulses are in the range of hundreds of picoseconds indicating that the pulses build up from spontaneous emission noise. The long turn-on delay, $t_{on}(\lambda_2)$ = 3.58 ns, for photons at wavelength λ_2 to reach 10% of their steady state value is due to the oscillations when switching states. The 10% to 50% rise time is $t_{rise}(\lambda_2)$ = 0.52 ns. The standard deviation, σ, of the measured timing jitter for photon at wavelength λ_2 to build up from the spontaneous emission background is $\sigma_2(\lambda_2)$ = 283 ps at point 2 in Fig. 2(a).

Fig. 3.5(b) is the measured switching transient when a -9 mA pulse applied to the laser switches the device from state 2 to state 1. The negative electrical pulse applied to the laser at state 2 decreases the carrier density to below the λ_2 lasing threshold of the device. As the device can lase at wavelength λ_1 at a lower n, the carrier density decreases until its reaches its equilibrium value for lasing at λ_1. The photons at λ_1 build out of the spontaneous emission noise resulting in the slow turn-on delay,

$t_{on}(\lambda_1)$, of 1.52 ns. The 10% to 50% rise time is $t_{rise}(\lambda_1)$ = 0.38 ns. The measured timing jitter for the rising edge when λ_1 builds up has $\sigma_4(\lambda_1)$ = 418 ps, at point 4 in Fig. 3.5(b). The measured turn-on delay is consistent with the reported intermodal switching (between two different longitudinal modes) of 0.5 nm in 0.5 ns [3.3] and 7.4 nm in 8 ns [3.4].

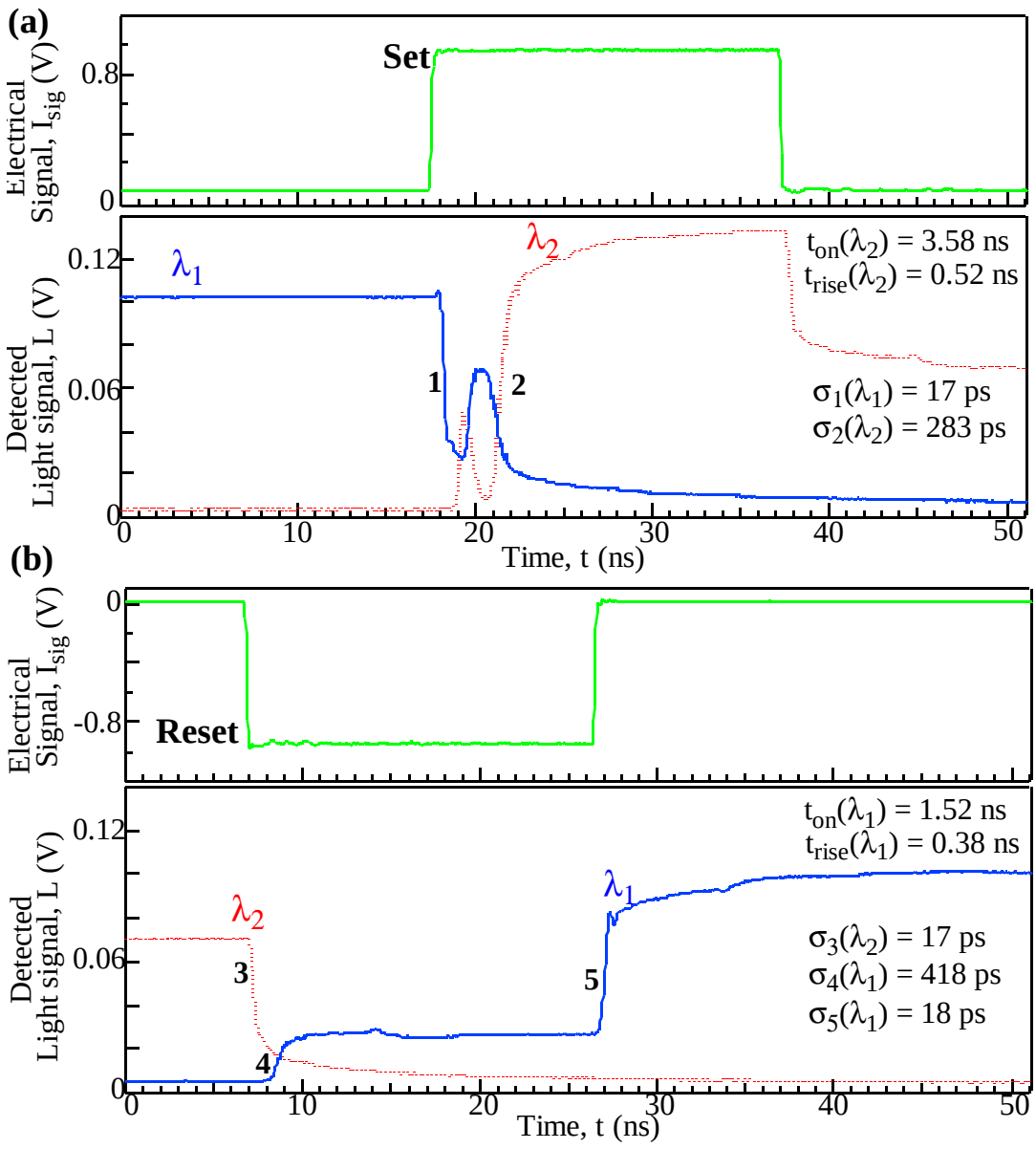

Fig. 3.5 Shows switching transients of the electro-optical SR flip flop.

The laser is biased at a DC bias current of I_{gain} = 50 mA with the absorber biased at V_{sat} = 0.9 V. The positive (negative) going pulse mimics S = 1, R =0, input (S = 0, R =1). The S = 0, R = 0 input equivalent to having no electrical pulse input to the electro-optical SR flip flop. (a) shows the measured transient response of the device to the set. The set signal is a 9 mA pulse 20 ns in duration. The laser switches lasing wavelength from λ_1 to λ_2 due to this input. The turn-on delay, $t_{on}(\lambda_2)$, for photons at wavelength λ_2 to reach 10% of their steady state value is 3.58 ns. The 10% to 50% rise time, $t_{rise}(\lambda_2)$, is 0.52 ns. The measured jitter of the detected optical waveform at wavelength λ_1 at point 1 and at wavelength λ_2 at point 2 has a standard deviation, σ, of $\sigma_1(\lambda_1)$ = 17 ps and $\sigma_2(\lambda_2)$ = 283 ps respectively. (b) illustrates the measured response to the reset signal. The reset signal is a -9 mA pulse, 20 ns in duration. It switches the lasing wavelength back to λ_1 with $t_{on}(\lambda_1)$ = 1.52 ns. The 10% to 50% rise time, $t_{rise}(\lambda_1)$, is 0.38 ns. The measured jitter of the detected optical waveform at wavelength λ_2 at point 3 and at wavelength λ_1 at points 4 and 5 has a σ of $\sigma_3(\lambda_2)$ = 17 ps, $\sigma_4(\lambda_1)$ = 418 ps and $\sigma_5(\lambda_1)$ = 18 ps respectively.

3.2.4 Optical reset

The speed of operation of the electro-optic SR flip-flop is limited to the 100 MHz range due to the turn-on delay as well as timing jitter when switching between states by applying an electrical pulse. When switching to λ_1 (λ_2) by applying a set (reset) signal photons at λ_1 (λ_2) have to build up from the spontaneous emission noise whose intensity is about four orders of magnitude less than the light intensity at the lasing wavelength. This causes the long rise times as well as large timing jitter when switching wavelengths. Switching to λ_1 (λ_2) by applying an optical pulse at λ_1 (λ_2) is a method to reduce the turn-on delay and timing jitter when switching states. The injected photons at wavelength λ_1 (λ_2) increase the background photon number at λ_1 (λ_2) when switching to λ_1 (λ_2), reducing turn-on delay. The number of photons injected to switch states is relatively fixed, compared to the photon number fluctuations in the spontaneous emission background, reducing timing jitter when switching states. The wavelength of photons injected should match the λ_1 (λ_2).

The measured transient switching characteristic to an optical 'reset' is shown in Fig. 3.6. The absorber is biased at 0.95 V. At I_{gain} = 71 mA the laser emits at wavelength λ_1 at a relatively lower carrier density, n, in the laser gain medium while at a relatively higher n lasing occurs at λ_2. The 'set' signal is a 11 mA electrical pulse 1 ns in duration. The 'reset' signal is an optical pulse at wavelength λ_1 and 1.5 ns in dura-

tion. During the reset pulse an estimated 70 μW of light is coupled into the laser. The 'reset' signal switches the light output from λ_2 to wavelength λ_1 as seen in Fig. 3. The measured turn-on delay is $t_{tran}(\lambda_1)$ = 0.18 ns. The measured 10% to 50% rise time is $t_{rise}(\lambda_1)$ = 0.13 ns. During the build up of photons at wavelength λ_1 the measured jitter at point 4 has σ_4 (λ_1) = 18 ps.

The optical 'reset' signal switches the laser from state 2, lasing at wavelength λ_1, to state 1, lasing at wavelength λ_2. The carrier density in the semiconductor laser, n, decreases when switching from state 2 to state 1. The optical reset signal besides injecting photons at wavelength λ_1 also decreases the carrier density, n, which switches the laser from state 2 to 1. An optical 'set' pulse at wavelength λ_2 applied to the laser, at the lower carrier density state 1, will decrease n in the cavity and hence will not switch the laser to state 2 with higher carrier density.

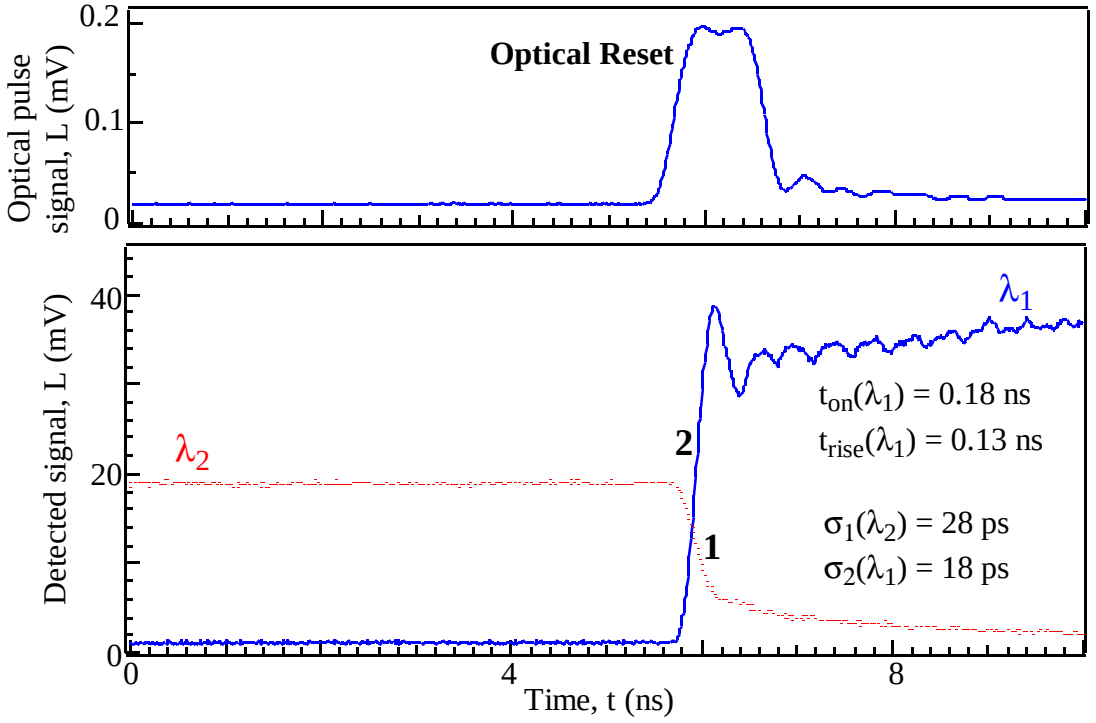

Fig. 3.6 Shows the measured device response to a 70 μW optical 'reset' pulse.

The laser is biased at a DC bias current of I_{gain} = 71 mA with the absorber biased at V_{sat} = 0.95 V. An optical pulse at wavelength λ_1, 1.5 ns in duration is the reset signal. It switches the lasing wavelength back to λ_1. The measured turn-on delay, $t_{tran}(\lambda_1)$, is 0.18 ns. The measured 10% to 50% rise time, $t_{rise}(\lambda_1)$, is 0.13 ns. The measured jitter of the detected optical waveform at wavelength λ_2 at point 1 and at wavelength λ_1 at point 2 has $\sigma_1(\lambda_2)$ = 28 ps and $\sigma_2(\lambda_1)$ = 18 ps respectively.

3.3 Switching between states at the same BG defined wavelength

The simulation results presented in chapter 2 section 6 indicate that the device is capable of lasing at multiple states at the same nominal optical wavelength. In this section we study the transient dynamics when switching between the same nominal wavelength.

Fig. 3.7 shows the L-I_{gain} curve of the laser in the external cavity with the absorber biased at 0.95 V. The coupling between the AR coated facet of the laser and the lensed SMF is adjusted to obtain high output power at 50 mA DC bias current to the gain section. At a DC bias current between 80 mA to 100 mA there are two possible states, 1 and 3, at which the laser lases at wavelength λ_2. Between these two states there is another state, 2, with laseing at wavelength λ_1. The discontinuities as well as the small hysteresis loops in the L-I_{gain} characteristic are due to the reflection back into the laser from the broad area detector used to detect the light output. Measured L-I_{gain} characteristics of the laser with index matching gel at the end of the fiber used to couple to the broad area detector do not have these features.

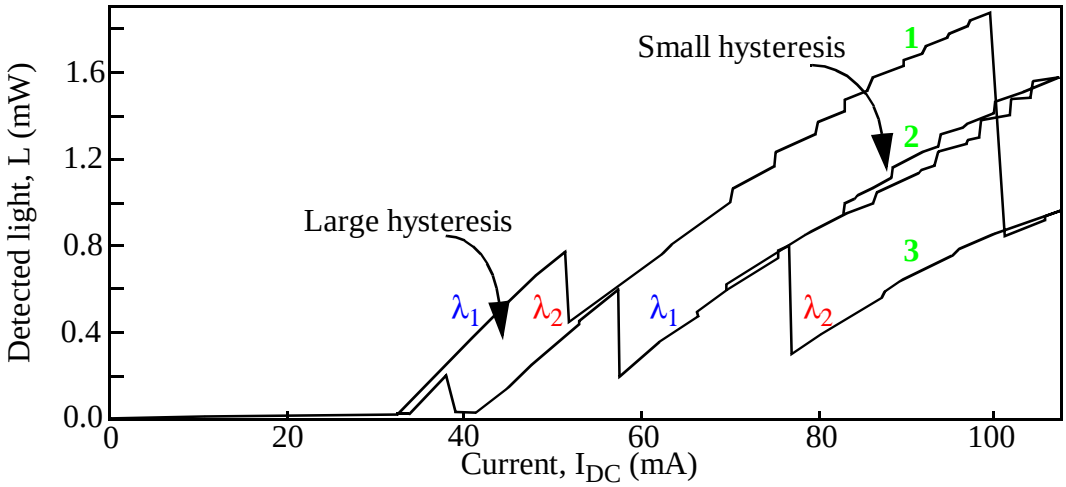

Fig. 3.7 shows results of measuring the light versus gain-section current (L-I_{gain}) characteristic of the laser in an external cavity for saturable absorber voltage, V_{sat} = 0.95 V.
When the laser is biased at I_{gain} = 80 mA to 100 mA the laser can lase at wavelength λ_1 at state 2 and λ_2 at states 1 and 3.

Switching is possible between states 1 and 3 by applying an electrical pulse for a short duration as seen in Fig. 3.8. The laser is biased at I_{gain} = 90 mA. A 20 ns, +13 mA electrical pulse switches the laser from state 1 to 3 while a 20 ns, -13 mA pulse resets the laser back to state 3.

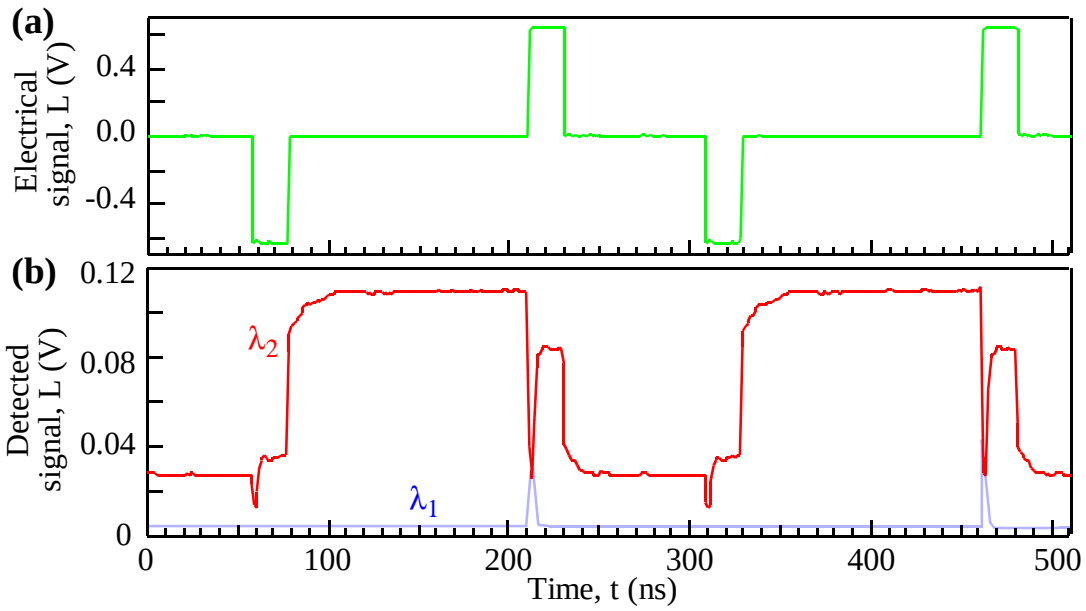

Fig. 3.8 Shows is the measured switching transients when electrical pulses are used to switch the MCL between states 1 and 3 as seen in Fig. 3.7.
A 13 mA electrical pulse 20 ns in duration applied to the laser in state 1 switches it to state 3. The device in state 3 is switched back to state 1 by applying a -13 mA electrical pulse 20 ns in duration. **(a)** Time trace of the electrical set/rest signal. **(b)** Shows the characteristic of the device when switching between states 1 and 3 lasing at nominal optical wavelength λ_1.

Fig. 3.9(a) shows the results of the switching between state 1 to 3 when a 13 mA current pulse is applied to the laser gain section. Initially there is a rapid decrease in the output light intensity at wavelength λ_2 followed by a long tail. During a portion on the tail there is a burst of photons at wavelength λ_1. The optical wavelength separation of lasing light at states 1 and 3 is smaller than the 0.1 nm resolution bandwidth of the monochromator. Hence the measured transients do not show the lasing light at state 1 turning off and the lasing light corresponding to state 3 growing from the spontaneous emission background. Although it is not clear from Fig. 3.9(a), the timing jitter of $\sigma_1(\lambda_2)$ = 98 ps and $\sigma_2(\lambda_2)$ = 935 ps at nominal wavelength λ_2 measured at points 1 and 2 of the transient switching characteristic indicate that photons corresponding to lasing state 1 of the device have to die before photons corresponding to state 3 at the same nominal wavelength can build up from the spontaneous emission noise.

The carrier density in the laser gain medium, n, increases when switching from state 1 to state 3. When switching from state 1 to state 3 n passes through an intermediate value corresponding to state 2 when lasing is possible at nominal wavelength λ_1. This causes the optical pulse at wavelength λ_1 during the switching transient. As this pulse builds up from the spontaneous emission noise the measured timing jitter at the rising edge of this pulse is in the 100s of ps range.

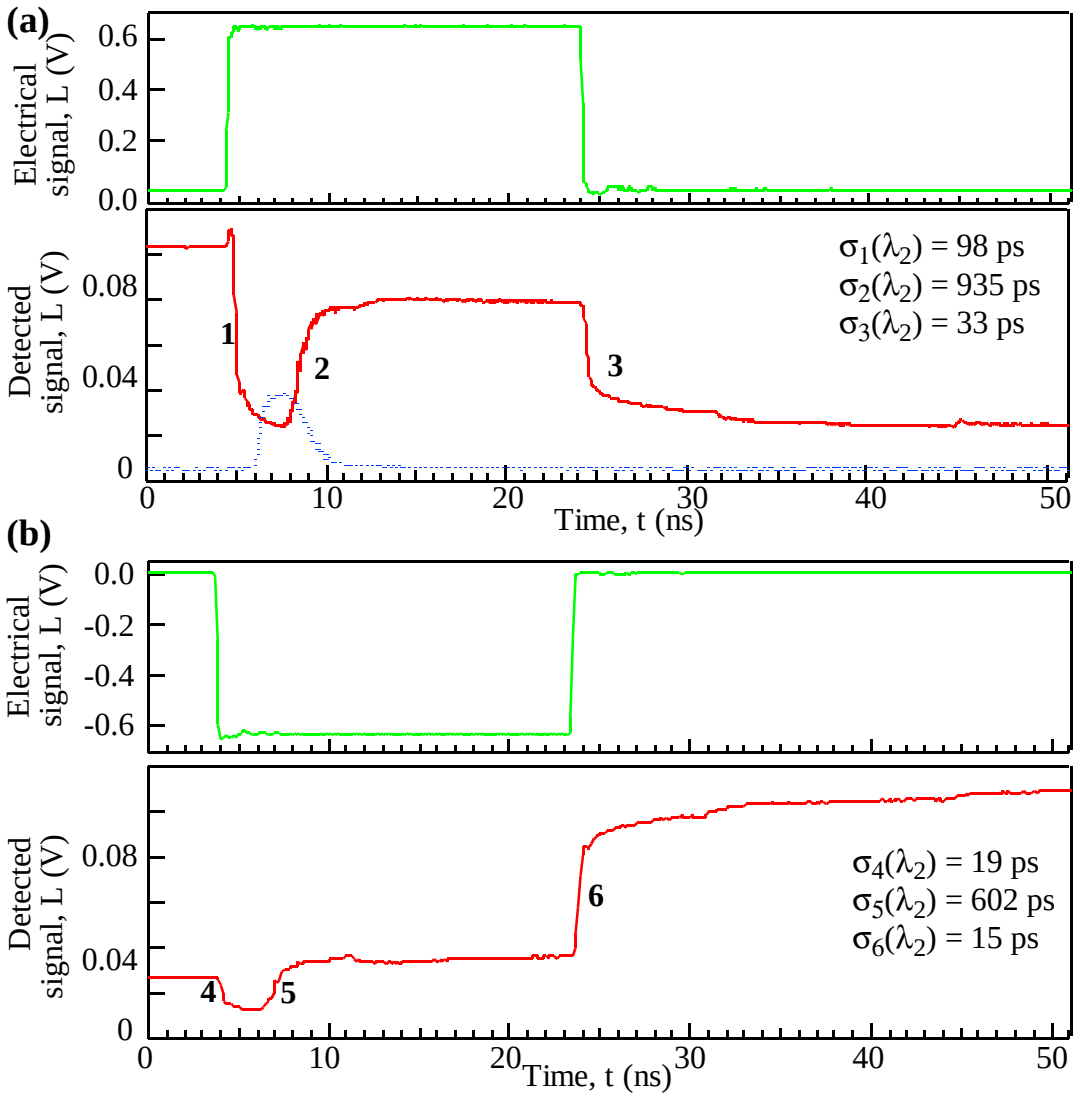

Fig. 3.9 Shows the measured transient response of the device when switching between states 1 and 3 as

illustrated in Fig. 3.6. The laser is biased at a DC bias current of 90 mA with the absorber biased at 0.95 V.
(a) Shows the measured transient response when a 13 mA pulse 20 ns in duration switches the laser from state 1 to 3. **(b)** Illustrates the measured response when switching from state 1 to 3. The laser switches back from state 3 to 1 when a -13 mA pulse 20 ns in duration is applied to the laser.

Fig. 3.9(b) is the measured transition from state 3 to 1 when the -13 mA, electrical pulse of 20 ns duration is applied to the laser. The timing jitter of $\sigma_4(\lambda_2)$ = 19 ps and $\sigma_5(\lambda_2)$ = 602 ps at nominal wavelength λ_2 measured at points 4 and 5 of the transient switching characteristic indicates that photons corresponding to lasing state 3 of the device have to die before photons corresponding to state 1 at the same nominal wavelength can build up out of the spontaneous emission noise. This causes the the notch in the time trace of light intensity at wavelength λ_2 during the initial phase of the switching transient. n decreases when switching from state 3 to state 1. When switching from state 3 to state 1, n passes through an intermediate value corresponding to state 2 when lasing is possible at nominal wavelength λ_1. This causes ane optical pulse at wavelength λ_1 during the switching transient. Although the optical pulse at wavelength λ_1 is not clearly seen in Fig. 3.9(b), other experiments performed by us confirm this phenomena.

3.4 Optical switching

3.4.1 Experiment

A schematic diagram of the experimental arrangement is shown in Fig. 3.10(a). The multiple quantum well laser emitting at 1.3 μm used for the experiments described in ref. [3.6] is AR coated on one side. The laser obtains optical feedback from two BG embedded in a lensed SMF approximately 80 cm from the lensed end. The 2 mm long fiber BG gratings are spaced 1 cm apart with center wavelengths at 1308.81 nm and 1311.346 nm with a -3 dB optical bandwidth of 0.475 nm and 0.555 nm respectively. Peak reflectivity of the BGs is 70%. The photon cavity round-trip time is ~ 8 ns. The coupling efficiency between the AR-coated laser and the lensed fiber with the embedded Bragg gratings is adjusted so that the device lases at wavelength λ_{HOT} [7]. The

laser has a threshold current of 14 mA in the external cavity.

A tunable laser is obtained by placing another AR-coated laser emitting at 1.3 μm in an external cavity with optical feedback from a bulk diffraction grating. The wave-length of the light output, is tuned by rotating the diffraction grating. The light output of the tunable laser is collected from the cleaved facet using a lensed SMF. The light is then passed through an isolator and a lithium niobate switch before it is injected into the multi-cavity laser at the cleaved facet (non-AR coated facet). The light output from the SMF containing the Bragg gratings is collected at the detector.

The steady state light versus intensity L-I_{DC} characteristics of the laser in this cavity with no optical input is shown in Fig. 3.10(b). The threshold current of the laser in the external cavity is I_{th} = 14 mA and the inset in the figure shows the spectrum under steady-state current I_{DC} = 25 mA.

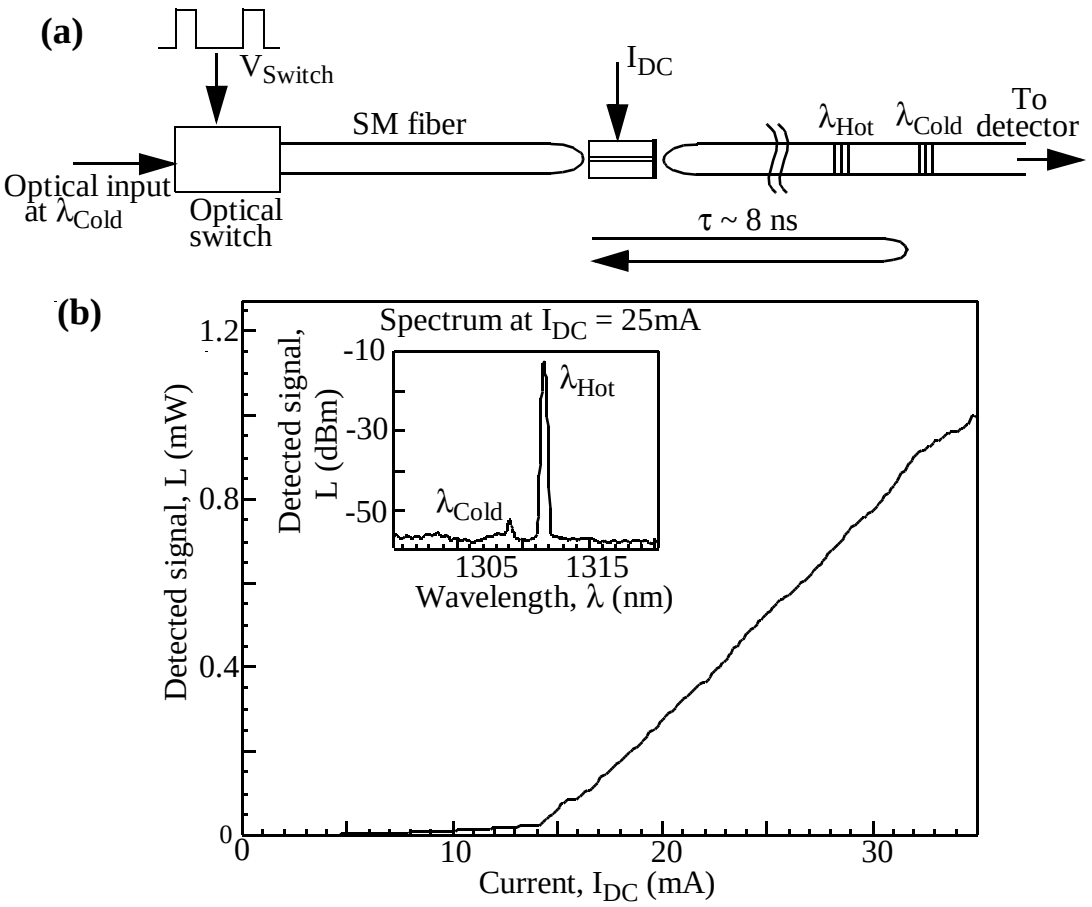

Fig. 3.10 Shows experimental arrangement and the measured staticcharacteristics of the MCL. **(a)** Shows a schematic of the experimental arrangement to study the dynamics of wavelength switching using an optical input. The BG gratings embedded in the SMF fiber are spaced 1 cm apart with center wavelengths at λ_{Cold} = 1308.81 nm and λ_{Hot} = 1311.346 nm with a -3 dB optical bandwidth of 0.475 nm and 0.555 nm respectively and peak reflectivity of 70%. **(b)** The measured detected light output (L) versus DC bias current (I_{DC}) for the laser in the external cavity with no optical input. The inset shows the optical spectrum of the light output at I_{DC} = 25 mA. The lasing wavelength is λ_{Hot}.

Fig. 3.11 shows initial results of cavity switching using light input. The laser is biased at current I_{DC} = 35 mA. Fig. 3.11(a) is the measured optical spectrum of laser light output without any optical input. Lasing emission occurs at a BG defined wavelength, λ_{HOT} = 1311.4 nm. When light is coupled into the laser at the wavelength λ_{COLD} = 1308.9 nm the wavelength of the lasing emission switches to λ_{COLD} as seen in Fig. 3.11(c). The optical discrimination is greater than -30 dB. The estimated optical power coupled into the laser is about 0.2 mW. The output optical power of the laser is

greater than 1mW. When the wavelength of the light input is not a BG defined wavelength the light output has components both at the wavelength of the optical input and λ_{HOT}. This case is shown in Fig. 3.11(b). Results obtained in the DC cavity/wavelength experiments are consistent with the results obtained by Hildebrand et al. in reference [3.5].

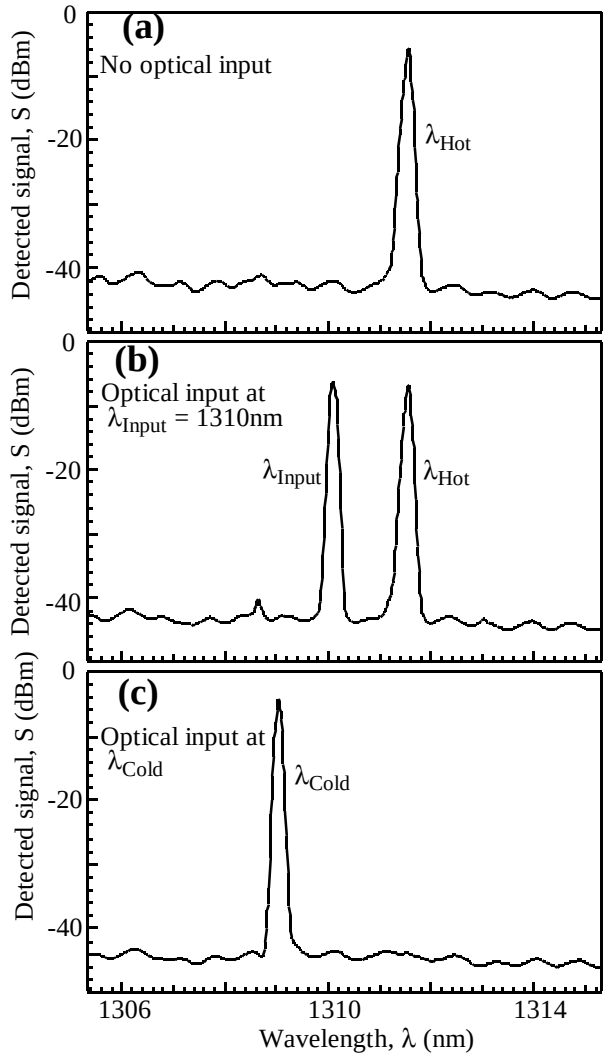

Fig. 3.11 Shows the results of cavity switching using optical input.
The experimental arrangement used in the experiment is similar to the one shown in fig. 4.1(a) except that the light input is not passed through the optical switch. The laser is biased at I_{DC} = 35 mA. The estimated optical power coupled into the laser is 200 μW. **(a)** Shows the optical spectrum of the light output with no optical input. The laser is lasing at λ_{Hot}. **(b)** The optical spectrum of the light output

when light at 1310 nm is coupled into the laser. The light output of the laser has components both 1310 nm and at λ_{Hot}. **(c)** The measured optical spectrum when light at λ_{Cold} is coupled into the laser. The wavelength of the light output is λ_{Cold} demonstrating cavity switching using an optical input.

Shown in Fig. 3.12 (a) are the transients involved in switching to the cold wavelength, λ_{COLD}, due to injection of light at the cold wavelength. The amount of power injected is estimated to be approximately 200 μW. The laser is biased at I_{DC} = 18 mA. The time taken to reach 50% of the steady state value when switching to λ_{COLD} is less than 2 round trips, comparable to the value obtained from numerical simulation using our model presented in the next section. Shown in Fig. 3.12 (b) are the transients involved in switching back to the hot wavelength after the light injection is turned off. It takes several round trips to reach steady state lasing at λ_{HOT}. Further, it is interesting to note the presence of a "shoulder" in the fall-off of cold photons. This is predicted by our model and is attributed to two regimes involved in the transients. During regime (a) the carrier density increases, at the expense of cold photons, to a value so as to maintain lasing at the cold wavelength. This occurs during the first couple of roundtrips after light injection is turned off. The hot photons in the cavity build up at the expense of cold photons and carrier density during regime (b). The carrier density now decays to a value such that it supports lasing at λ_{HOT}.

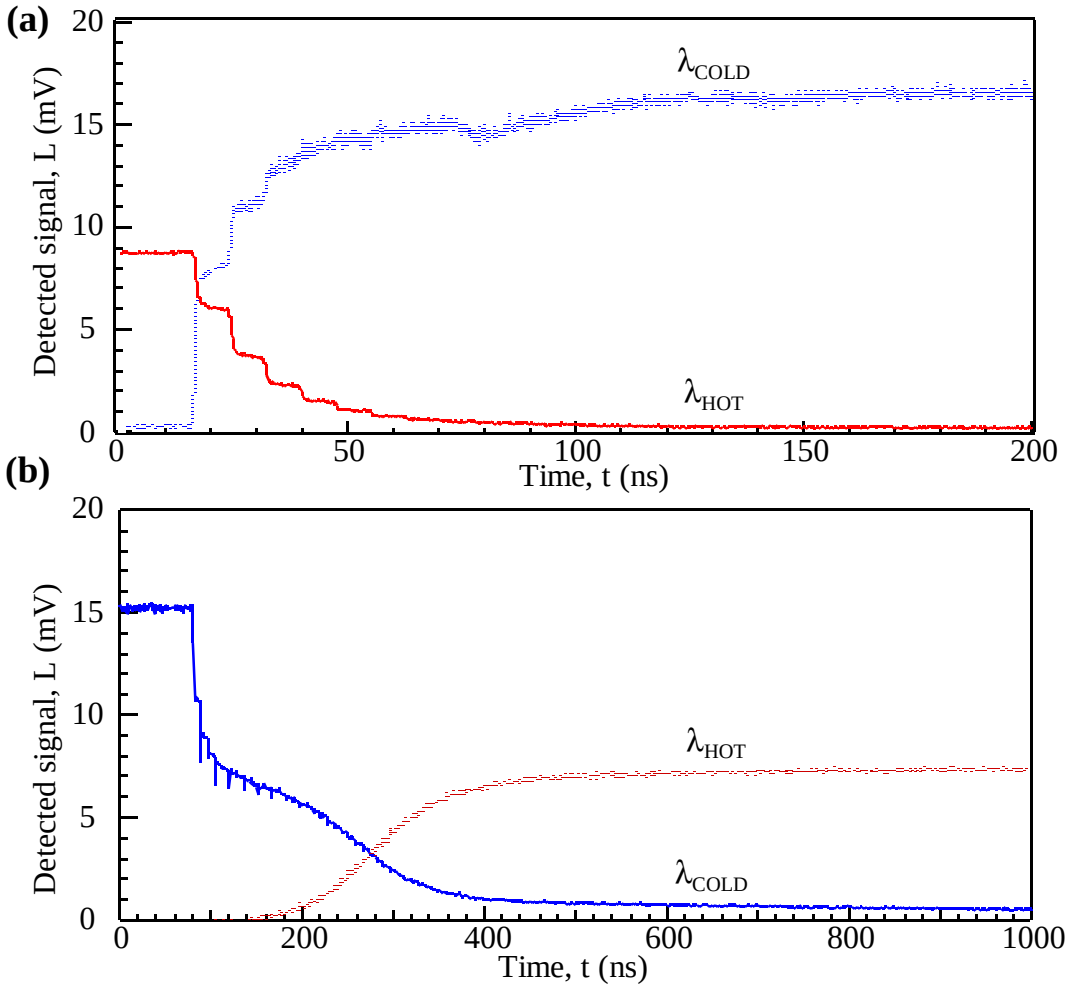

Fig. 3.12 The transient switching response obtained experimentally when cold light is injected into the cavity.
The device is biased, at I_{DC} = 18 mA, slightly above the threshold current (I_{th} = 14 mA). The output of the laser at this bias current before any optical injection is ~ 150 μW. We estimate that about 200 μW at λ_{COLD} is injected into the laser. (a) The transients involved in switching to λ_{COLD} with the injection of light. (b) Temporal response involved in switching back to λ_{HOT} when the light injection is turned off.

3.4.2 Model and results of numerical simulation

Spatially dependent photon density rate equations [6] are used to model the multi-cavity laser. In the model

$$\frac{d}{dt}\mathbf{S}^{+}(\lambda_i) + v_g\frac{d}{dz}\mathbf{S}^{+}(\lambda_i) = (G_i - \kappa_i)\mathbf{S}^{+}(\lambda_i) + (\beta_i/2)R_{sp} \qquad \text{(Eq. 3.1)}$$

$$\frac{d}{dt}\mathbf{S}^{-}(\lambda_i) + (-v_g)\frac{d}{dz}\mathbf{S}^{-}(\lambda_i) = (G_i - \kappa_i)\mathbf{S}^{-}(\lambda_i) + (\beta_i/2)R_{sp} \qquad \text{(Eq. 3.2)}$$

$$\frac{d}{dt}N(z,t) = \frac{I}{eV} - \sum_{i=cold}^{hot} G_i(\mathbf{S}^{+}(\lambda_i) + \mathbf{S}^{-}(\lambda_i)) - R_{sp} \qquad \text{(Eq. 3.3)}$$

where S^+ is the photon density moving to the right, S^- is the photon density moving to the left, $N(z,t)$ is the electron carrier density, v_g is the photon group velocity, G_i (κ_i) is the optical gain (internal loss) at wavelength λ_i, R_{sp} is the spontaneous emission power and β_i is the spontaneous emission factor. The boundary condition at the cleaved facet of the laser for photons at optical wavelength λ_{COLD} is

$$\mathbf{S}^{+}(0;t;\lambda_{cold}) = R_1 \times \mathbf{S}^{-}(0;t;\lambda_{cold}) + \mathbf{S}_{inj} + k\sqrt{S_{inj} \times R_1 \times \mathbf{S}^{-}(0;t;\lambda_{cold})} \qquad \text{(Eq. 3.4)}$$

where S_{inj} is the number of photons injected into the cavity from the non-AR coated facet side and R_1 is the reflectivity of the cleaved facet. The square root term takes into account the interference due to the coherent addition of the electric fields. For the sake of simplicity, the constant k in the equation is set to unity. The boundary condition for photons at the hot wavelength at the cleaved facet of the laser is

$$\mathbf{S}^{+}(0;t;\lambda_{HOT}) = R_1 \times \mathbf{S}^{-}(0;t;\lambda_{HOT}) \qquad \text{(Eq. 3.5)}$$

The boundary conditions at the AR coated facet of the laser are

$$\mathbf{S}^{-}(L_C;t;\lambda_{COLD}) = R_{COLD} \times C^2 \times \mathbf{S}^{+}(L_C;(t-\tau_{COLD});\lambda_{COLD}) \qquad \text{(Eq. 3.6)}$$

$$\mathbf{S}^{-}(L_C;t;\lambda_{HOT}) = R_{HOT} \times C^2 \times \mathbf{S}^{+}(L_C;(t-\tau_{HOT});\lambda_{HOT}) \qquad \text{(Eq. 3.7)}$$

where R_1 is the reflectivity (at both the wavelengths) of the non-AR coated facet, $\tau_{HOT\,(COLD)}$ is the round-trip time for the hot (cold) photons, C is the optical coupling factor between the semiconductor laser and the lensed single mode fiber, and $R_{HOT(COLD)}$ is the reflectivity of the grating at the corresponding wavelength. To simplify our analysis, although the FWHM of the Bragg grating may contain more than one external-cavity longitudinal mode, we solve only the single-mode rate equations.

An AR-coated semiconductor laser of cavity length, L_C = 300 μm and external cavity

lengths of L_{COLD} = 6.67 cm and L_{HOT} = 5.0 cm is used. The non-AR coated facet has a reflectivity, R_1 = 0.32 at both the wavelengths and the reflectivity of the gratings at their respective center wavelengths is R_{HOT} = 0.90 and R_{COLD} = 0.90. The coupling between the semiconductor laser and the lensed single mode fiber, C = 0.45. Internal loss in the semiconductor laser diode of 10 cm^{-1} at the hot and cold wavelength is assumed. A linear model of the gain is used in our analysis with a gain slope of 4.40×10^{-16} $cm^{-2}s^{-1}$ at the cold wavelength and 4.70×10^{-16} $cm^{-2}s^{-1}$ at the hot wavelength. Homogeneous gain compression of 2×10^{-17} cm^3 and spontaneous emission factor of $\beta = 10^{-4}$ at both the wavelengths is assumed. The values chosen are typical of 1.3 μm InGaAsP lasers [7] and we assume that λ_{HOT} and λ_{COLD} are approximately 1.3 μm with about 10.0 nm separation between them.

The numerical simulation was done by S. M. K. Thiyagarajan. The simulated device has a threshold of I_{DC} = 9 mA in the external cavity. If the active region is excited by a constant D.C. bias current, $I_{DC} > I_{th}$, the laser produces photons at the hot wavelength when $S_{inj} = 0$. However, when photons at the cold wavelength (~100 μW) are continuously injected as shown in Fig. 3.13(a), we see wavelength switching as shown in Fig. 3.13(c and d). The injection of cold photons alters the effective photon lifetime (optical loss) and thereby causes wavelength switching. This is confirmed by the fact that the average carrier density decreases after the laser switches to λ_{COLD}. Fig. 3.13(b) shows the transient response of the average carrier density in the semiconductor during wavelength switching. The presence of steps/discontinuities at each round trip time, a signature of external cavity laser buildup[3.8][3.9], is clearly seen in Fig. 3.13(b-d). Further, it is of interest to note that the 50% rise time for switching to the cold wavelength is only 2-3 round trips.

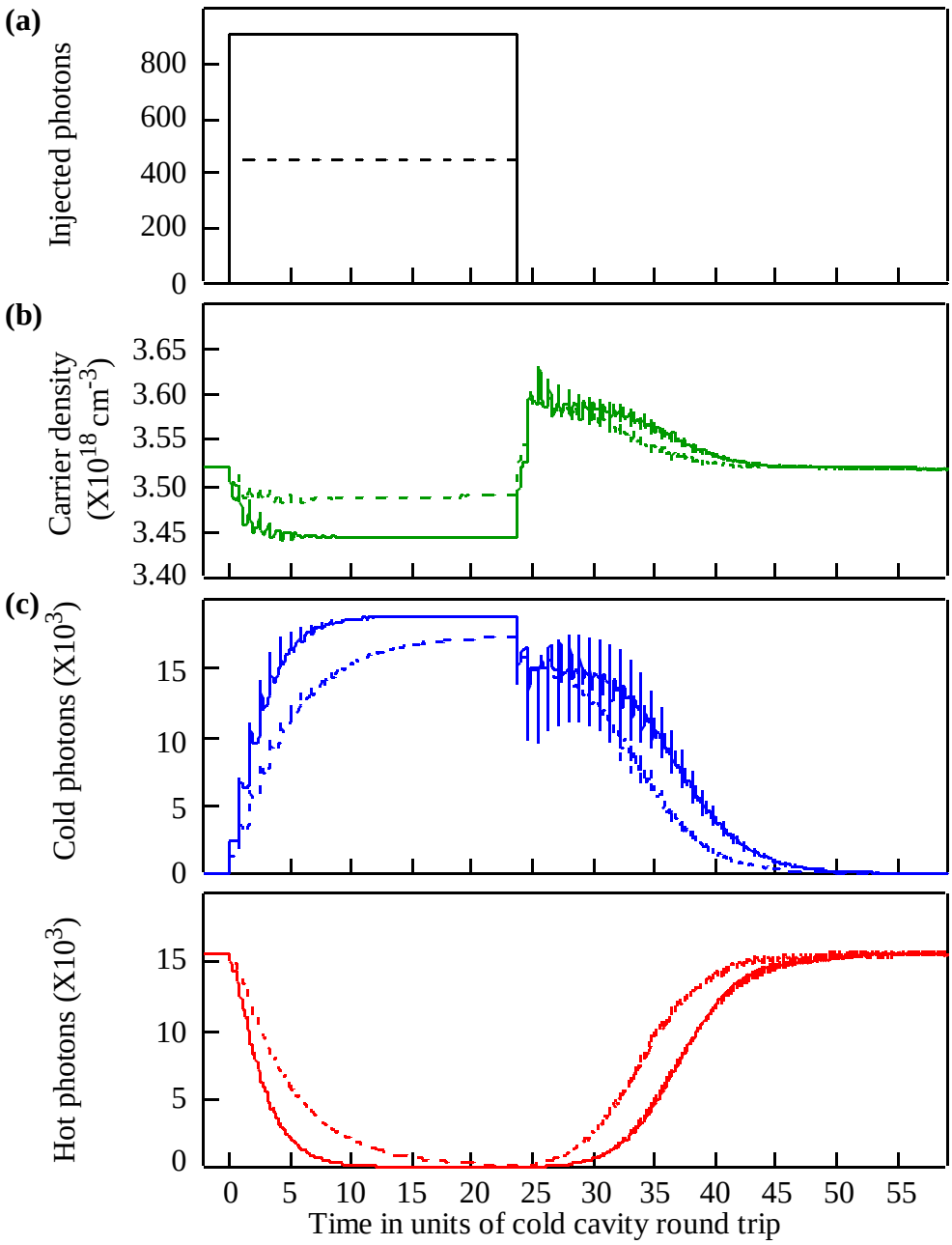

Fig. 3.13 The simulated transient switching response when a fixed number of cold photons are continuously injected into the lasing region.
The laser is biased at I_{DC} = 18 mA and the threshold current I_{th} = 9 mA with a light output of ~1.75 mW from the non-AR coated facet before cold photons are injected. The dashed curves correspond to a smaller photon injection and the solid curves for the larger photon injection. (a) The number of cold photons injected into the cavity (~ 200 μW for the solid curve and ~100 μW for the dashed curve) to effect wavelength switching. (b) The temporal response of the average carrier density within the semiconductor region during wavelength switching. (c) The dynamics of the build up /decay of the total

number of cold photons in the cavity during wavelength switching. (d) The total number of hot photons in the cavity as a function of time.

After the photon injection is turned off, we see from the figure that the laser switches back to lasing at λ_{HOT} and P_{COLD} decreases. The ringing in P_{HOT} after switching back to lasing at λ_{HOT} is due to the presence of an external cavity and the ringing decays down after a few round trips. It is of interest to note that switching back to λ_{hot} takes about 10-20 round trips. Switching back from λ_{COLD} to λ_{HOT} consists of 2 regimes, namely, regime(a) consisting of the first 2-3 round trips after turning off light injection and regime(b) about 10-20 roundtrips after regime(a). During regime (a), the average carrier density in the active region increases to a value so as to sustain laser oscillation at λ_{COLD}. This increase in the carrier density is accounted for by a decrease in the number of cold photons in the cavity. However, the laser is still lasing at λ_{COLD} but with fewer number of cold cavity photons. Regime (b) consists of the buildup of hot photons and decay of cold photons and carriers to the value present before any light injection. This is analogous to the case when the laser switches from lasing at λ_{HOT} to λ_{COLD}. However, it takes longer to switch back to λ_{HOT} because of the relative values of gain/loss at this carrier density for both the wavelengths.

The effect of decreasing the CW photon injection on the switching transients can also be seen from Fig. 3.13 (dashed curves). Decreasing the photon injection, causes a decrease in the change in effective cold photon lifetime, i.e. decrease in the difference between effective cold photon lifetime and hot photon lifetime. This causes the rise time to increase and the number of cold photons to decrease. The time needed to switch back to λ_{HOT} after a lower light injection is turned off is smaller. This is due to an increase in the number of hot photons present, just before turning off light injection, at lower injection levels.

Although our model is very simplistic, e.g. we have ignored mode pulling due to

injection locking, bistability, hysteresis etc., it nonetheless predicts qualitatively the experimental results presented earlier.

3.5 Conclusion

In this chapter we have studied the cavity switching dynamics of the MCL. The switching time of the MCL operating as a SR flip-flop is limited by the timing jitter as well as turn-on delay of photons building up from the spontaneous emission noise to between 1 and 10 ns. The timing jitter as well as the turn-on delay are dramatically reduced when switching to a lasing state if the device is seeded using an optical pulse by photons at the wavelength corresponding to that state. The switching time in this case is about 0.3 ns. As the optical pulse decreases n in the semiconductor it cannot be used to switch the device from a state with a lower steady state n to a state with higher steady state n. We also see that the coupling between the carrier and photon dynamics while switching states causes oscillations in the light output thus increasing the switching time.

Optical injection is also used to select the lasing cavity of the MCL. The cavity switches when coherent light injection is used to select the lasing cavity in about 2 round-trips.

Results presented in this chapter indicate that for high speed wavelength switching (less than 100 ps) carrier densities in the different sections of the device should not change while switching wavelengths. Fast switching times also mean that the MSR of the light output is low so as to reduce the photon turn-on time. This condition may be relaxed if coherent optical injection is used to switch the lasing wavelength.

3.6 References

3.1 K. Berthold, A. F. J. Levi, T. Tanbun-Ek and R. A. Logan, "Wavelength switching in InGaAs/InP quantum well lasers," Appl. Phys. Lett., **56**, pp. 122-124 (1990).

3.2 A. P. Kanjamala, and A. F. J. Levi, "Wavelength switching in multi-cavity lasers," Appl. Phys. Lett., **71**, pp. 300-302 (1997).

3.3 F. Delorme, P. Gambini, M. Puleo, and S. Slempkes, "Fast tunable 1.5 μm distributed Bragg reflector laser for optical switching applications," Electron. Lett., **29**, pp. 41-43 (1993).

3.4 B. Glance, U. Koren, R. W. Wilson, D. Chen, and A. Jourdan, "Fast optical packet switching based on WDM," IEEE Photon. Technol. Lett., **4**, pp. 1186-1188 (1992).

3.5 O. Hildebrand, M. Schilling, W. Idler, D. Baums, W. Idler, K. Dutting, G. Laube, and K. Wunstel, "The Y-laser - a multifunctional device for op[tical communication-systems and switching-networks," J. Lightwave Technol., **11**, pp. 2066-2075 (1993).

3.6 K. Kojima, "High-power, high-efficiency, highly uniform 1.3 μm InGaAsP/InP strained MQW lasers," Optical Fiber Communications Conference, OSA Technical Digest Series (ISBN 1-55752-368-1) **8**, pp. 253-254, 1995.

3.7 R. Lang, "Injection locking properties of a semiconductor laser," IEEE J. of Quant. Elec., **18**, pp. 976-983 (1982).

3.8 N. A. Olsson, and W. T. Tsang, "Transient effects in external cavity semiconductor lasers," J. Quantum Electron., **19**, pp. 1479-1481 (1983).

3.9 J. O'Gorman, A. F. J. Levi, D. Coblentz, T. Tanbun-Ek, and R. A. Logan, "Cavity formation in semiconductor-lasers," Appl. Phys. Lett., **61**, pp. 889-891 (1992).

Chapter 4 : Cavity switching using RF modulation

4.1 Introduction

The emergence of wavelength division multiplexing as a viable method to transmit information has spurred the need for high speed wavelength tunable lasers [4.1]. In a tunable laser a control input, which varies the wavelength dependent loss/gain, is used to select the lasing wavelength. Bragg gratings (BGs) with different center wavelengths define distinct laser cavities of a multi-cavity laser (MCL). The different cavities of a MCL have distinct photon cavity round-trip times due the differences in the cavity lengths. In MCLs, the effective gain/loss, is dependent on the cavity round-trip time. Hence, a large RF signal tuned to the photon cavity round-trip time of a BG defined cavity of MCL, could be used to select the wavelength defined by that BG as the lasing wavelength. A similar idea is used to select the lasing wavelength of actively mode-locked optical pulses from a laser diode using radio frequency (RF) modulation in Refs. [4.2] and [4.3]. In Refs. [4.2] and [4.3] a chirped grating is used to provide optical feedback. Recently, Huhse and co-workers recognized that the lasing wavelength could be switched using an RF signal in gain switched self-seeded external cavity lasers [4.4].

The next section presents experimental results of wavelength selection of lasing light output from a MCL by applying an RF signal to the laser gain section. Section 4.3 presents a detuning curve for the pulse width of optical pulses versus RF signal frequency obtained from the MCL when modulated by an RF signal. Experimentally measured transient dynamics of cavity switching using an RF signal is presented in section 4.4. Results of numerical simulation of cavity switching using the travelling wave model of the laser is discussed in section 4.5. Section 4.6 presents an experimental demonstration of digital data transmission using the RF signal to select the transmission optical wavelength. It also presents results that show that the MCL can

be used to transmit wavelength encoded digital data. Timing jitter of the mode locked pulses when switching the lasing cavity is presented in section 4.7.

4.2 Wavelength selection using RF signal

Semiconductor lasers have a resonance at the photon cavity round-trip time. In monolithic semiconductor laser devices the round-trip time is a few picoseconds corresponding to an RF frequency of 70 to 140 GHz. As the device packaging parasitics prevent the laser from responding to signals in that frequency range this resonance is often ignored when studying laser dynamics. In external cavity lasers where the frequency corresponding to the round-trip time is usually in the GHz range or less this resonance is clearly seen in the small signal RF response of the laser [4.5]. In this section the resonance is used to select the wavelength of the pulsed light output of the MCL.

Inset in Fig. 4.1(a) shows a schematic of the experimental arrangement. Optical emission at λ = 1.3 μm wavelength from the anti-reflection (AR) coated side of a multi-quantum well semiconductor laser diode [4.6] is coupled with 45% efficiency into a lensed single-mode fiber containing 10 Bragg gratings. The fiber gratings [4.7],[4.8],[4.10] are spaced 2 mm apart with center wavelengths placed at approximately 1 nm intervals covering the spectral range from λ = 1307 nm to λ = 1316 nm. The steady-state light-current (L-I) characteristics of the laser diode in this cavity is shown in Fig. 4.1(b). The threshold of the laser in the external cavity is I_{th} = 9 mA and the inset in the figure shows the optical spectrum under steady-state current bias, I_{DC}

= 30 mA.

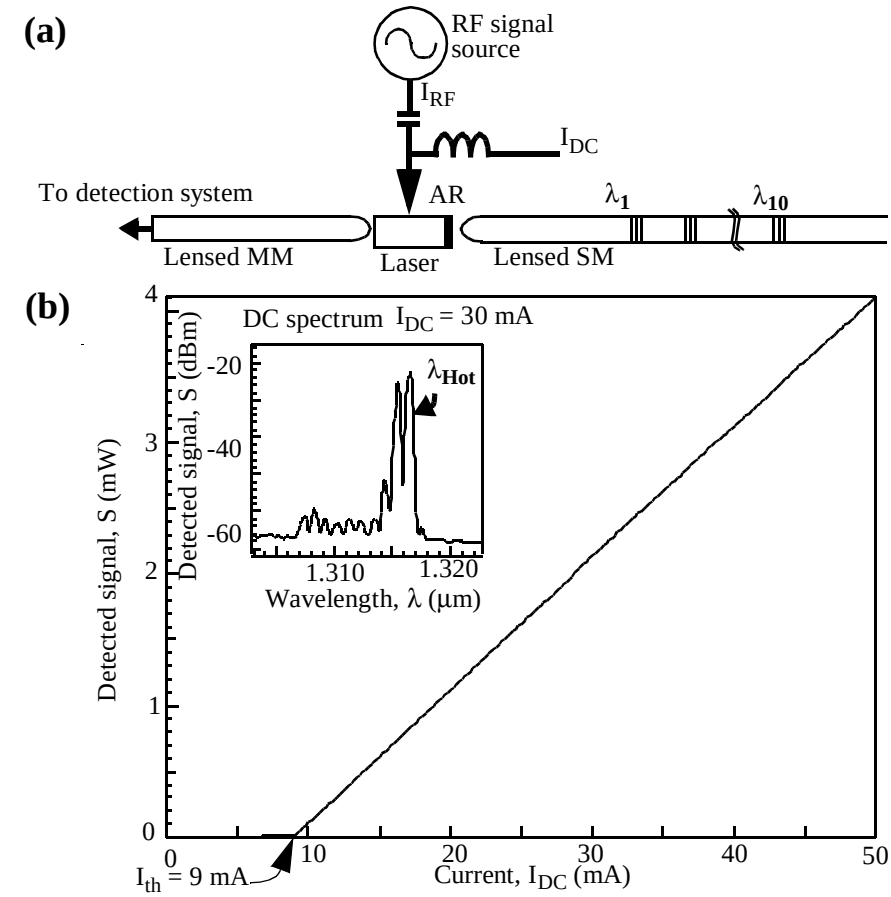

Fig. 4.1 Shows the experimental arrangement and the static device characteristics of the MCL. **(a)** Experimental arrangement to study the transient characteristics of an external cavity actively mode-locked laser diode. The AR coated laser obtains optical feedback from BGs embedded in the single mode fiber which is used to define lasing wavelength λ, cavity length L, and resonance frequency f. **(b)** External cavity laser diode L-I characteristic showing I_{th} = 9 mA. The insert shows the optical spectrum for I_{DC} = 30 mA with λ_{Hot} = 1316.5 nm. The as-cleaved multi-quantum well laser diode had I_{th} = 6 mA.

Actively mode-locked light output is switched to a particular wavelength by applying a radio frequency (RF) signal to the diode which corresponds to a grating-defined photon cavity round-trip time, τ_{CAV}. Any one of the wavelengths determined by the BG is selected by applying an RF signal at the appropriate frequency and mode-locking the laser light output as shown in Fig. 4.2.

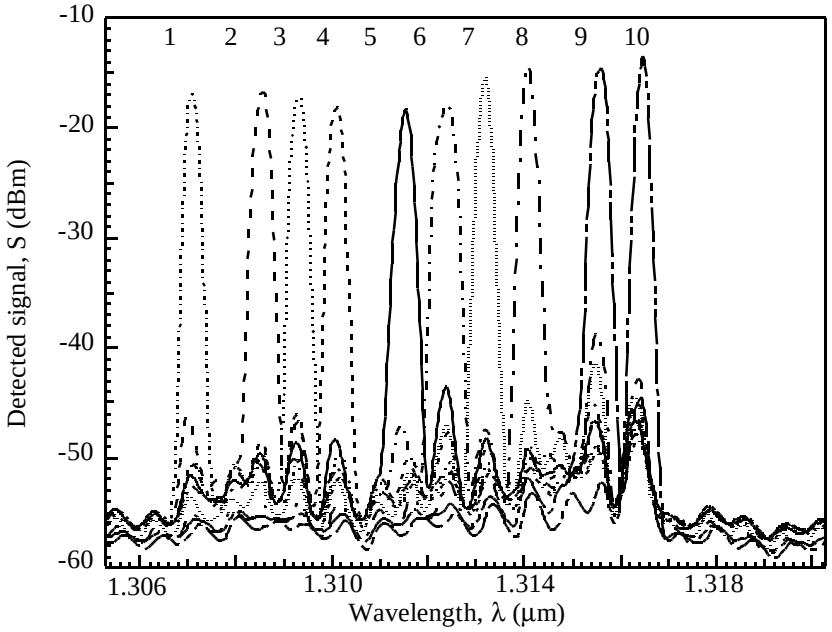

Fig. 4.2 Optical Spectra obtained when the RF signal modulating the laser is used to select wavelength of laser light emission.
The laser is in the external cavity shown in Fig. 1. The single mode fiber contains BGs 2mm apart centered at 10 different wavelengths. The optical wavelengths of the gratings are about 1nm apart. The laser is biased at 11mA. RF Signals used to select the 10 wavelengths are : 1:

1: 2.320GHz selects λ at 1307nm. 2: 2.280GHz selects λ at 1308.5nm.
3: 2.16GHz selects λ at 1309.3nm 4: 2.058GHz selects λ at 1310nm.
5: 1.992GHz selects λ at 1311.5nm. 6: 1.932GHz selects λ at 1312nm.
7: 1.84GHz selects λ at 1313.2nm. 8: 1.769GHz selects λ at 1314nm.
9: 1.722GHz selects λ at 1315.5nm. 10:1.632GHz selects λ at 1316.4nm.

The optical discrimination ratio is greater than -25dB.

4.3 Detuning curve

Active mode-locking results in gain modulation due to the injection of RF current at the frequency corresponding to the photon cavity round-trip time. Active mode locked lasers emit short optical pulses at the photon cavity round-trip time. Laser diodes also emit short pulses when gain switched. Unlike gain switching, the pulse width of active mode locked pulses is influenced by frequency of the applied RF signal. As the frequency of the applied RF is tuned to lower frequencies than the photon cavity round-trip frequency, f_{CAV}, the pulse width of the modelocked pulses decreases [4.10]. The laser partially compensates for the detuning by advancing the

phase of the pulse. For large negative detuning the laser is no longer mode locked and there is a rapid increase in optical pulse width. The pulse width increases as the applied RF frequency is tuned higher than f_{CAV}.

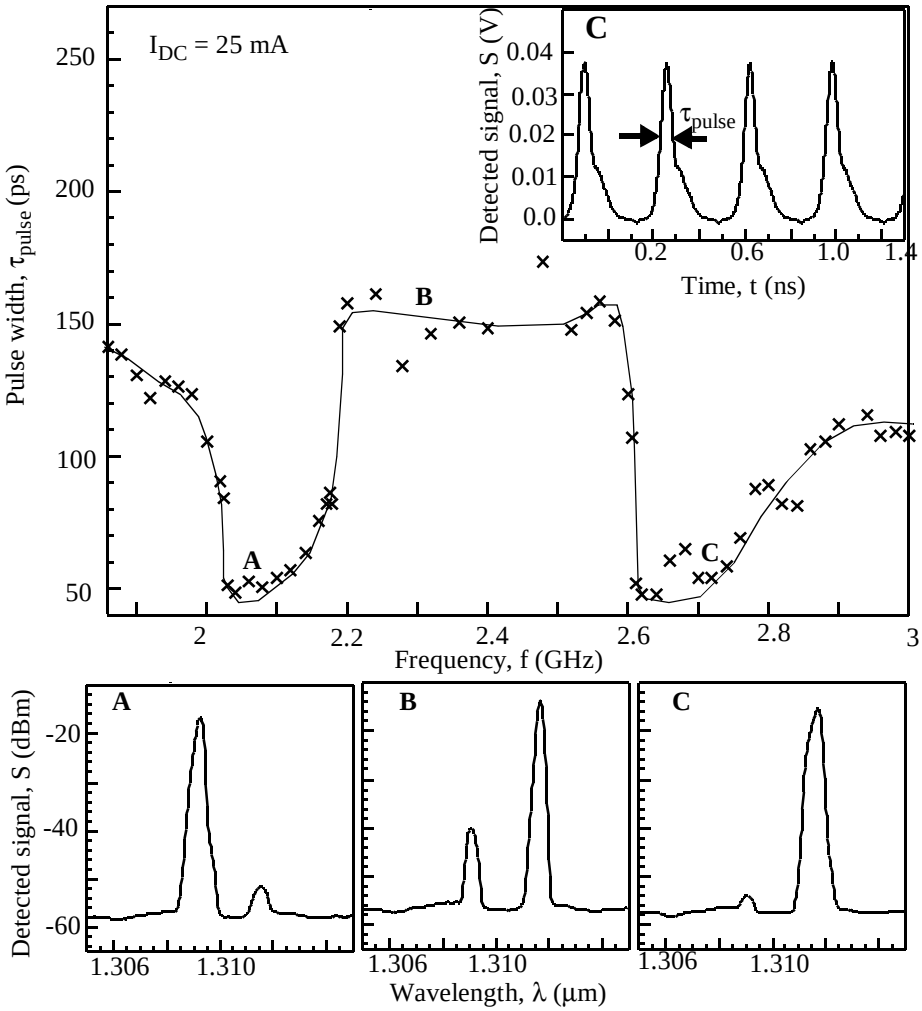

Fig. 4.3 Measured full width half maximum pulse width τ_{pulse} as a function of applied RF for an actively mode-locked external fiber grating cavity laser diode.
The laser is biased at I_{DC} = 25 mA and a small fraction of the applied 24 dBm RF signal power is absorbed by the laser due to impedance mismatch. The linear BGs are 1 cm apart, centered at wavelength λ = 1309 nm and λ = 1312 nm, and exhibit cavity resonances at 2.14 GHz and 2.74 GHz.

Fig. 4.3 shows measured optical pulse width, τ_{pulse}, as a function of RF detuning for an external cavity formed using linear fiber gratings centered at λ = 1312 nm and λ = 1309 nm spaced 1 cm apart. As expected for an actively mode-locked device

[4.10], τ_{pulse} decreases sharply as the applied RF approaches cavity resonances defined by the two Bragg gratings from lower frequencies. τ_{pulse} increases gradually as the RF frequency is tuned higher than the photon cavity round-trip frequency. The minima in pulse width at frequency f = 2.14 GHz and f = 2.74 GHz correspond to 1/ τ_{CAV} for each Bragg grating defined cavity. The locking range is determined by the approximate 2 mm length of the linear Bragg grating.

4.4 Switching transients

An RF signal applied to the MCL at a photon cavity round-trip frequency of a BG defined cavity selects that BG defined cavity as the lasing cavity. In this section the cavity switching transients are measured.

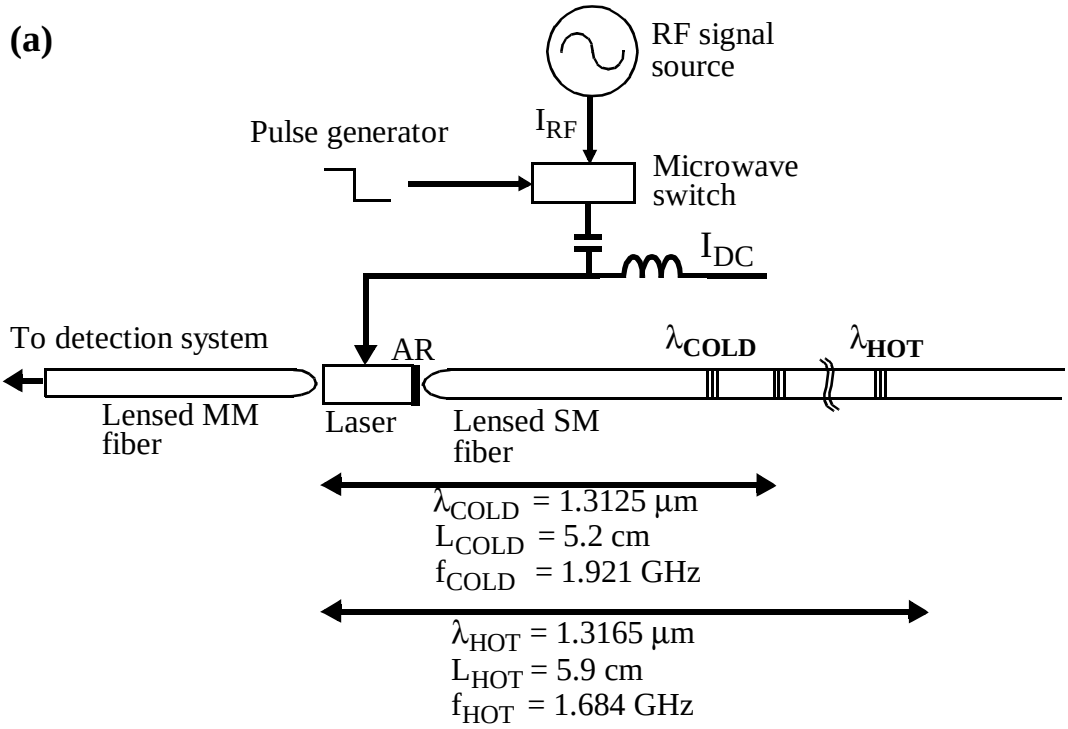

Fig. 4.4 Experimental arrangement to study the transient characteristics of an external cavity actively mode-locked laser diode.
The AR coated laser obtains optical feedback from Bragg gratings embedded in the single mode fiber which is used to define lasing wavelength λ, cavity length L, and resonance frequency f.

Fig. 4.4 shows the experimental arrangement used to measure transient response. Spectrally resolved transient response is measured using a microwave switch to gate the RF signal, a spectrometer to select detected wavelength, a high-speed detector and sampling oscilloscope.

Fig. 4.5 illustrates results of measuring transient response using a microwave switch to turn on the RF signal applied to the laser diode. As shown in Fig. 4.5(a), the applied RF signal has a 1 ns response time. In these experiments the diode is biased at I_{DC} = 30 mA so that prior to applying the RF signal the laser light output has spectral components at λ = 1316.5 nm and λ = 1315.5 nm (see Fig. 4.5(d)). If the applied RF signal selects a mode-locked lasing wavelength which is already lasing we define this to be a "hot photon cavity". The results shown in Fig. 4.5(b) indicate that it takes approximately two photon cavity round-trips after the RF signal, f_{HOT} = 1.684 GHz, is applied for the laser to switch its mode-locked output to the wavelength λ_{HOT} = 1316.5 nm. If the applied RF signal selects a mode-locked lasing wavelength which is not already lasing we define this to be a "cold photon cavity". The results in Fig. 4.5(c) show that by applying an RF signal, f_{COLD} = 1.921 GHz, the lasing wavelength can be switched to λ_{COLD} but it takes 5 photon cavity round-trips for the λ = 1316.5 nm wavelength component to decay after which the spectral intensity at λ_{COLD} starts to grow with a 50% rise time of 7 photon cavity round-trips.

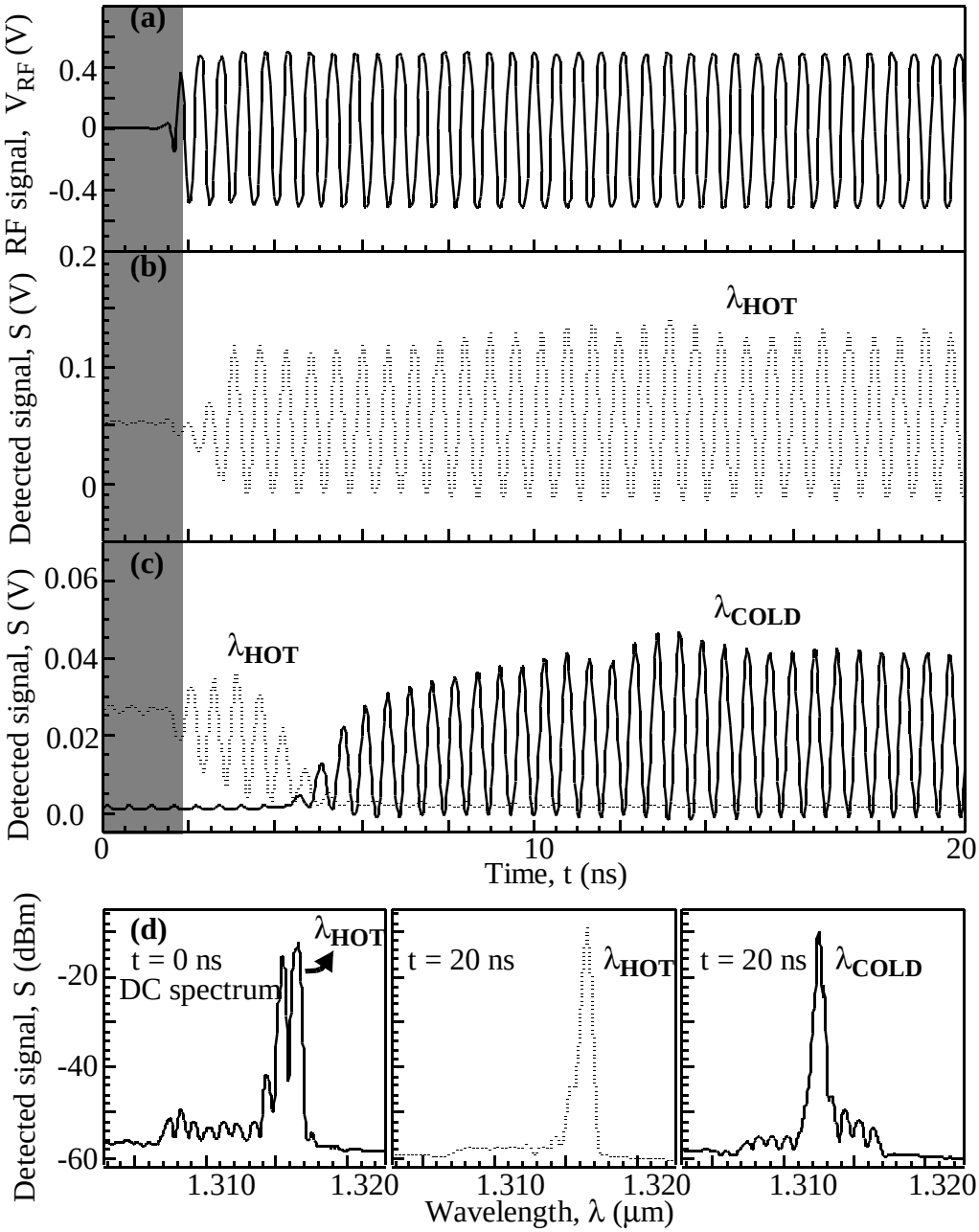

Fig. 4.5 Transient response of the MCL when switching the lasing cavity using an RF signal to modulate the semiconductor gain section.
(a) Transient RF waveform applied to the laser diode. 24dBm of RF signal power incident on the laser is used to switch the optical wavelength of the light output. **(b)** Hot photon cavity response to achieve active mode-locking using f_{HOT} = 1.684 GHz, λ_{HOT} = 1316.5 nm and I_{DC} = 30 mA. **(c)** Cold photon cavity response to achieve active mode-locking using f_{COLD} = 1.921GHz, λ_{COLD} = 1312.5 nm and I_{DC} = 30 mA. It takes 5 photon cavity round-trips for the λ = 1316.5 nm wavelength component to decay after which the spectral intensity at λ_{COLD} starts to grow with a 50% rise time of 7 photon cavity

round-trips. **(d)** Optical spectrum at the indicated times.

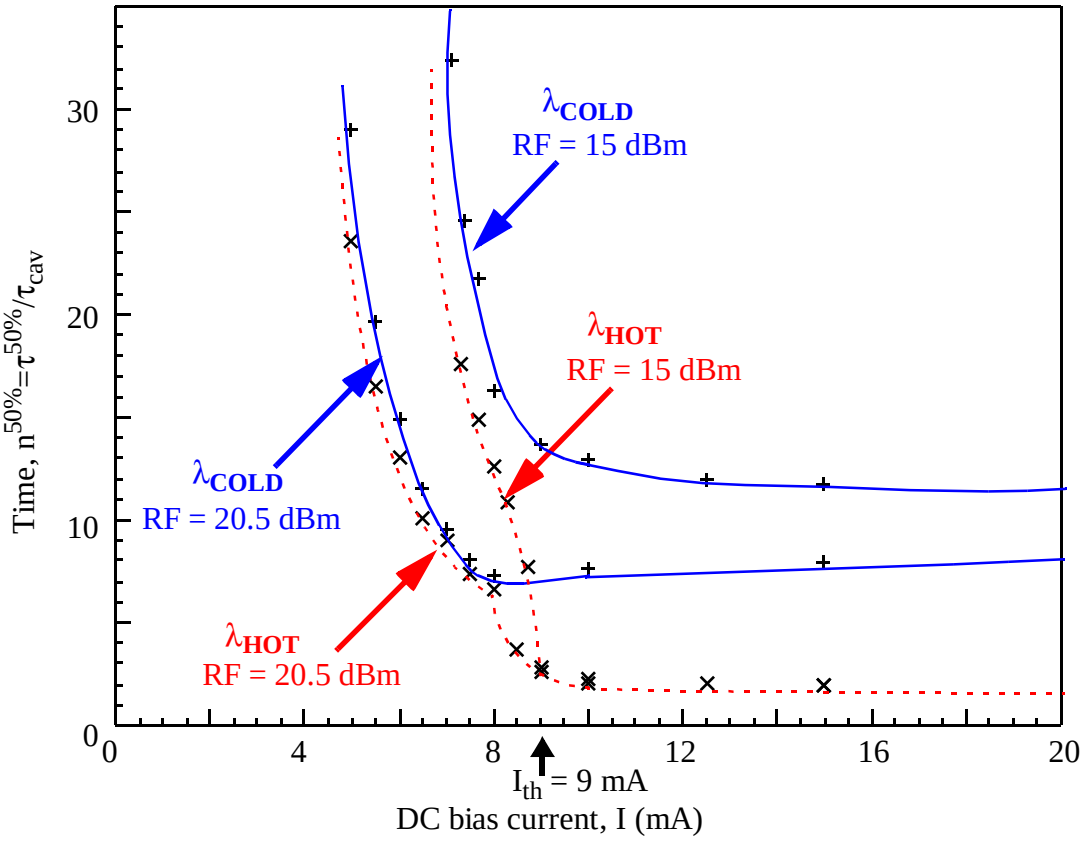

Fig. 4.6 Normalized transient time, $n^{50\%} = \tau^{50\%}/\tau_{CAV}$, for the laser to reach 50% of the steady-state response after the switch is turned on for different bias conditions.
Above threshold, the transient time for λ_{HOT} is 2 round-trips independent of I_{DC} and incident RF signal power while that for λ_{COLD} decreases with increase in RF signal power. Below threshold, the transient response of λ_{HOT} tends to that of λ_{COLD}, increasing with decrease in I_{DC} and RF signal power.

The transient time $\tau^{50\%}$ to reach 50% of the steady-state value after the switch is turned on can be normalized to τ_{CAV} by defining $n^{50\%} = \tau^{50\%}/\tau_{CAV}$. In Fig. 4.6 we show results of measuring $n^{50\%}$ as a function of I_{DC} for both hot and cold photon cavities and for different applied RF signal powers. When $I_{DC} > I_{th}$ the value of $n^{50\%}$ for the hot photon cavity is independent of the RF signal power and I_{DC}. For $I_{DC} < I_{th}$ the transient response time increases rapidly with decreasing I_{DC}. Below threshold $n^{50\%}$

decreases with increasing RF signal power.

The transient response time of the cold photon cavity decreases with increase in RF signal power. Above threshold $n^{50\%}$ for λ_{COLD} is independent of I_{DC} and depends on the RF signal power. Below threshold there is an increase in the transient time for λ_{COLD} with decrease in I_{DC} at all RF signal power levels. The increase in $n^{50\%}$ with decrease in DC bias current just below threshold is more rapid for λ_{HOT} than for λ_{COLD}. As the laser is biased further below threshold the transient response time for λ_{HOT} tends towards that of λ_{COLD}. This suggests that the transient response time when switching lasing wavelength and cavity length depends on the number of "hot photons", photons corresponding to the wavelength and lasing cavity switched to, present initially before the RF signal is turned on.

4.5 Model and numerical simulation

Spatially dependent photon density rate equations [4.11] are used to model the multi-cavity laser. We use the model described in section 3.4.2 with boundary condition for the cold wavelength at the non-AR coated facet modified from equation Eq. 3.4 to

$$\mathbf{S}^{+}(0;t;\lambda_{COLD}) = R_1 \times \mathbf{S}^{-}(0;t;\lambda_{COLD}) \qquad \text{(Eq. 4.1)}$$

where R_1 is the reflectivity, at both the wavelengths, of the non-AR coated facet. To simplify our analysis, although the FWHM of the Bragg grating may contain more than one external cavity longitudinal mode, we solve only the single mode rate equations.

The numerical simulation presented in this section was done by S. M. K. Thiyagarajan. The threshold current of the simulated device is, $I_{th} \sim 9$ mA. The simulated L_{out}-I characteristics match that of the experimental device seen in Fig. 4.1. Lack of carrier pinning above threshold due to gain compression is seen in the simulations.

Fig. 4.7(a) shows the rectifying action of the laser diode on RF current flow. After time t = 0, the sinusoidal current amplitude is $I_{RF} = 3xI_{th}$ superimposed on a steady-state current I_{DC} = 18 mA. In the model, only positive current flows through the diode. Shown in Fig. 4.7(b) and (c) is the calculated temporal evolution of wavelength switching in the multi-cavity laser due to an RF signal tuned to the cold cavity resonance. The RF signal drives the laser below threshold during portions of the negative half cycle and hence causes gain switching to occur. Since the RF signal is tuned to the cold cavity resonance, the average dynamic gain seen by the cold wavelength is larger than that seen by the hot wavelength. Hence, the lasing wavelength changes from the hot wavelength to the cold wavelength. Fig. 4.7(c) shows that about 7-8 round-trips are needed to switch to the cold wavelength. The transient switching time is determined by the relative dynamic gain at each wavelength and the fact that photons at the hot wavelength must first be reduced before increasing the number of photons at the cold wavelength. There are some spike-like features in the optical power output at the hot wavelength even after the average value has been suppressed. This is due to the difference in the round-trip times for the hot and cold photons which affect each other directly through gain compression and indirectly through carrier density variation.

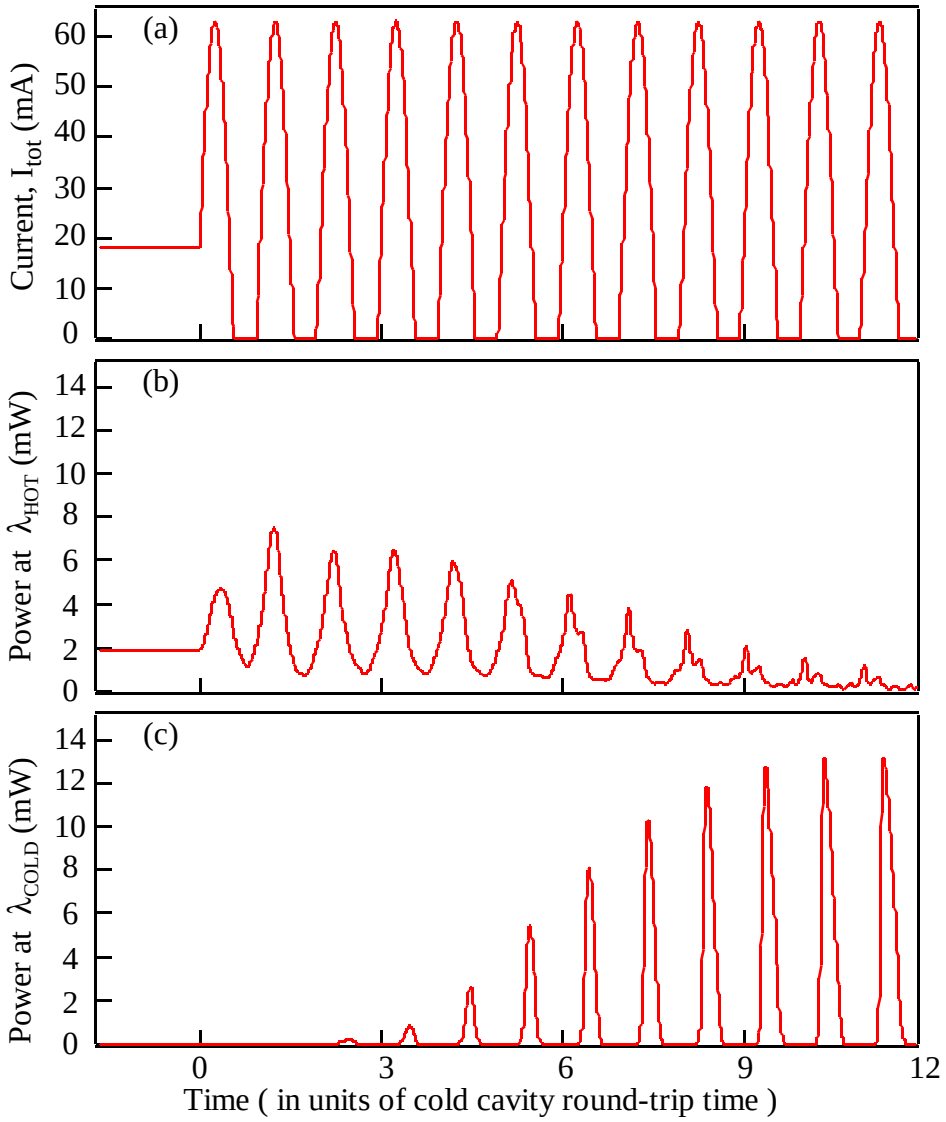

Fig. 4.7 Transient switching response when an RF signal tuned to the cold cavity resonance is turned on.
(a) Total current, I_{tot}, input to the laser, with $I_{DC} = 2xI_{th}$ and $I_{RF} = 3xI_{th}$. **(b)** The response of the hot photons. **(c)** Pulse build-up dynamics of the cold photons. It takes about 7 round-trips for the cold wavelength to build up and reach 50% of the steady state intensity. Dashed curve is the light output at the hot wavelength and the solid curve is the light output at the cold wavelength.

Fig. 4.8 shows the effect of bias current I_{DC} and the RF current I_{RF} on the calculated rise time for hot and cold switching. It is of interest to note that switching to the cold wavelength takes longer than switching to the hot wavelength. This is because hot

photons in the cavity must first be suppressed before significant build up of the cold photons. Further, the trends shown here agree qualitatively with the experimental results shown in Figure 4. The only discrepancy is in the case of switching to λ_{COLD} for a given RF current I_{RF}, as the bias current I_{DC} is increased above threshold. In this situation, the numerical results indicate that the switching time should increase with an increase in the bias current I_{DC} while the experimental results show that it is independent of the bias current. Naively, one expects the number of hot photons in the cavity to affect the switching transients and they increase with I_{DC}. Hence, we expect our simulations to show an increase in the cold switching time with an increase in I_{DC} above threshold. Our results show this result but the experiments do not. We tentatively ascribe the discrepancy to the simplistic model used which does not take into account the effects of modelocking and the residual reflectivity of the anti-reflection coated facet [4.12].

As shown in Fig. 4.8, the cold switching time decreases with an increase in RF current independent of the bias current. This is to be expected since RF modulation decreases the effective dynamic loss seen at the cold wavelength compared to the hot wavelength. For hot switching time, an increase in the RF modulation causes a faster turn on when biased below threshold since this decreases the effective dynamic loss at the hot wavelength. This and the cold switching case are analogous to the case wherein the turn on delay of an on-off modulated laser depends on the modulation depth. However, when the laser is biased above threshold, this effect is negligible since the device is already lasing and has hot photons in the cavity. Hence, the hot switching time is independent of the RF power when biased above threshold. An analogy would be the almost negligible dependence of the turn-on delay of an above threshold (on-on) modulated laser on the modulation depth. Intuitively, we expect the time taken to switch to λ_{COLD} to decrease, when the spectral separation between λ_{HOT} and λ_{COLD} is decreased. This is confirmed by our simulations whose results (not

shown in figure) indicate a decrease of 2 round-trips in the rise time for switching to λ_{COLD}, independent of the bias current I_{DC}, when the differential gain at λ_{COLD} is increased by approximately 2 percent. Hence, we believe that the transients are determined by the relative values of the dynamic gain and loss at both the wavelengths.

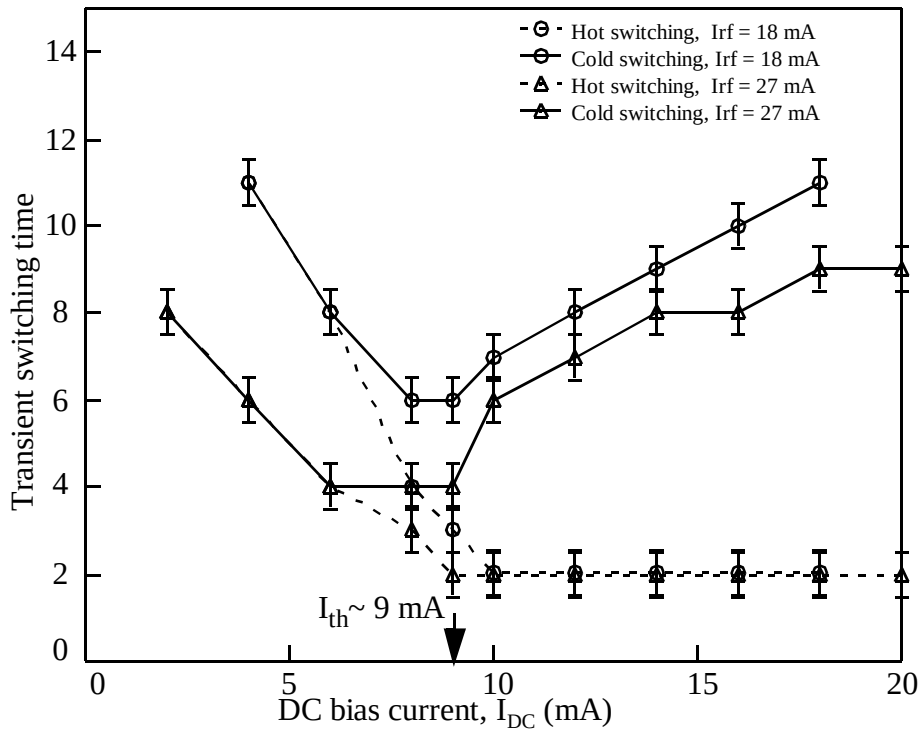

Fig. 4.8 Simulation results for cavity switching time of the MCL when the gain section is modulated by an RF signal.
Transient switching time for cold cavity switching (solid curve) and hot cavity switching (dashed curve),is plotted as a function of the DC bias current, I_{DC}, for the different indicated RF currents, I_{RF}. Note that the RF source is a voltage source capable of supplying the indicated maximum current. However, the total current $I_{tot} = (I_{DC}+I_{RF} \sin\omega_{RF}t)$ into the laser is always non-negative at any time instant. If I_{tot} becomes negative, the current into the laser is clamped to zero. The error bars in the figure are due to an uncertainty of a round-trip in the rise time.

4.6 Data transmission experiments

In the MCL the BGs define the possible wavelengths of the light output. So when an RF signal selects one of the BG defined cavities as the lasing cavity the wavelength of the pulsed light output is well defined and repeatable. The MCL is at least one order

of magnitude less sensitive to temperature variations than the DFB or DBR lasers. The results presented in this chapter indicate that an RF signal can select the wavelength of the pulsed light output of an MCL with an optical discrimination of greater than -40 dB. It is possible to switch the lasing wavelength of the MCL in about 10 photon cavity round-trips. Hence, the MCL is potentially a cheap, simple and fast wavelength selective source for applications such as WDM. In this section results of digital data transmission experiments using the MCL as the transmitter are presented.

Fig. 4.9 shows the experimental arrangement used for our data transmission experiments. A 300 μm long multiple quantum-well Fabry Perot semiconductor laser diode [4.6] has a 0.1% reflecting anti-reflection (AR) coated mirror on one side and a 32% reflecting cleaved mirror on the other. Optical emission at wavelength λ = 1310 nm from the AR coated side of the diode is coupled with 40% efficiency into a lensed single-mode fiber containing two adjacent BGs. The 1 mm long BGs have center wavelengths λ_1 = 1311.7 nm and λ_2 = 1310.4 nm, 75% reflectivity, and -3 dB optical linewidth of 0.24 nm (42.7 GHz) and 0.26 nm (46.2 GHz) respectively. The two BGs define distinct laser cavities at precise optical wavelengths. The photon cavity round-trip time in the multi-cavity laser (MCL) at wavelength λ_1 (λ_2) is approximately 112 ps (138 ps) with resonant RF frequency at f_1 = 8.950 GHz (f_2 = 7.240 GHz).

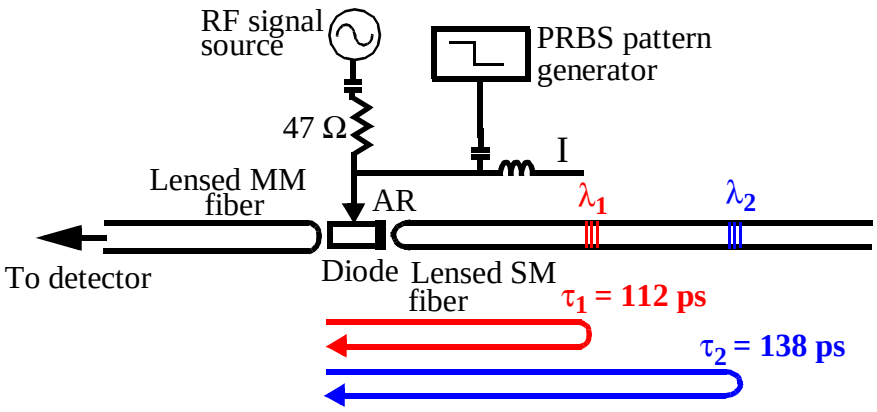

Fig. 4.9 Shows the xperimental arrangement.

Optical emission at λ = 1300 nm wavelength from the anti-reflection (AR) coated side of a multi-quantum well semiconductor laser diode is coupled with 40% efficiency into a lensed single-mode fiber containing two BGs. The BGs have center wavelengths λ_1 = 1311.7 nm and λ_2 = 1310.4 nm, reflectivity of 75%, and -3 dB optical bandwidth of 0.24 nm and 0.26 nm respectively.

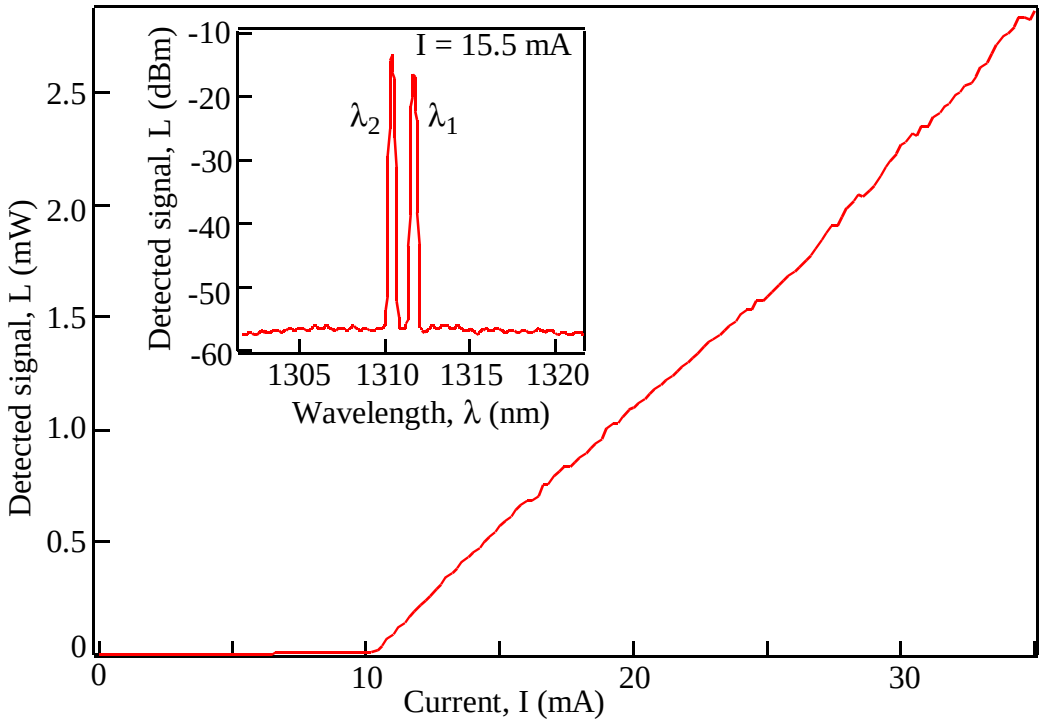

Fig. 4.10 Measured L-I of the MCL. The inset shows the measured optical spectrum when I = 15.5 mA.
Lasing occurs at wavelengths λ_1 and λ_2 corresponding to the two BGs.

The steady-state light-current (L-I) characteristics of the MCL diode with threshold current I_{th} = 10.5 mA is shown in Fig. 4.10. Small discontinuities in the L-I curve are likely due to mode hopping between longitudinal external cavity modes. The inset to Fig. 4.10 shows the optical spectrum of the MCL biased at constant current I = 15.5 mA with lasing at both BG wavelengths.

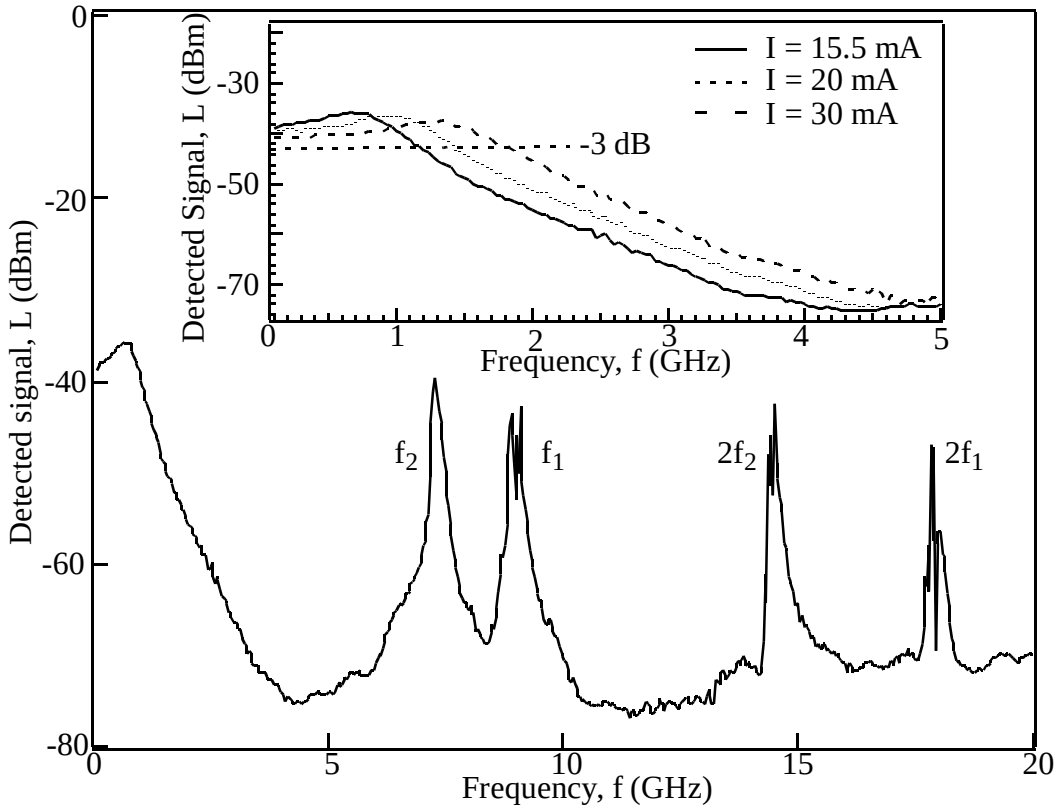

Fig. 4.11 Measured small-signal RF response of the MCL at a steady-state current bias of I = 15.5 mA. The baseband -3 dB optical bandwidth of the MCL at I = 15.5 mA is 1.2 GHz. The RF spectrum of the MCL shows 'out of band' peaks at f_1 and f_2 and their higher harmonics corresponding to the inverse photon cavity round-trip times at wavelengths λ_1 and λ_2 respectively.

The measured small-signal RF response of the MCL shown in Fig. 4.11 has 'out of band' peaks at f_1 and f_2, and their higher harmonics, corresponding to the photon cavity round-trip times of the two BG-defined cavities. At a bias of I = 15.5 mA the 'baseband' -3 dB optical bandwidth is 1.2 GHz. The inset to Fig. 4.11 shows that this -3 dB frequency increases with bias current. Gb/s digital data transmission is possible within this baseband.

Modulating the laser with a RF signal at f_1 (f_2) selects lasing wavelength λ_1 (λ_2). The RF power launched from the signal generator is 16 dBm and the laser is biased to a steady-state current I = 15.5 mA. Mode-locked pulses at λ_1 (λ_2) have a -3 dB optical

bandwidth of 0.28 nm (0.24 nm). Digital data encoded as a small signal amplitude modulation of 3 mA on the RF signal at f_1 (f_2) is applied to the MCL. A 1 Gb/s non-return to zero pseudo-random bit stream (NRZ PRBS) is generated by a pattern generator. The received optical signal is measured using a detector with a -3 dB optical bandwidth of 1.44 GHz. Fig. 4.12(a) shows the BER versus measured eye opening relative to the clock edge. The measured phase margin at a BER of 10^{-7} is 840 ps and the optical spectrum of the transmitted signal seen in the inset to Fig. 4.12(a) has a MSR of -30 dB. The measured phase margin for data transmitted with no applied RF is approximately the same as when the RF signal is used to select the lasing wavelength.

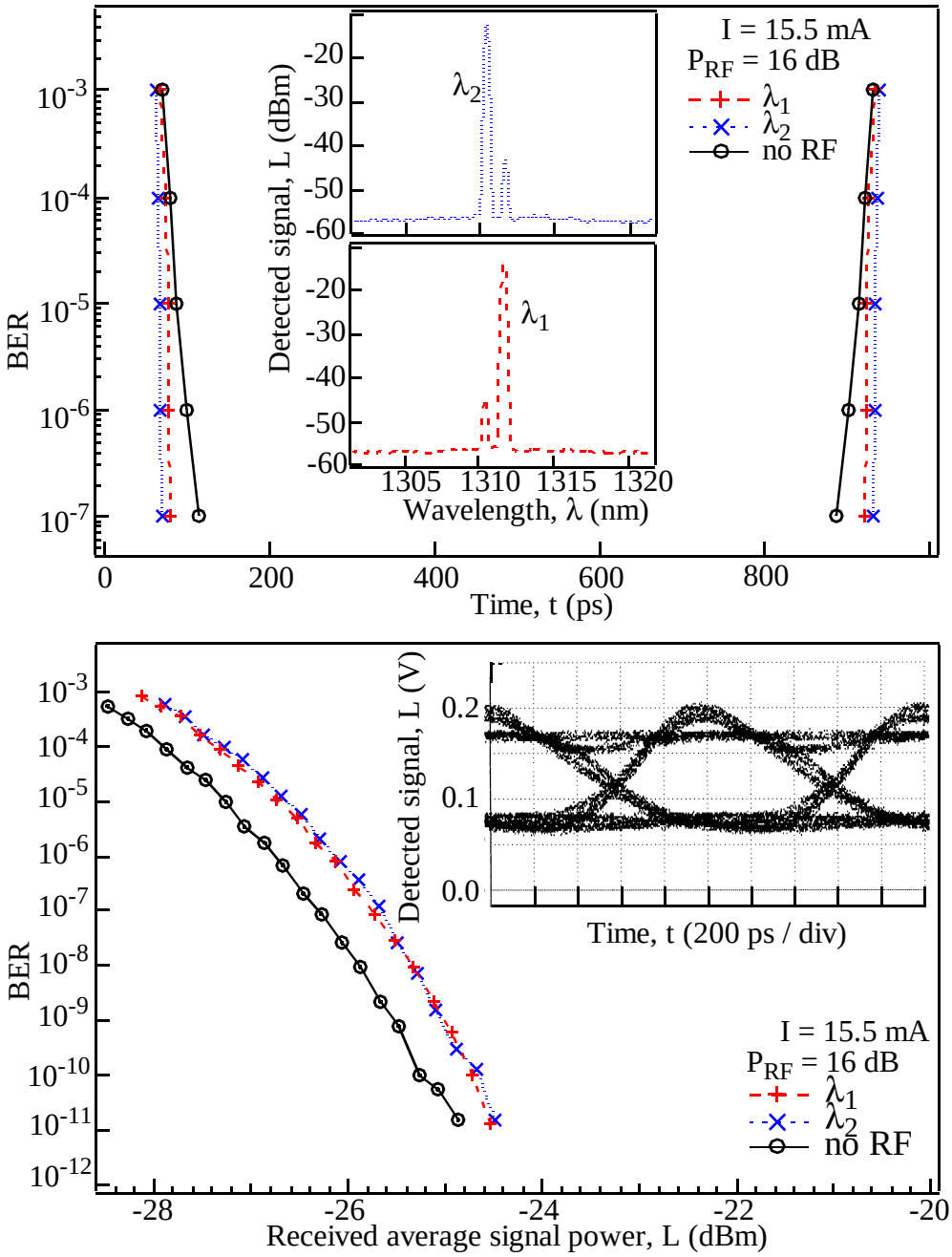

Fig. 4.12 Measured results of digital data transmission at an optical wavelength selected using an RF signal.

(a) Measured BER versus eye opening relative to clock edge. A 2^7 - 1 NRZ PRBS is transmitted at 1 Gb/s. A 16 dBm RF signal launched by the signal generator at f_1 = 8.95 GHz (f_2 = 7.24 GHz) is used to select λ_1 (λ_2). The phase margin at a BER of 10-7 is 840 ps. The inset shows the time averaged optical spectrum of the MCL when transmitting digital data at λ_1 (λ_2). **(b)** Measured BER versus average

received optical signal power at λ_1 (λ_2). Inset is eye diagram of received signal for a 1 Gb/s 2^7 - 1 NRZ PRBS transmitted at wavelength λ_1.

Measured BER versus average received optical signal power is shown in Fig. 3(b). Light is collected using a lensed multimode fiber (MMF) and is passed through an optical attenuator before being detected. There is no measurable noise floor with a BER as low as 10^{-11} and digital data was transmitted at wavelength λ_1 (λ_2) for over two hours with no errors. The inset to Fig. 4.12(b) shows the eye diagram of the received signal at λ_1. Experiments without a RF signal to select the lasing wavelength indicate that there is a -0.5 dBm power penalty when the RF signal is used to select the lasing wavelength. Thus, our preliminary results suggest that the MCL is a possible candidate for use in WDM systems which require selectable multi-wavelength sources.

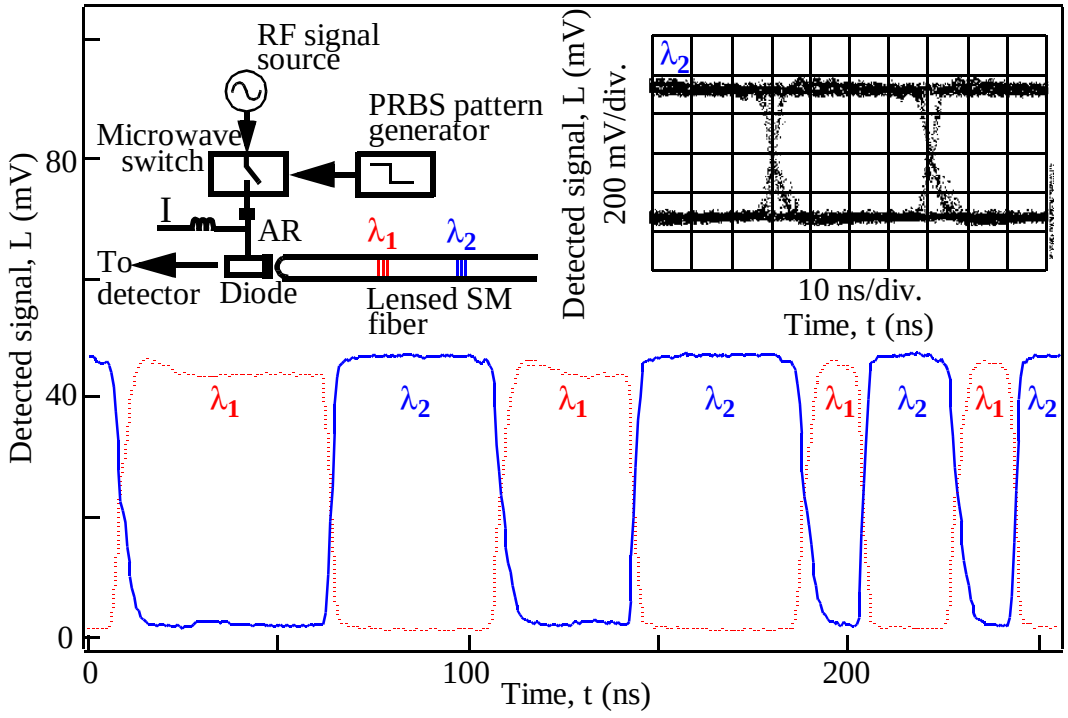

Fig. 4.13 Measured waveform of wavelength-encoded 2^7 - 1 NRZ PRBS transmitted at wavelengths λ_1 and λ_2.

The transmitted 25 Mb/s signal has a BER of less than 10^{-9}. Inset shows a schematic diagram of the

experimental arrangement and the eye diagram of the received signal at wavelength λ_2. Biased at current I = 25 mA, the laser has emission at wavelength λ_1. The 23 dBm RF signal at frequency f_2 incident on the laser is turned on and off using a microwave switch. A logical-high data input turns the microwave switch on and the RF signal selects lasing wavelength λ_2.

Wavelength-encoded data transmission is also possible using a MCL diode. In our initial experiments the laser is biased at I = 25 mA and the coupling efficiency between the MCL and the lensed SMF with embedded BGs is adjusted so that the device lases at wavelength λ_1. A schematic of the experimental arrangement is shown as an inset to Fig. 4.13. A 23 dBm RF signal at frequency f_2 selects λ_2 as the lasing wavelength. In our first experiments, the RF signal applied to the laser is turned on and off using a microwave switch. Logical-high data input turns the switch on and is encoded as emission at wavelength λ_2. Logical-low data input turns the switch off and is encoded as emission at wavelength λ_1. Wavelength-encoded NRZ PRBS is transmitted at 25 Mb/s with a BER of less than 10^{-9}. Fig. 4.13 shows a measured time-trace of the transmitted signal at wavelengths λ_1 and λ_2. The eye diagram of the transmitted signal at λ_2 is shown as an inset to Fig. 4.13. At present the microwave switch used in our experiment limits the wavelength switching rate to less than 100 Mb/s. Although with some RF signal processing the switch has a 0.5 ns rise time the fall time of the switch limits the speed of operation. However, experiments on the transient response of wavelength switching in MCLs indicate that Gb/s data rates are possible in such MCL devices.

4.7 Jitter

Fig. 4.14(a) shows a schematic diagram of the experimental arrangement to measure the steady state pulse jitter of optical pulses at both λ_{HOT} and λ_{COLD}. A SM fiber with two BG gratings centered at λ_{HOT} = 1311.4 nm and λ_{COLD} = 1308.8 nm provides optical feedback to the AR coated laser used for the experiments on pulse jitter. The laser is described in section 2. The laser is modulated by an RF signal with a fre-

quency f_{HOT} = 2.14 GHz (f_{COLD} = 2.738 GHz), corresponding to the photon cavity round-trip time, to select λ_{HOT} (λ_{COLD}) as the lasing wavelength. The RF signal power incident on the laser is 23 dBm. Fig. 4.14(b) shows the measured steady state pulse jitter as a function of DC bias current for optical pulses at wavelengths λ_{HOT} and λ_{COLD}. The RF signal used to select the lasing cavity is split and a portion is used to trigger the high speed digital sampling oscilloscope. The measured electrical jitter of the experimental arrangement is 2 ps. The pulsed light output from the MCL passes through a monochromator before being detected using a optical detector with a -3 dB optical bandwidth of 16 GHz. The output of the detector is fed to the oscilloscope.

The pulse timing jitter for pulses at λ_{HOT} is equal to that for a pulse at λ_{COLD} up to about 30 mA. Below 30 mA the RF signal is large enough to ensure complete wavelength switching to λ_{COLD} as seen in Fig. 4.14(c). Above 35 mA the MSR when switching to λ_{COLD} drops and this coincides with an increase in steady state pulse jitter for λ_{COLD} as seen in Fig. 4.14(b). Above 35 mA the pulse jitter at λ_{HOT} varies significantly with DC bias current. This may be due to back-reflections from the fiber connectors and the front face of the fiber lens collecting light from the laser.

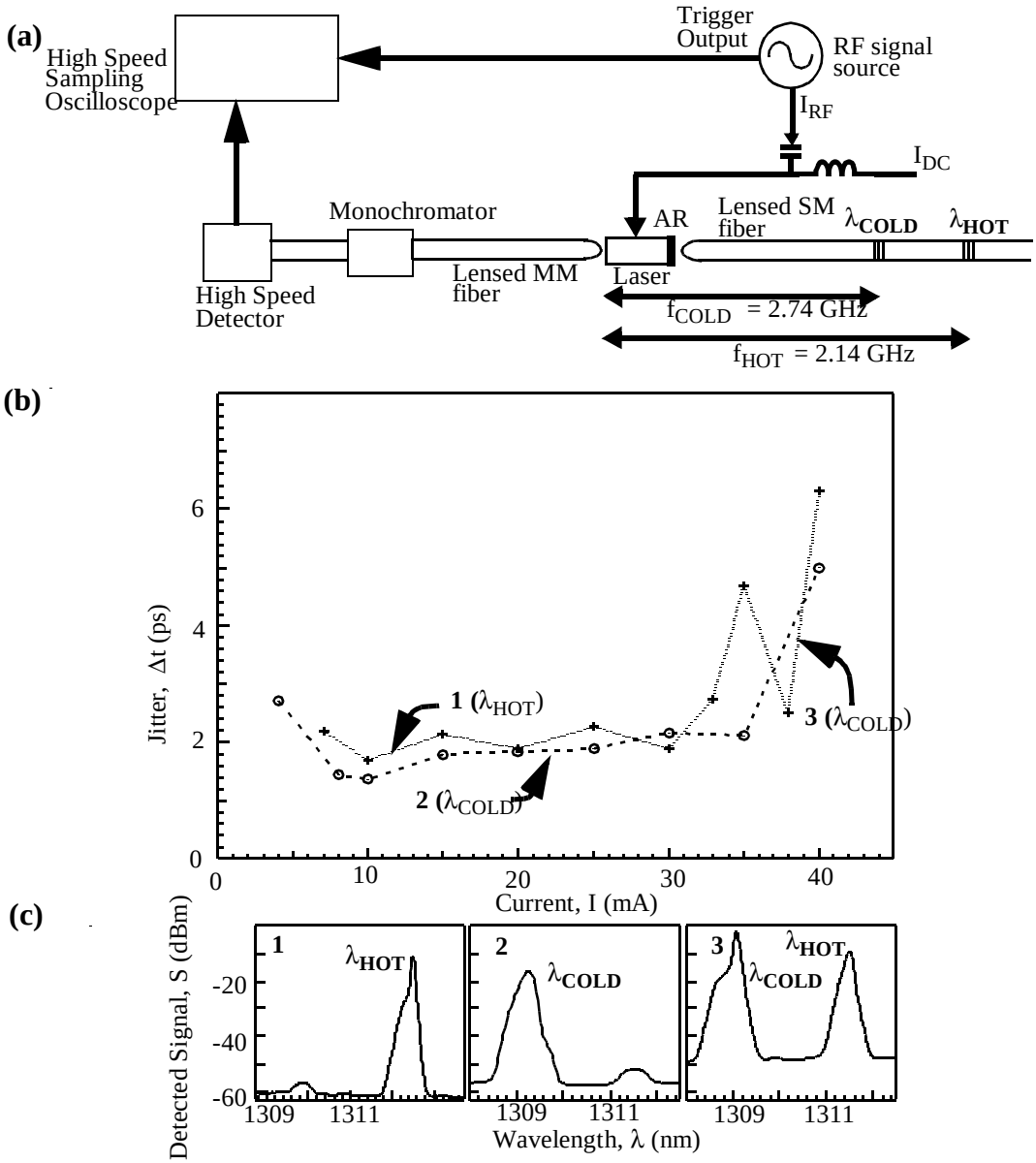

Fig. 4.14 (a) The experimental arrangement for the steady state pulse jitter.
(b) Measured steady state jitter as a function of bias current for optical pulses at λ_{HOT} = 1311.4 nm, and λ_{COLD} = 1308.8 nm. The SM fiber contains two BGs. The laser is modulated at frequency of f_{Cold} = 2.14 GHz and at f_{Hot} = 2.738 GHz to select λ_{HOT} and λ_{COLD} respectively. **(c)** Shows the measured optical spectra at the indicated points along the graph in Fig. 4.14(b).

Fig. 4.15(a) shows the experimental arrangement used to measure timing jitter of the optical pulses at wavelengths λ_{COLD} and λ_{HOT} as a function of pulse position. The

laser is biased at 20 mA. The RF signal power incident on the laser is 23 dBm. The RF signal used to select the wavelength of the light output is fed to a trigger head which generates a trigger signal in the 100 KHz range. This signal is used to trigger the rest of the instruments. The measured timing jitter of the experimental arrangement is 7 ps. The RF signal modulating the MCL is turned on and off by a microwave switch which is controlled by a pulse generator. The light output of the MCL is detected as in the previous experiment.

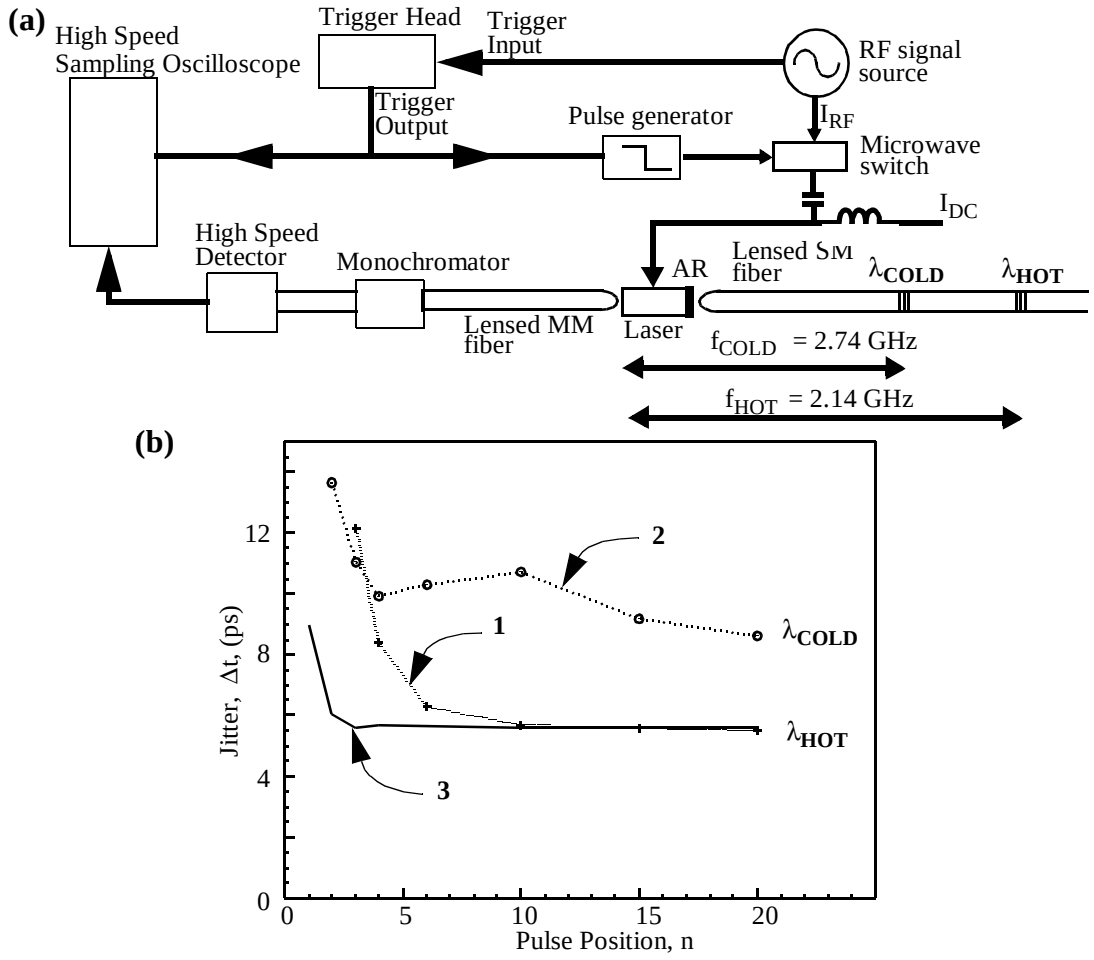

Fig. 4.15(a) Schematic of the experimental arrangement to measure pulse jitter versus pulse position. **(b)** Measured jitter as a function optical pulses position at λ_{HOT} = 1312 nm, and λ_{COLD} = 1309 nm after an RF signal is applied to select the optical wavelength. The laser is modulated at frequency of f_{HOT} = 2.14 GHz and f_{COLD} = 2.738 GHz to select λ_{HOT} and λ_{COLD} respectively. The RF signal power

incident on the laser is 13 dBm. Curves 1 and 2 show the measured pulse timing jitter for pulses at λ_{HOT} and λ_{COLD} respectively, with the laser biased at 20 mA. The SM lensed fiber collecting light from the AR coated side of the laser is optimally aligned for maximum coupling efficiency. Curve 3 is the measured pulse jitter at λ_{HOT} with the SM lensed fiber aligned at an angle to the laser and the DC bias of the laser changed to 35 mA to minimize jitter.

Measured variation of jitter with optical pulse position is shown in Fig. 4.15. The measured steady state jitter for optical pulses at wavelengths λ_{COLD} and λ_{HOT} in the experimental arrangement is 8 ps and 6 ps respectively. Experimental results shown in Fig. 4.14(b) indicate that the steady state pulse jitter for the two wavelengths should be the same. The difference in the steady state value of jitter between λ_{COLD} and λ_{HOT} is due to the electrical triggering mechanism used for the experiment which has a measured timing jitter of 7 ps.

Timing jitter of optical pulses at λ_{COLD} reach their steady state value in 5 pulses of λ_{COLD}. The timing jitter of the first few pulses at the wavelength λ_{HOT} is dependent on the experimental arrangement. When the lensed SM fiber collecting the light from the AR coated side of the laser is optimally aligned the jitter of the first few pulses varied with time and bias current. Any slight movement of the lensed multimode (MM) fiber collecting light from the non AR coated side of the laser also caused a variation of the jitter of the initial pulses. A possible cause of the instability is the back-reflections of light back into the laser from the surface of the lens and mis-aligned connectors. Under these conditions the timing jitter of optical pulses at λ_{HOT} reach their steady state value after 10 pulses. The lensed SM fiber collecting light from the AR coated side of the laser is aligned at an angle to the laser diode. This minimizes the back-reflections of light from the lens surface back into the laser. Under these conditions the timing jitter of the initial pulses is more stable over time although it varies with bias current. The experimental conditions are tweaked to minimize pulse jitter. The laser is biased at 35 mA. Under these conditions the timing jitter of pulses at λ_{HOT} reaches a steady state value in 3 pulses.

Further work is necessary to understand the factors affecting timing jitter. Both the intensity as well as the phase of the light reflected back into the laser cavity affect the linewidth of the light output. Narrowing or broadening of emission line were predicted and observed to occur at very low feedback levels (<-50 dB) [4.14] [4.15]. Effects of feedback on the spectra of DC biased semiconductor lasers have been extensively studied [4.16] [4.17]. The turn-on jitter measurement is sensitive to slight movements indicating that besides the magnitude of the unwanted optical feedback, its phase also affects the timing jitter of the first few pulses. The effect of the light fed back from the surface of the SMF lenses collecting light from the facets of the laser may be studied by placing the semiconductor laser in an external cavity with optical feedback from a bulk optic BG. To minimize unwanted reflections a carefully selected AR coated optical lens should be used to collimate the light in the external cavity. The effect of an SMF lens collecting the light output from the cleaved facet can then be studied in a controlled manner. Translation stages with submicron translational resolution are needed to study the effect of the phase of the light fed back to the device on the its characteristics. After the effects of reflections from the lens surface on the device characteristics are determined the effect of optical feedback from misaligned SMF connectors can then be studied.

4.8 References

4.1 C. A. Brackett, "Dense wavelength division multiplexing networks : Principles and applications," IEEE J. Select. Areas Commun., **8**, pp. 948-964 (1990).

4.2 P. A. Morton, V. Mizrahi, P. A. Andrekson, T. Tanbun-Ek, R. A. Logan, P. Lemaire, D. L. Coblentz, A. M. Sergent, K. W. Wecht, and P. F. Sciortino Jr., "Mode-locked hybrid soliton pulse source with extremely wide operating frequency range," IEEE Photonics Technol. Lett., **5**, pp.28-31 (1993).

4.3 J. Yu, D. Huhse, M. Schell, M. Schulze, D. Bimberg, J. A. R. Williams, L. Zhang, and I. Bennion, "Fourier-transform-limited 2.5 ps light pulses with electrically tunable wavelength (15 nm) by hybridly modelocking a semiconductor laser in a chirped Bragg grating fibre external cavity," Electon. Lett., **31**, pp. 2008-2009 (1995).

4.4 D. Huhse, M. Schell, W. Utz, D. Bimberg, J. A. R. Williams, L. Zhang, and I. Bennion, "Fast wavelength switching of semiconductor-laser pulses by self-seeding," Appl. Phys. Lett., **69**, pp. 2018-2020 (1996).

4.5 J. E. Bowers, P. A. Morton, A. Mars, and S. W. Corzine, "Actively mode-locked semiconductor lasers," IEEE J. Quantum. Electron., **25**, pp. 1426-1439 (1989).

4.6 K. Kojima, "High-power, high-efficiency, highly uniform 1.3 μm InGaAsP/InP strained MQW lasers," Optical Fiber Communications Conference, OSA Technical Digest Series (ISBN 1-55752-368-1) **8**, pp. 253-254, 1995.

4.7 K. O. Hill, Y. Fujii, D. C. Johnson, and B. S. Kawasaki, "Photosensitivity in optical fiber waveguides : Application to reflection filter fabrication," Appl. Phys. Lett., **32**, pp. 647-649 (1978).

4.8 L. Zhai, A. J. Lowery, and Z. Ahmed, "Locking bandwidth of actively mode-locked semiconductor-lasers using fiber-grating external cavities," IEEE J. Quantum Electron., **31**, pp. 1998-2005 (1995).

4.9 G. A. Ball, W. H. Glenn, and W. W. Morey, "Programmable fiber optic delay-line," Photonics Technol. Lett., **6**, pp. 741-743 (1994).

4.10 J. P. van der Zeil, "Actively mode locking of double heterostructure lasers in an external cavity," J. Appl. Phys., **52**, 4435-4446 (1981).

4.11 J. E. Bowers, P. A. Morton, A. Mar and S. W. Corzine, "Actively mode-locked semiconductor lasers," IEEE J. of Quant. Elec., **25**, pp. 1426-1439 (1989).

4.12 A. P. Kanjamala and A. F. J. Levi, "Transient-response of wavelength switching in multicavity mode-locked laser-diodes," Appl. Phys. Lett., **69**, pp. 3647-3649 (1996).

4.13 J. O'Gorman, A. F. J. Levi, D. Coblentz, T. Tanbun-Ek, and R. A. Logan, "Cavity formation in semiconductor-lasers," Appl. Phys. Lett., **61**, pp. 889-891 (1992).

4.14 K. Kikuchi and T. Okoshi, "Simple formula giving spectrum-narrowing ratio of semiconductor laser output obtained by optical feedback," Electron. Lett., **18**, pp. 10-12 (1982).

4.15 F. Farve, D. LeGuen and J. C. Simon, "Optical feedback effects upon laser diode oscillation field spectrum," IEEE J. Quantum Electron., **18**, pp. 1712-1717 (1982).

4.16 B. Tromborg, J. H. Osmundsen and H. Olesen, "Stability analysis for a semiconductor laser in an external cavity," IEEE J. Quantum Electron., **20**, pp. 1023-1032 (1984).

4.17 R. W. Tkach, A. R. Chraplyvy, "Regimes of feedback effects in 1.5 mm distributed feedback lasers," J. Lightwave Technol., **4**, pp. 1655-1661 (1986).

Chapter 5 : Conclusions and future work

5.1 Summary and conclusions

In this thesis an attempt is made to understand the static and dynamic characteristics of a MCL consisting of an AR coated semiconductor laser in an external cavity with optical feedback from narrow BGs embedded in a singlemode fiber.

The residual facet reflectivity of the AR coated facet, even with reflectivity as low as 10^{-3}, plays a crucial role in determining the device characteristic of the MCL due to coupled cavity effects. The optical cavity between the cleaved semiconductor facet of the AR coated semiconductor laser and the fiber BG is one cavity of the MCL. The semiconductor laser cavity between the AR coated semiconductor facet and the cleaved semiconductor facet forms a second cavity. Optical loss is minimized and lasing occurs at a BG defined wavelength when a peak in the spontaneous emission background of the semiconductor cavity coincides with the BG defined wavelength. In this manner the small residual reflectivity of the AR coated facet can cause a large mode suppression ratio (MSR) when selecting lasing wavelengths.

Decreasing optical coupling efficiency between the semiconductor diode and the SMF causes an increase in threshold carrier density. An increase in carrier density in the semiconductor causes a decrease in the refractive index and moves the FP peaks of the semiconductor cavity to shorter wavelengths. By changing the coupling efficiency between the AR coated semiconductor laser and a SMF containing two BGs with distinct center wavelengths, coupled cavity effects are used to select the lasing wavelength with a MSR of greater than -35 dB.

In a two-section laser the carrier density is not pinned above threshold. Experimental results show that changing the bias current applied to one of the sections of an AR coated two section laser in a BG defined external cavity shifts the spontaneous emis-

sion peaks of the AR coated laser to shorter wavelengths. This effect is used to demonstrate wavelength coding using a two-section laser in an external cavity with optical feedback from two FBGs.

In MCL besides the interference effects of the composite cavity, the reflection spectrum of the BG also plays a crucial role in determining the lasing characteristics of the device. If residual facet reflectivity of the AR coating is reduced to zero the MCL has a unique lasing solution at any bias current when the optical bandwidth of the BG is greater than the mode spacing of the cavity modes. The device has multiple lasing solutions at the same bias current even with a perfect AR coating if the bandwidth of the BG is comparable to the mode spacing of the external cavity modes. The device also has multiple lasing states at the same bias current due to coupled cavity effects if the effective reflectivity of the BG approaches that of the AR coated facet of the laser.

The MCL is used to build an electro-optic flip-flop by switching between the multiple lasing states at the same bias current using electrical pulses to set and reset the device. When the flip-flop switches between two states with lasing at optical wavelengths corresponding to the two BGs the switching time is in the ns range even though the photon cavity round trip time is 68 ps. The switching time when switching between lasing states at the same nominal wavelength using electrical set and reset pulses is also in the ns range. The speed of operation of the electro-optic SR flip-flop is limited to about 100 MHz by the turn-on delay as well as timing jitter when switching between states by applying electrical pulses. Switching to a wavelength state of the flip-flop by coherently injecting photons into the device at that wavelength reduces the turn-on delay and timing jitter. As the coherent optical pulse applied to the device lowers the carrier density, n, in the laser gain medium it will not switch the flip-flop to a lasing state with higher carrier density.

Semiconductor lasers have a resonance at the photon cavity round-trip time. Hence, a

large RF signal tuned to the photon cavity round-trip time of a BG defined cavity of the MCL, selects the wavelength defined by that BG as the lasing wavelength. This novel technique switches the lasing cavity with an optical discrimination of greater than -40 dB. The transient switching time depends on the number of "hot photon" present initially before the RF signal is applied to accomplish the switching. Above threshold the transient response time of the hot photon cavity is 2 round trips independent of the DC bias level and RF signal power while that of the cold photon cavity decreases with increase in RF signal power. Below threshold the transient time of the hot photon cavity tends to that of the cold photon cavity, increasing with decrease in I_{DC} and RF signal power. Using this basic idea, out of band RF modulation of a MCL is used to precisely select lasing optical wavelength for digital data transmission at 1 Gb/s.

5.2 Future work

5.2.1 Stability of the experimental arrangement

Packaging of the AR coated semiconductor lasers in an external cavity with optical feedback from FBGs is the main factor determining long term stability of these hybrid devices. The alignment between the lensed SMF and the AR coated laser needs to be maintained in all three dimensions to within a fraction of a wavelength to prevent mode hopping. The experimental arrangement that we use to perform experiments on the MCL is stable for about 10 to 15 minutes. Improvements of the packaging to ensure long term stability will help to study the MCL in a much more controlled manner than currently possible. Besides, the packaging problem needs to be solved before the MCL can be used to build functional optoelectronic devices.

5.2.2 Model of the MCL

The model of the MCL presented in this thesis is a first cut at simulating a fairly complex device. The wavelength selectivity of the MCL results from coherent interference of light feedback into the semiconductor laser from the FBGs with the light

reflected from the AR coated facet of the laser. Hence, the phase response of the FBG and the coupling efficiency between the AR coated laser and the SMF as a function of optical wavelength, ignored in the model, affect the device characteristics. Results presented in [5.1] [5.2] indicate that the phase and magnitude of the reflections from the lens surface collecting light from the AR coated facet as well as the cleaved facet of the laser result in oscillations in the coupling of about 0.2 dB. The light feedback to the laser from the lens surface will coherently interfere with the lasing light. The model indicates that reflection from the AR coated facet of the laser with a reflectivity of 10^{-3} plays a crucial role in the device characteristics. Hence, the reflections from the surfaces of lenses used for collecting the light need to be included in the model.

In the model of the MCL the reflectivity of the FBG as a function of wavelength is assumed to be Gaussian to simplify calculations. The reflectivity of a typical FBG has a more complicated dependence on wavelength as derived in Refs [5.3] [5.4]. This dependence of the reflectivity of a FBG as a function of wavelength needs to be included in the model. We also assume that there is a single lasing mode. Lasing occurs at a wavelength approximately equal to the center wavelength of the FBG. This assumption is valid when the BW of the FBG is comparable to the cavity mode spacing. But in longer cavities when the cavity mode spacing is smaller than the FBG bandwidth the device lases in multiple longitudinal modes and this is no longer the valid.

A number of experiments to study the cavity switching dynamics of the MCL are presented in this thesis. Although the cavity switching characteristics of the MCL are qualitatively understood, to gain insight into the switching transients a dynamic model of the device which includes interference effects of the composite cavity as well as BG bandwidth is essential. The simplest case of cavity switching using optical injection is modeled in section 3.4.2. As this model does not include effects due the BG bandwidth limitations it is not suitable to model the dynamics of the MCL when

operating as a flip-flop. A physically sound dynamic model of the MCL is a daunting task especially if one does not linearize the coupled nonlinear system as is usually done when simulating the dynamics of coupled cavity lasers [5.9].

An accurate dynamic model of the device will also require a model of the transient response of the FBG. There have been experimental and theoretical studies on pulse propagation through uniform and non-uniform FBG structures for the case where the spectral bandwidth of the incident pulse is narrower than that of the BG response [5.5] [5.6], the spectral bandwidth of the pulse is broader than the FBG [5.7] and of the impulse response of the FBGs [5.8]. If the propagation time through the FBG is of the same order or a factor of 10 less than the propagation through the entire MCL the transient response of the grating needs to be included in any accurate dynamic model of the device.

5.2.3 Novel devices

A semiconductor laser diode in a photon cavity containing a mirror whose optical bandwidth is less than the classical cavity mode spacing can have multiple lasing states at the same bias current. This idea can be used to build novel monolithic as well as hybrid devices which have multiple stable states at the same bias current. If one is able to switch between the stable states these devices can be used to build optical memory elements, flip-flops, latches and quantizers. The hybrid optical flip-flop demonstrated in section 3.2.2 operates in the 100 MHz range. Scaling the device size as well as seeding the device with photons corresponding to the final state will increase the switching speed. Successful demonstration of these devices in the 10s of GHz range is crucial for high speed all optical networks.

5.3 References

5.1 C. A. Edwards and H. M. Presby, "Coupling-sensitivity comparison of hemispheric and hyberbolic microlenses," Appl. Opt., **32**, pp. 1573-1577 (1993).

5.2 W. Bludau and R. Rossberg, "Characterization of laser-to-fiber coupling techniques by their optical feedback," Appl. Opt., **21**, pp. 1933-1939 (1982).

5.3 A. Yariv, "Coupled-mode theory for guided-wave optics," IEEE J. Quantum Electron., **9**, pp. 919-933, (1973).

5.4 H. Kogelnik, "Theory of optical waveguides," in Guided-Wave Optoelectronics, T. Tamir, Ed. New york : Springer-Verlag, 1990.

5.5 D. Taverner, D. J. Richardson, J. -L. Archambault, L. Reekie, P. St. J. Russell, and D. N. Payne, "Experimental investigation of picosecond pulse reflection from fiber gratings," Opt. Lett., **20**, pp. 282-284 (1995).

5.6 J. E. Sipe, L. Poladian and C. Martijn de Sterke, "Propagation through nonuniform grating structures," J. Opt. Soc. A, **11** (4), pp. 1307-1320 (1994).

5.7 L. R. Chen, S. D. Benjamin, P. W. E. Smith and J. E. Sipe, "Ultrashort pulse reflection from fiber gratings : A numerical investigation," J. Lightwave Technol., **15** (8), pp. 1503-1512 (1997).

5.8 A. Carballar and M. A. Muriel, "Phase reconstruction from reflectivity in fiber Bragg gratings," J. Lightwave Technol., **15**, pp. 1314-1322 (1997).

5.9 L.A.Coldren and T.L.Koch, "Analysis and design of coupled-cavity lasers- Part 2 : Transient analysis," IEEE J. Quantum Electron., **20**, pp. 671-682 (1984).